



HAL
open science

Dynamics and rheology of a suspension of vesicles and red blood cells

Giovanni Ghigliotti

► **To cite this version:**

Giovanni Ghigliotti. Dynamics and rheology of a suspension of vesicles and red blood cells. Data Analysis, Statistics and Probability [physics.data-an]. Université Joseph-Fourier - Grenoble I, 2010. English. NNT: . tel-00554161

HAL Id: tel-00554161

<https://theses.hal.science/tel-00554161>

Submitted on 10 Jan 2011

HAL is a multi-disciplinary open access archive for the deposit and dissemination of scientific research documents, whether they are published or not. The documents may come from teaching and research institutions in France or abroad, or from public or private research centers.

L'archive ouverte pluridisciplinaire **HAL**, est destinée au dépôt et à la diffusion de documents scientifiques de niveau recherche, publiés ou non, émanant des établissements d'enseignement et de recherche français ou étrangers, des laboratoires publics ou privés.

Université de Grenoble



THESE
pour obtenir le grade de
DOCTEUR DE L'UNIVERSITE DE GRENOBLE

Spécialité: Physique des Matériaux

Arrêté ministériel : 7 Août 2006

Présentée et soutenue publiquement par

Giovanni Ghigliotti

le 9 Décembre 2010

**Dynamique et rhéologie d'une suspension
de vésicules et globules rouges**

Thèse dirigée par Chaouqi Misbah

Jury

Président: Dr. Bart van Tiggelen
Rapporteurs: Dr. Andrea Mazzino
Prof. Petia Vlahovska
Examineurs: Prof. Dominique Barthès-Biesel
Prof. Stefano Guido
Dr. Didier Jamet
Dr. Chaouqi Misbah
Dr. Jacques Prost

Thèse préparée au sein du Laboratoire de Spectrométrie Physique
dans l'École Doctorale de Physique de Grenoble

Dynamics and rheology of a suspension of vesicles and red blood cells

Giovanni Ghigliotti

PhD Thesis

Grenoble, December 9th 2010

PhD Thesis supervised by Chaouqi Misbah
and prepared at Laboratoire de Spectrométrie Physique
UMR 5588 Université Joseph Fourier - CNRS
Grenoble, France

CONTENTS

Contents	v
1 Introduction	1
1.1 Blood flow, red blood cells and vesicles	1
1.2 Contributions of this work	2
1.3 Organization of the work	5
2 Introduction en Français	7
2.1 Ecoulement sanguin, globules rouges et vésicules	7
2.2 Contributions de ce travail	9
2.3 Organisation du travail	12
3 Complex fluids	15
3.1 Particles in suspension	16
3.2 The study of complex fluids: rheology	22
4 The model for vesicles	27
4.1 Vesicles as a minimal energy configuration	27
4.2 The model for the curvature	29
4.3 Hydrodynamical model	32
4.4 Basic dynamics in linear shear	38
4.5 Vesicles to model red blood cells in two dimensions	40
5 The numerical methods	43
5.1 A moving interface problem	43
5.2 Boundary Integral Method	44
5.3 Phase Field Method	48
5.4 Comparison between the numerical methods	52
5.5 Alternative Boundary Integral implementation	53
6 Dilute suspension of vesicles	57
6.1 The effective viscosity	62
6.2 The normal stress difference	65
6.3 Instantaneous stress in the tumbling regime	65
6.4 Dependence on shear rate	68

6.5	Comparison with drops	71
6.6	Comparison with three dimensional theory and experiments	75
6.7	Highly deflated vesicles	76
7	Vesicles in a Poiseuille flow	83
7.1	Introduction	83
7.2	The physical system	84
7.3	The fast Multipole Method	85
7.4	Numerical tests	86
7.5	One dimensional vesicle sets	87
8	Vesicles in a curved flow	93
8.1	Cross-streamline migration	93
8.2	Unbounded vortex	94
8.3	Couette flow	100
9	Conclusions and perspectives	105
10	Conclusions et perspectives	107
	Appendices	111
A	The stress tensor of a dilute suspension of particles	113
A.1	Mean stress tensor for a particle suspension	114
A.2	Suspension of liquid particles	118
A.3	Loss of symmetry of the mean stress tensor	125
A.4	Two-dimensional Einstein coefficient	127
B	Rheology of a tumbling filament	131
B.1	Qualitative interpretation	132
B.2	Rigorous argument	133
C	Migration driven by normal stress difference	137
D	The computation of effective viscosity in a Couette cell	139
E	The Fast Multipole Method	143
E.1	Multipole expansion	144
E.2	Local expansion	145
	Bibliography	149

INTRODUCTION

The subject is presented. The state of the art at the beginning of the thesis is summarized and the contributions of this PhD work are detailed.

1.1 Blood flow, red blood cells and vesicles

Blood flow has since centuries attracted the attention of scientists. Blood is a non homogeneous material, formed mainly by a fluid (the plasma) and red blood cells (RBCs). These cells can deform under flow and undergo complicated dynamics, conferring to the blood amazing and nontrivial flow properties.

A description based on a continuum model has first been attempted by Poiseuille in the middle of 19th century, leading to the well-known relationship between flux, pressure drop and geometry in a circular duct that bears his name. In the 1930's Fåhræus and Linqvist found deviations from Poiseuille's law [FL31]: while flowing blood through thin tubes, the blood viscosity derived from the flow rate at a given driving pressure using Poiseuille's law decreased with decreasing diameter of the tubes. This effect has been later explained as being a consequence of the radial displacement (towards the center) of RBCs [PSG96] within the tubes.

Later in the 1970s, clear experimental evidence has been given to the peculiar microscopic dynamics of red blood cells, the so-called tank-treading motion [FSLSS78]. This motion takes place in a shear flow and consists of a stationary RBC shape associated to a tangential movement of the membrane. This ingredient could solve issues in the interpretation of the blood flow properties [PSG96] and is peculiar to particles surrounded by a membrane.

Nowadays, although many features of blood flow are understood, many questions remain unanswered. These questions are linked on one side to the fundamental understanding of the underlying physics (why RBCs move in the radial direction, which is transverse to the flow? How does their

deformation affect the flow?), and on the other to the biological relevance of physiological conditions (what is the role of the *glycocalyx* layer on the vessel walls? Do RBCs have an active role in vascular morphogenesis?).

This thesis deals with the first set of problems, those that are more related to physics, and in particular fluid mechanics and the interactions between fluids and other structures (as the RBC membrane and the vessel walls).

In order to grasp the fundamentals of blood flow and link them to the microscopic properties of the RBCs, we consider a model system consisting in a suspension of *vesicles* in a fluid. Vesicles are fluid drops delimited by a lipid bilayer, similar to the one surrounding living cells (but without membrane proteins and other biological structures).

From a mechanical point of view, a suspension of vesicles is a *complex fluid*: that is, it belongs to the class of polymer melts, emulsions, foams, particle suspensions. . . This gives to vesicle suspensions both a fundamental interest and the possibility to compare with many other systems, ‘similar’ in some aspects, that have been studied since long [Ein06, Ein11, Tay32, Wei47, CN61].

This thesis deals both with the dynamics of vesicles immersed in a fluid and with the flow properties of the suspension, i.e. the *rheology*.

The long-term goal is to contribute to the knowledge of blood flow, and the short-term goal is the understanding of the fundamental mechanisms underlying the dynamics of vesicles and their link to rheology.

The method employed is the one of numerical simulations, carried out in two dimensions. The choice of dimension two (instead of the more realistic three) is motivated by the great geometrical simplifications that one gets by dropping one dimension, allowing for a deeper understanding of the underlying physics. In addition, this will allow us to explore a wide range of parameters, a task that become quite prohibitive in three dimensions.

1.2 Contributions of this work

The state of the art

At the beginning of this thesis (2007) the dynamics of vesicles had been studied analytically, numerically and experimentally since several years. More precisely, a rough analytical model was proposed in 1982 [KS82]. This model was incorporating a quasi-inextensible membrane, but vesicles were treated as *undeformable* liquid ellipsoids. Nevertheless, this model was able to reproduce tank-treading motion. Only in 1996 deformations were taken into account, and this was done through numerical simulations

[KWSL96]. Soon after, experiments on the deformation of vesicles under flow started [dHBvdE⁺97]. From that moment, many studies investigated the dynamical behavior of a vesicle under flow: analytical calculations [Oll97, Sei99], experiments [ALV02, VMP04, KS05, MVA⁺06], and simulations [CM99b, BM02, BRS⁺04, NG04]. Only in 2006 a precise analytical theory, able to implement deformations, has been developed [Mis06].

In 2007, the dynamics of a single vesicle was being refined, with a new type of motion discovered only one year before [Mis06]. The corresponding parameter space was not extensively explored (and even its dimension was under debate [KFM09]) and two-dimensional effects were not separated from the three-dimensional ones. The rheology of a dilute suspension of vesicles was only partially understood [DM07] and experimental data were lacking. The interactions between vesicles were not studied.

During my thesis, the number of investigations on the dynamics and rheology of suspensions of vesicles carried out in our and other institutions sensibly increased. Theory has been improved [VG07, DBP⁺07, LTV08, DVM08, DVM09], becoming more and more quantitative. Experiments measured the dynamics of vesicles [CKPM08, DKSS09, DKS09, VCM⁺09] and the rheology of dilute and semi-dilute suspensions [KSS08, VMP⁺08]. Several new numerical approaches have been developed [Low09, VGZB09, RVB10, KL10, STL⁺10], simulations focused in particular on the behavior in microchannels [KRC⁺08, RVB10] and on interactions between vesicles [MNG09].

Contributions of the present work

This work brings several contributions to the knowledge of vesicle suspensions, both to dynamics and rheology. They are detailed in the following paragraphs, together with the context in which they are situated.

The behavior of a dilute suspension of vesicles (i.e. a suspension in which interactions between vesicles are disregarded) has been analyzed in detail, and all the relevant parameters have been widely examined. The contributions to this topic can be summarized around two points:

Characterization and interpretation of the rheology of a dilute suspension

An exhaustive study of the rheology of a dilute suspension of vesicles has been carried out. Although the basic behaviors had already been published [DM07, KSS08, VMP⁺08], the results were nontrivial and not completely understood. The study of all the parameters contributing to the dynamics in a simple situation (a single vesicle in an unbounded linear shear flow) and the comparison with similar systems (drops and rigid rods) allowed to give a clear interpretation of the link between the microscopic dynamics and the overall rheological behavior. In particular, the peculiar role in both dynamics and rheology of the vesicle membrane has been elucidated. This topic is treated in chapter 6. This work gave rise to a publication in *Journal of Fluid Mechanics* [GBM10].

Tumbling without viscosity contrast

The dynamics of vesicles has been studied most of the time close to the spherical limit, or at moderate deflation: no results concerning the dynamical or rheological behavior of highly deflated vesicles were available. In a joint work with Prof. G. Biroš (applied mathematician at *Georgia Tech*, USA), we carried out simulations of extremely deflated vesicles. We could find a surprising result, i.e. the presence of a rigid body motion (*tumbling*) in a region of the parameter space where it was not expected (that is, when the fluids inside and outside the vesicle have the same viscosity). This subject is presented in section 6.7, where an interpretation has also been given. The first results are published in *Esaim: Proceedings* [GSK⁺09].

After the study of the behavior of a dilute suspension, the analysis moved towards more complex situations: we considered a suspension of vesicles in a flow with a nonlinear profile (Poiseuille flow, which is parabolic) and in a confined device (a Taylor-Couette cell, composed by two coaxial cylinders that shear the fluid in the gap between them), that creates a flow with curved flow lines, as described in the following paragraphs.

Interactions in Poiseuille flow

A collaboration with H. Selmi (applied mathematician at *Ecole Polytechnique de Tunisie*, Tunisia) made possible the precise simulation of suspensions containing few tens of vesicles, thanks to the implementation of a fast solver based on the *fast multipole method*. We studied the behavior of an

array of vesicles lying on the centreline of a parabolic velocity profile, in order to mimic red blood cells in a capillary. Hydrodynamic interactions are very strong and generate the formation of clusters, characterized by a nonuniform distribution of vesicle positions. This has led us to the discovery of the existence of a maximal vesicle number in the cluster, above which one or few vesicles detach from the remaining ones, bringing to important spatial reorganization. This work is presented in chapter 7. The first results are accepted for publication in *Discrete and Continuous Dynamical Systems - Series B*.

Behavior in a curved flow

The analysis of the motion of a vesicle in a velocity field with curved flow lines revealed an amazing behavior: vesicles migrate perpendicularly to the flow, in the direction of concavity of the flow lines. This behavior is found to be common to many other entities, as drops and elastic polymers. Despite its observation dates back to thirty years ago, no explanation was suggested. The analysis revealed the proportionality of the migration velocity to a rheological quantity, the first normal stress difference. An explanation of the phenomenon has been proposed, and it may apply to other deformable particles.

The analysis continued with the study of a microscopic Couette device containing several vesicles. Vesicles organize in very ordered structures despite the extremely low volume fraction. The explanation given here relies on the mechanism for inward migration discussed above and hydrodynamic interactions. This topic is presented in chapter 8. An article has been submitted to *Physical Review Letters*.

1.3 Organization of the work

The contents of this work are organized as follows.

In chapter 3 we introduce complex fluids, in particular those that are closely related to vesicles and red blood cells, together with the basic concepts that one needs to characterize the flow properties of a fluid (i.e. *rheology*).

Chapter 4 is dedicated to the description of the model for vesicles; the constitutive equation for the membrane is introduced, together with the evolution equation for the fluid. A short overview of the basic dynamics of a vesicle under flow is given. The applicability of the model of vesicles to red blood cells is also discussed.

The numerical methods, used to obtain all the results presented hereafter, are detailed in chapter 5. This chapter contains three sections, each one dedicated to a different numerical code.

Chapter 6 contains an extensive description of the dynamics and the rheology of a dilute suspension of vesicles in a simple flow. This dense chapter presents all the fundamental behaviors and gives interpretations for them. It provides the tools that will be necessary to investigate more complex situations.

Chapter 7 is dedicated to the analysis of the behavior of sets of vesicles in a Poiseuille flow. Interactions between vesicles play here a nontrivial role that affects deeply the dynamics of the system.

Chapter 8 investigates the behavior of vesicles in a flow with curved flow lines. Results are presented for the peculiar dynamics of a single vesicle in this kind of flow, and for the more complex case of a collection of vesicles in a bounded system (Taylor-Couette cell).

Chapter 9 briefly summarizes the results obtained in this work and presents a series of perspectives.

Appendix A derives the expressions used for the computation of the rheological quantities all along this work.

In appendix B it is shown how a very simple system (a filament tumbling in a shear flow) happens to be of great help in the interpretation of the rheology of a suspension of vesicles.

Appendix C shows some fundamental concepts of fluid mechanics that can help the understanding of the dynamics of deformable particles in a curved flow.

Appendix D details the derivation of a formula for the rheological quantities in a Taylor-Couette cell.

Finally, in Appendix E the fast multipole method (FMM), used to sensibly decrease the computing time of a part of the simulations, is presented.

INTRODUCTION EN FRANÇAIS

Le sujet est présenté. L'état de l'art au début de de la thèse est résumé et les contributions apportées par ce travail sont détaillées.

2.1 Ecoulement sanguin, globules rouges et vésicules

L'écoulement sanguin a attiré l'attention des chercheurs scientifiques depuis des siècles. Le sang est un matériau non homogène, formé principalement par un fluide (le plasma) et des globules rouges. Ces cellules peuvent se déformer sous l'effet de l'écoulement et montrer des dynamiques complexes, donnant au sang des propriétés d'écoulement très particulières.

Une description basée sur un modèle continu a été proposée par Poiseuille au milieu du 19^{ème} siècle, conduisant à la relation bien connue qui porte son nom entre le flux, le saut de pression et la géométrie dans un tube circulaire. Dans les années 1930, Fåhræus et Linqvist ont observé des déviations à la loi de Poiseuille [FL31]: en faisant écouler du sang à travers des capillaires fins, la viscosité dérivée du flux et du saut de pression diminuait à mesure que diminuait le diamètre du capillaire. Cet effet sera par la suite expliqué comme étant une conséquence du déplacement radial (vers le centre) des globules rouges à l'intérieur des capillaires [PSG96].

Plus tard, dans les années 1970, une preuve expérimentale claire de la dynamique particulière des globules rouges, appelée *tank-treading* ('chenille de char' en anglais) a été apportée [FSLSS78]. Ce mouvement, typique des particules dotées d'une membrane, survient dans un écoulement de cisaillement et consiste en une forme stationnaire du globule, associée à un mouvement tangentiel de la membrane. Cette découverte majeure a permis de résoudre des questions dans l'interprétation des propriétés d'écoulement du sang [PSG96].

Aujourd'hui, bien que plusieurs caractéristiques de l'écoulement du sang soient comprises, beaucoup de questions demeurent sans réponse. Ces

questions sont, d'un côté, liées à la compréhension fondamentale de la physique sous-jacente (pourquoi les globules rouges se déplacent-ils radialement, perpendiculairement à l'écoulement imposé? Comment leur déformation influence-t-elle l'écoulement?), et de l'autre à l'interprétation biologique des conditions physiologiques (quel est le rôle de la couche de *glycocalyx* sur les parois des capillaires? Est-ce que les globules rouges ont un rôle actif dans la morphogenèse vasculaire?).

Cette thèse s'occupe de la première catégorie de problèmes, ceux qui sont le plus liés à la physique, et en particulier à la mécanique des fluides et à l'interaction entre fluide et structures (telles que les membranes des globules ou les parois des vaisseaux).

Pour saisir les mécanismes fondamentaux de l'écoulement du sang et les relier aux propriétés microscopiques des globules rouges, on considère un système modèle constitué d'une suspension de vésicules dans un fluide. Les vésicules sont des gouttes liquides délimitées par une double couche lipidique, similaire à celle qui délimite les cellules vivantes (mais sans les protéines de membrane ou autres structures biologiques).

D'un point de vue mécanique, une suspension de vésicules est un *fluide complexe*, c'est à dire, elle appartient à la classe des polymères fondus, émulsions, mousses, suspensions de particules, ... Ceci donne aux suspensions de vésicules à la fois un intérêt fondamental et la possibilité d'être comparées avec d'autres systèmes, 'similaires' en certains aspects, qui ont fait l'objet d'études depuis longtemps [Ein06, Ein11, Tay32, Wei47, CN61].

Cette thèse s'occupe à la fois de la dynamique de vésicules immergées dans un fluide et des propriétés d'écoulement de la suspension, c. à d. la *rhéologie*.

L'objectif à long terme est de contribuer à la connaissance de l'écoulement sanguin, et l'objectif à court terme est la compréhension des mécanismes fondamentaux sous-jacents à la dynamique des vésicules et de leur lien à la rhéologie.

La méthode utilisée est la simulation numérique, menée en deux dimensions. Le choix de la dimension deux (à la place de la plus réaliste trois) est motivé par les grandes simplifications géométriques que l'on obtient en abandonnant une dimension, permettant une meilleure compréhension de la physique sous-jacente.

2.2 Contributions de ce travail

L'état de l'art

Au debut de cette thèse (2007) la dynamique des vésicules avait été étudiée analytiquement, numériquement et expérimentalement depuis plusieurs années. Plus précisément, un modèle analytique simplifié a été proposé en 1982 [KS82]. Ce modèle incorporait une membrane quasi-inextensible, mais les vésicules étaient traitées comme des ellipsoïdes liquides *indéformables*. Néanmoins, ce modèle a été capable de reproduire le mouvement de tank-treading. C'est seulement en 1996 que les déformations ont été prises en compte, et ceci grâce à des simulations numériques [KWSL96]. Peu après, les expériences de déformation sous écoulement ont débuté [dHBvdE⁺97]. Depuis, plusieurs études ont été consacrées au comportement dynamique d'une vésicule sous écoulement: calculs analytiques [Oll97, Sei99], expériences [ALV02, VMP04, KS05, MVA⁺06] et simulations [CM99b, BM02, BRS⁺04, NG04]. Mais c'est seulement en 2006 qu'une théorie analytique précise, capable de prendre en compte les déformations, a été développée [Mis06].

En 2007, la description de la dynamique d'une vésicule était en train d'être affinée, avec un nouveau type de mouvement découvert seulement une année auparavant [Mis06]. L'espace des paramètres correspondant n'était pas exploré de manière systématique (et même sa dimension était en débat [KBM09]) et les effets bidimensionnels n'étaient pas séparés des effets tridimensionnels. La rhéologie d'une suspension diluée de vésicules était comprise seulement en partie [DM07] et des mesures expérimentales manquaient. Les interactions entre vésicules n'étaient pas étudiées.

Pendant ma thèse, le nombre d'études sur la dynamique et sur la rhéologie de suspensions de vésicules, menées dans notre laboratoire ou ailleurs, a augmenté fortement. La théorie a été améliorée [VG07, DBP⁺07, LTV08, DVM08, DVM09], devenant de plus en plus quantitative. Des expériences ont mesuré la dynamique de vésicules [CKPM08, DKSS09, DKS09, VCM⁺09] et la rhéologie de suspensions diluées et semi-diluées [KSS08, VMP⁺08]. Plusieurs nouvelles approches numériques ont été développées [Low09, VGZB09, RVB10, KL10, STL⁺10], se focalisant sur le comportement en microcanaux [KRC⁺08, RVB10] et sur les interactions entre vésicules [MNG09].

Contributions du travail présenté

Ce travail apporte plusieurs contributions à la connaissance des suspensions de vésicules, à la fois pour la dynamique et pour la rhéologie. Elles sont détaillées dans les paragraphes suivants, ainsi que les contextes dans lesquels elles se situent.

Le comportement d'une suspension diluée de vésicules (c. à d. une suspension dans laquelle les interactions entre vésicules sont négligées) a été étudié en détail, et tous les paramètres relevant ont été analysés. Les contributions à ce sujet peuvent être résumées autour de deux points :

Caractérisation et interprétation de la rhéologie d'une suspension diluée

Une étude approfondie de la rhéologie d'une suspension diluée de vésicules a été menée. Bien que les comportements fondamentaux aient déjà été publiés [DM07, KSS08, VMP⁺08], les résultats étaient complexes et pas complètement interprétés. L'étude de tous les paramètres qui contribuent à la dynamique dans une situation simple (une vésicule dans un écoulement de cisaillement linéaire non borné) et la comparaison avec des systèmes similaires (gouttes et fibres rigides) a permis de donner une interprétation claire du lien entre la dynamique microscopique et le comportement rhéologique du système. En particulier, le rôle précis de la membrane de la vésicule à la fois dans la dynamique et dans la rhéologie a été élucidé. Ce sujet est traité dans le chapitre 6. Ce travail a donné lieu à une publication dans le *Journal of Fluid Mechanics* [GBM10].

Tumbling sans contraste de viscosité

La dynamique des vésicules a été étudiée la plupart du temps dans une configuration proche de la limite sphérique, ou à dégonflement modéré : aucun résultat sur la dynamique ou sur la rhéologie d'une suspension de vésicules hautement dégonflées n'était disponible. Dans un travail en collaboration avec le professeur G. Biroş (mathématicien appliqué à *Georgia Tech*, USA), on a réalisé des simulations numériques de vésicules hautement dégonflées. On a ainsi mis en évidence un résultat surprenant, la présence d'un mouvement de corps rigide, *tumbling*, ('mouvement de bascule' en anglais) dans une région de l'espace des paramètres où il n'était pas attendu (c. à d. quand les fluides à l'intérieur et à l'extérieur de la vésicule ont la même viscosité). Ce sujet est présenté dans la section 6.7, où une interprétation a été aussi

donnée. Les premiers résultats ont été publiés dans *Esaim: Proceedings* [GSK⁺09].

Après l'étude du comportement d'une suspension diluée en cisaillement linéaire, l'analyse s'est portée sur des situations plus complexes: on a considéré une suspension de vésicules dans un écoulement avec un profil non linéaire (écoulement de Poiseuille, qui est parabolique) puis dans un système confiné (cellule de Taylor-Couette, composée de deux cylindres coaxiaux qui cisailent le fluide contenu dans l'interstice entre eux), qui crée un écoulement avec des lignes courbes, comme décrit dans les paragraphes suivants :

Interactions dans un écoulement de Poiseuille

Une collaboration avec H. Selmi (mathématicien appliqué à l'*Ecole Polytechnique de Tunisie*, Tunisie) a rendu possible la simulation de suspensions contenant plusieurs dizaines de vésicules, grâce à l'implémentation d'un solveur rapide basé sur la *méthode multipolaire rapide*. On a étudié le comportement d'un ensemble unidimensionnel de vésicules sur l'axe d'un écoulement de Poiseuille, dans le but d'imiter les globules rouges dans les capillaires. Les interactions hydrodynamiques sont très fortes et génèrent la formation de paquets, caractérisés par une distribution non uniforme des positions des vésicules. Ceci nous a amené à la découverte de l'existence d'un nombre maximal de vésicules par paquet, au dessus duquel une ou plusieurs vésicules se détachent des autres, générant une réorganisation spatiale conséquente. Ce travail est présenté dans le chapitre 7. Les premiers résultats sont acceptés pour publication dans *Discrete and Continuous Dynamical Systems - Series B*.

Comportement dans un écoulement courbe

L'analyse du mouvement d'une vésicule dans un champ de vitesse possédant des lignes d'écoulement courbes a dévoilé un comportement particulièrement intéressant : les vésicules se déplacent perpendiculairement à l'écoulement (*migrent*), dans la direction de la concavité des lignes d'écoulement. Ce comportement a été aussi observé pour plusieurs autres entités, comme gouttes et polymères élastiques. Bien que ce phénomène ait été observé il y a trente ans, aucune explication n'avait été suggérée. L'analyse a révélé que la vitesse de migration est proportionnelle à une propriété rhéologique, qui est la première différence des contraintes normales.

Une explication de ce phénomène a été proposée, qui pourrait s'appliquer à d'autres particules déformables.

L'étude s'est ensuite orientée vers un dispositif de Couette microscopique contenant plusieurs vésicules. Les vésicules s'organisent en structures hautement ordonnées malgré la très faible concentration. L'explication donnée ici repose sur le mécanisme de migration vers l'intérieur discuté ci-dessus et sur les interactions hydrodynamiques. Ce sujet est présenté dans le chapitre 8. Un article a été soumis à *Physical Review Letters*.

2.3 Organisation du travail

Les contenus de ce travail sont organisés ainsi.

Dans le chapitre 3 on introduit les fluides complexes, en particulier ceux qui sont proches des suspensions de vésicules et globules rouges, avec les concepts de base dont on a besoin pour caractériser les propriétés d'écoulement d'un fluide (c. à d. la *rhéologie*).

Le chapitre 4 est dédié à la description du modèle pour les vésicules ; l'équation constitutive de la membrane est introduite avec l'équation d'évolution pour le fluide. Un résumé sur les dynamiques de base d'une vésicule sous écoulement est présenté. L'applicabilité du modèle 'vésicule' aux globules rouges est discutée.

Les méthodes numériques utilisées pour obtenir tous les résultats présentés par la suite sont détaillées dans le chapitre 5. Ce chapitre contient trois sections, chacune dédiée à un code numérique différent.

Le chapitre 6 contient une description détaillée de la dynamique et de la rhéologie d'une suspension diluée de vésicules dans un écoulement simple. Ce chapitre particulièrement dense présente tous les comportements fondamentaux et en donne des interprétations. Il fournit les outils nécessaires pour étudier des situations plus complexes.

Le chapitre 7 est dédié à l'analyse du comportement d'ensembles de vésicules dans un écoulement de Poiseuille. Les interactions entre vésicules jouent ici un rôle complexe qui influence profondément la dynamique du système.

Le chapitre 8 examine le comportement de vésicules dans un écoulement courbe. Des résultats sont présentés pour la dynamique complexe d'une vésicule dans ce type d'écoulement, et pour le cas encore plus riche d'un ensemble de vésicules dans un système borné (dispositif de Taylor-Couette).

Le chapitre 10 résume brièvement les résultats obtenus dans ce travail et présente une série de perspectives.

L'annexe A contient les dérivations des expressions utilisées pour le cal-

cul des grandeurs rhéologiques tout le long de ce travail.

Dans l'annexe B on montre comment un système très simple (une fibre qui bascule dans un écoulement de cisaillement) peut être d'une grande aide pour l'interprétation de la rhéologie d'une suspension de vésicules.

L'annexe C montre des concepts fondamentaux de la dynamique des fluides qui peuvent aider à la compréhension de la dynamique de particules déformables dans un écoulement courbe.

L'annexe D détaille la dérivation d'une formule pour les grandeurs rhéologiques dans la cellule de Taylor-Couette.

Pour finir, dans l'annexe E, la méthode multipolaire rapide (FMM), utilisée pour diminuer sensiblement le temps de calcul, est présentée.

CHAPTER 3

COMPLEX FLUIDS

Complex fluids are defined and several examples are given. Rheology is introduced, the meaning of effective viscosity and normal stress difference and their link with the stress tensor are explained.

Les fluides complexes sont définis et plusieurs exemples donnés. La rhéologie est introduite, la signification de la viscosité effective et de la différence des contraintes normales et leur lien avec le tenseur des contraintes sont expliqués.

The first images that usually come to the mind when thinking to fluid mechanics are the ones connected to the flow properties of water and air: airplane design, dam engineering, waves in the ocean, tornadoes. . . Air and water belong to the class of the *simple fluids* (also called *Newtonian*), in contrast to another category, the so-called *complex fluids*, among which are found: polymer melts (plastic), foams, gels, biological liquids (blood, saliva), many food products (mayonnaise, mustard, ice cream) and then lava, mud, corn starch, . . . What do blood and mud have in common? The answer is, the presence of *mesoscopic structures*: red blood cells for blood and mineral particles for mud, in a suspension of ‘simple’ fluid (plasma and water, respectively). A simple fluid lacks these mesoscopic structures, and is formed by single molecules. Properties of simple fluids have been studied since long and the motion equation, the Navier-Stokes equation, is known since two centuries. Its most complicated consequence, turbulence, that is highly nonlinear, is from many points of view quite well understood nowadays (despite the lack of analytical solutions) [YO86].

On the other side, for nearly any complex fluid the governing equation is still unknown! This is due to the complex interplay between the macroscopic scale of the flow and the mesoscale structures, that does not allow for a simple continuum description.

3.1 Particles in suspension

As stated in the previous paragraph, complex fluids are materials composed by a fluid phase and some mesoscopic structures (i.e. structures at a scale intermediate between the molecular size and the macroscopic size of the system) dispersed in the fluid. In this section some kind of complex fluids are briefly described, the focus is on those that are related to vesicles and red blood cells.

Rigid spheres

One of the simplest complex fluids is a simple fluid suspending rigid spherical particles. The particles cannot deform, but can move in the fluid and interact with each other through hydrodynamical forces. Suspensions of rigid particles are found for example in paint, molten glass and smoke. The simplest way to model these systems is to assume that the particles are spherical. The flow properties of a dilute suspension of rigid spheres have first been studied by Einstein [Ein06, Ein11], who quantified the increase in the viscosity of the suspension due to the particles.

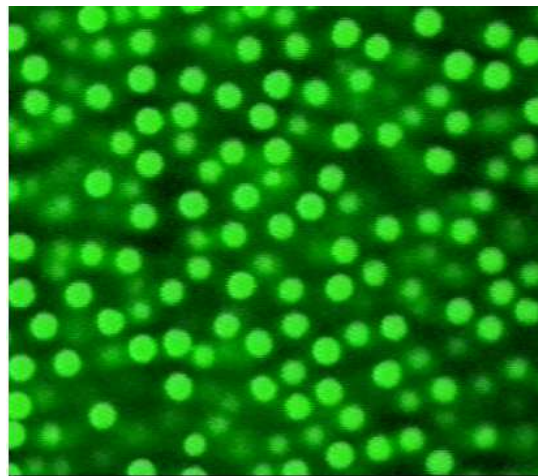


Figure 3.1: A suspension of rigid spheres ($\approx 2\mu\text{m}$ in diameter) used to model glasses [NEPW07].

Polymers

Polymer is a very generic word used to identify molecules that present themselves in the form of long chains. All plastics are composed by polymers,

DNA is a polymer too. The flow properties of a polymer melt are important for the production of synthetic materials (plastic, fabrics), so they have been widely studied during the last century, and they still are an active area of industrial research. In the last decades, the dynamics of DNA molecules in a fluid has received a lot of attention in relation to the increasing genetic studies in the medical sector [DZ79].

Due to the very large amount of materials that belong to this class, polymers can show very different conformations and confer the fluid different dynamical properties. For example, some polymers are very soft, have a rest shape that looks like a wool ball (*coil* state) that can be deformed (*stretched*) by the flow of the fluid in which they lay. Some others are stiff and do not deform under flow.

A suspension of polymers can have astonishing behaviors under flow that differ completely from the behavior of simple fluids. Examples are the *rod climbing* and the *die swell* effects, illustrated in figure 3.2. When a rod immersed in a polymeric fluid is rotated around its axis at high speed, the fluid is attracted towards the centre and ‘climbs’ the rod, while a Newtonian fluid would be projected towards the container walls. The same kind of fluid shows a huge increase in the section when coming out from a pipe, while a simple fluid would decrease (or slightly increase, depending on the velocity [BAH87]) its section, as water from a tap. These effects are both determined by positive *normal stress difference*, a quantity that will be introduced in the next section.

Drops

Drops are the simplest deformable particles that can be thought of in suspension in a fluid: a drop of another fluid. Drops (or bubbles) too have vast industrial applications, from the control of evaporation in nuclear reactors to production of alimentary emulsions such as mayonnaise. From a physical point of view, they are characterized by *surface tension*, a force that arises from negative interaction energy between the molecules of the fluid forming the drop. As a consequence, surface tension opposes (weakly) the increase in the surface area. Since this force drives the drops towards coalescence (i.e. the formation of bigger drops), sometimes the emulsions are stabilized with ‘surfactants’, substances that accumulate at the surfaces of the drops and create an energy barrier against coalescence (this is for example the role of the lecithin contained in the yolk in mayonnaise, which is an emulsion of oil and vinegar). A suspension of drops can behave very differently from a suspension of rigid particles: if the suspending fluid is sheared, the drops deform and can eventually burst (split in smaller drops). When they pass

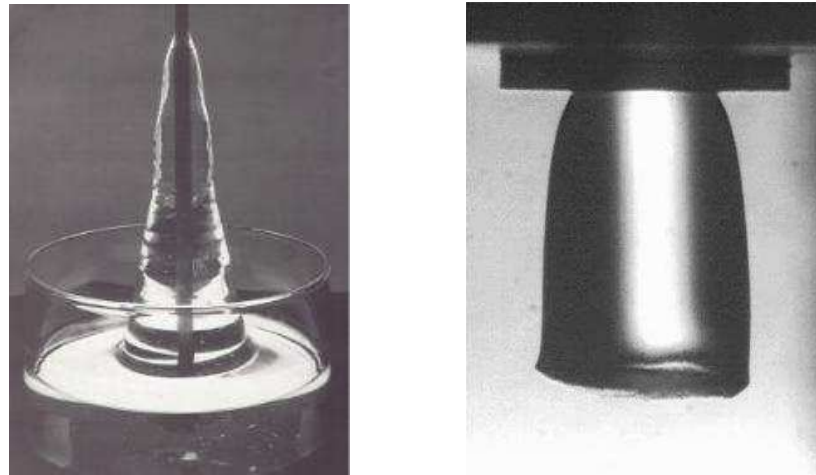


Figure 3.2: Examples of surprising flow behavior of a polymer melt. Left: *rod climbing* effect: when the rod immersed in the fluid is rotated around its axis at high speed, the polymer melt ‘climbs’ the rod. Right: *die swell*: the free surface of a polymer melt at the outlet of a pipe is divergent. Images extracted from <http://www.irc.leeds.ac.uk/mupp/flowSolve/> and <http://www.mie.utoronto.ca/labs/rheology/> respectively.

close one to another, they deform. All these behaviors influence the flow properties of the suspension.

Red blood cells

The blood flow has been at the centre of the attention of scientists since the 19th century (Poiseuille derived his famous equation for the flux of a Newtonian fluid in a pipe in 1838 with the aim of explaining blood circulation in capillaries). Blood is constituted by a simple fluid, the plasma, for around 55% of its volume. The remaining 45% is composed by red blood cells (RBCs), and white blood cells and platelets occupy together less than 1%. This is why the blood flow is mainly affected by plasma and red blood cells, and the other components can be neglected when attempting a mechanical modeling. Red blood cells have a biconcave shape whose diameter is around $8\mu\text{m}$ and are filled by a dense suspension of h emoglobin, a Newtonian fluid which is about seven times more viscous than water at physiological temperature, and responsible of oxygen delivery and carbon dioxide capture. The membrane of red blood cells is composed by a lipid bilayer (as all human cells), below which an elastic cytoskeleton is fixed, as sketched in figure 3.5. The membrane embeds different kinds of proteins, that perform

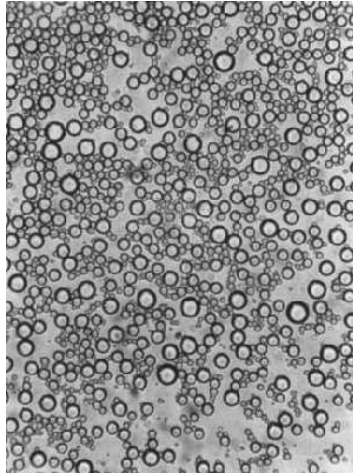


Figure 3.3: A suspension of oil drops in water stabilized with a surfactant to avoid coalescence [Pal00]).

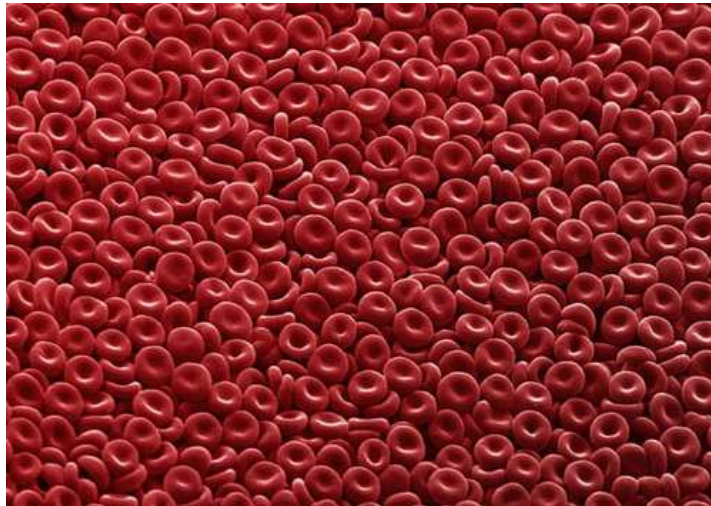


Figure 3.4: Red blood cells *in vitro*.

different tasks ranging from ion and molecule transport to intracellular signaling reception. The cytoskeleton, that has among others the function of preserving the cell integrity, is composed by filaments of a protein (spectrin) forming a two-dimensional network. The lipid bilayer is in the liquid state, resists strongly surface dilatation and opposes surface bending, while the cytoskeleton has elastic properties (it allows deformations but exerts a restoring force towards the original shape of the membrane). When red blood cells are formed in the bone marrow, they expel their nucleus, losing

3. COMPLEX FLUIDS

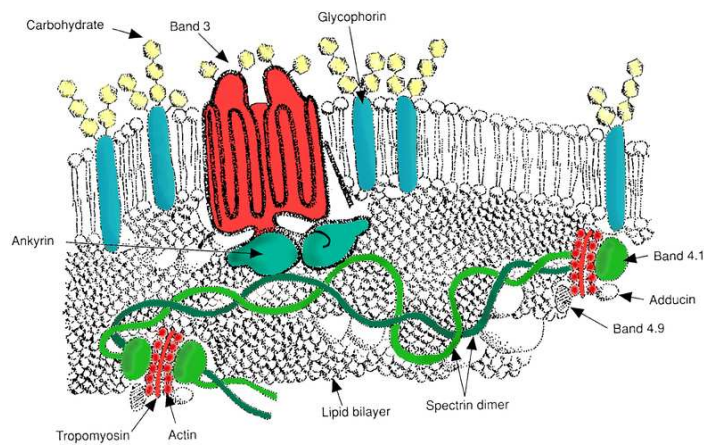


Figure 3.5: Sketch of the red blood cell membrane. The lipid bilayer is grayed, and the membrane proteins are in color, the green filaments are the actin network forming the cytoskeleton.

in this way a big part of their inner volume. This is why they are deflated in the typical biconcave shape. Red blood cells are highly deformable exactly because they don't have a nucleus. This characteristic allows the cells to pass through tiny capillaries that are even three-four times smaller than their rest diameter. A red blood cell under flow exhibits a highly nontrivial behavior: several dynamics are possible, depending on the details of the velocity field and the viscosity of the outer fluid, as it will be discussed at the end of chapter 4 [Bit86, AV08].

Capsules

Capsules are drops surrounded by elastic membranes, as rubber balloons filled with water. Their size can be comparable to blood cells, and are used in the medical sector for drug delivery or for cell therapy [LdGdSVG⁺07]. Capsules are also used to model red blood cells, since the elastic membrane mimics the cytoskeleton. The membrane resists in-plane shear (meaning that a restoring force is generated whenever a shear force is applied in the membrane plane) and weakly surface dilatation. In the models, often no resistance to bending is considered. Capsules can show several dynamical regimes, similar to red blood cells.

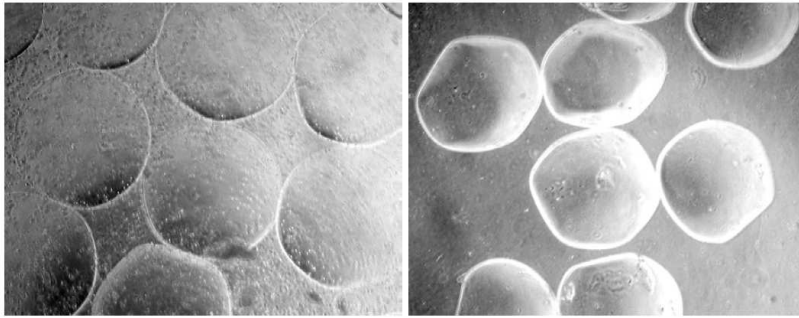


Figure 3.6: Polymeric microcapsules for medical use [LdGdSVG⁺07].

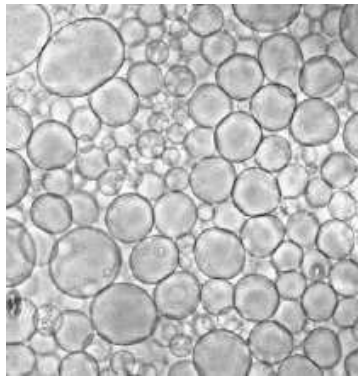


Figure 3.7: Giant Unilamellar vesicles produced by electroformation [ASM⁺92].

Vesicles

Vesicles are liquid drops surrounded by a phospholipidic bilayer. Vesicles of $\sim 1\mu\text{m}$ are used by living cells to transport nutrients and other substances. Artificial vesicles of $\sim 10\mu\text{m}$, named *giant unilamellar vesicles* (due to their size and to the single bilayer membrane that delimits them) are commonly used to model living cells, especially the ones, as red blood cells, that do not have a nucleus. The membrane has similar properties to the membrane of red blood cells, resisting strongly surface dilatation and opposing bending, but they don't have the elasticity arising from the cytoskeleton. Their properties are detailed in chapter 4.

3.2 The study of complex fluids: rheology

Simple incompressible fluids are characterized by two material parameters: their density ρ and their viscosity μ . The density affects the inertia of the motion, while the viscosity is at the origin of the *viscous force*, that conveys momentum between adjacent fluid elements having different velocities. Complex fluids can in general also display another kind of behavior: *elasticity*. The elastic behavior arises from the deformation of the mesoscopic structures contained in the fluid, that tend to relax to their equilibrium configuration. A typical example are polymer suspensions. Polymers can be thought to in this context, at least in a very crude approximation, as rubber bands stretched by the flow. When the intensity of the velocity gradient (called *shear rate*¹) varies, the stretched polymers change their length bringing with them the surrounding fluid. Elasticity may also arise from the interactions of non-deformable particles, as is the case of a suspension of rigid spheres, but in this case the microscopic picture is less trivial. So, in general a complex fluid can be defined *viscoelastic*.

Since the deformations of the mesoscopic structures depend on the intensity of the flow, the flow patterns depend on this microscopic parameter: *deformation*. Complex fluids show then a new kind of dependence on the intensity of the flow compared to simple fluids, that is not related to the appearance of turbulence at higher velocities. This dependence can cause a decrease (increase) of the viscosity of a complex fluid when the velocity gradient of the flow is increased: this behavior is known as *shear thinning* (*shear thickening*). Common examples of shear thinning fluids are paint (it is desirable for the paint on one side to be easy to be applied and on the other to stop flowing once spread), nail polish, ketchup. Shear thickening fluids are less common, but find anyway applications in different fields. An example is the coaxial self-locking car differential (when an axis starts to rotate much faster than the other, the shear thickening fluid placed among them stops the relative motion, while allowing for small velocity differences).

Complex fluids can also show *thixotropy*²: a viscosity decrease over time

¹The simplest flow that can be thought of is a uniform field of constant velocity, of the kind $\mathbf{u}(\mathbf{x}) = U\hat{\mathbf{e}}_x$, where U is a constant. This flow corresponds to a uniform translation of the system (the vesicle) in the x direction, and cannot deform it. So the minimal ingredient to influence the vesicle dynamics is *shear*, i.e. nonzero gradient of the velocity field. The simplest flow showing a nonzero gradient is a linear shear flow: $\mathbf{u}(\mathbf{x}) = \dot{\gamma}y\hat{\mathbf{e}}_x$. This velocity field has parallel flow lines and the pressure is constant everywhere, and will be used later in this section to introduce the flow properties of some fluids.

²From Greek: *thixis*, touch and *-tropy*, from *tropos*, changeable: ‘changeable with touch’.

at constant shear. Thixotropy is due to a structural change of the suspended phase, for instance the destruction (by the shear) of particle aggregates. A typical example is blood, in which red blood cells form aggregates (called *rouleaux*) when left at rest, which are destroyed if the blood is put under flow. Also some clays are thixotropic, and in case of an earthquake or other ground movements they can lead to apparent ‘soil liquefaction’.

The study of the flow properties is called *rheology* (from the Greek *rheo*, ‘stream’, and *-logos*, ‘one who deals with’). Typical analysis methods are measurements of the viscosity and of the elastic properties. The viscosity can be obtained via the simultaneous measurement of the force necessary to shear a sample of fluid and the shear rate itself. Elastic properties are typically retrieved via the phase difference between an oscillating driving force and the oscillating velocity of the sample.

Rheology as determination of the stress tensor

From a more formal point of view, rheology is the study of the components of the stress tensor describing a material. In fact, the stress tensor represents the response of the system to external forces, and contains thus all the information for the description of the motion.

The stress tensor $\boldsymbol{\sigma}$ is defined as the force density \mathbf{f} acting on a surface, defined by its normal \mathbf{n} , of a small material element:

$$\sigma_{ij} \equiv f_i n_j \quad (3.1)$$

The rheological quantities are functions of the components, or of combinations of components, of the stress tensor. A more precise definition of some rheological quantities is needed in order to set this link. In the following we focus on a system consisting of a fluid (either Newtonian or complex) between two parallel and infinite plates, separated by a distance L , one of which moves tangentially with respect to the other with a velocity U , as sketched in figure 3.8. The force surface density needed to maintain the motion of the plate is F . The definition of the rheological measures will be done using the macroscopic quantities (L, U, F) .

For a Newtonian fluid they can be equivalently defined for an infinitesimally small fluid element, using the microscopic counterparts of this triad (its size, the velocities of its surfaces and the forces applied to the surfaces themselves). The two definitions are equivalent due to the *homogeneity* of the fluid.

For a complex fluid instead, this scale invariance is lost due to the presence of structures at the mesoscale, that sets also a lower limit (through their

3. COMPLEX FLUIDS

size L_s) for a microscopic definition.

The conventional choice is then to define the rheological quantities in the macroscopic limit $L \gg L_s$ in which these quantities do not depend any more on the precise choice of L .

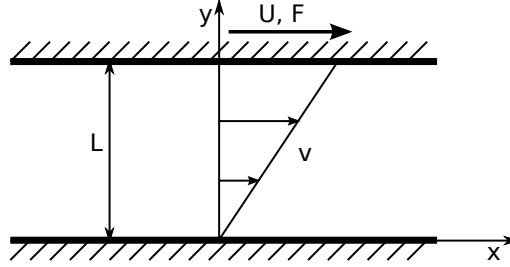


Figure 3.8: Schematic of the system used to define the rheological quantities.

Effective viscosity. The viscosity (denoted η) refers to the relation between shear forces and velocity gradient for a Newtonian fluid. Although its value is uniform in most situations³, it is a microscopic quantity defined everywhere in the fluid. Taken a fluid element and oriented the y axis in the direction of the shear, the shear forces are represented by σ_{xy} and the velocity gradient is $\partial_y v_x$. The viscosity is defined as $\eta = \sigma_{xy} / \partial_y v_x$. In the considered macroscopic setup, this definition is equivalent to

$$\eta = \frac{F}{U/L} \quad (\text{for a Newtonian fluid}) \quad (3.2)$$

that is the volume average of the microscopic (uniform) quantity.

We define then the *effective viscosity* as:

$$\eta_{eff} = \frac{F}{U/L} \quad (\text{for any fluid}) \quad (3.3)$$

Obviously for a Newtonian fluid $\eta_{eff} = \eta$, but the fact that the details of the flow are disregarded allows for the application of this definition to any material that can flow between the two considered plates (i.e. to all complex fluids). The effective viscosity represents the link between *stress* and *strain*, or equivalently force (F) and deformation (U/L , the velocity gradient). Since in our system the force is along the x axis and acts on a

³Spatial variations of the viscosity can be generated for instance by a temperature gradient.

surface normal to y , F represents the volume average of the xy component of the stress tensor, $F = \langle \sigma_{xy} \rangle$, so

$$\eta_{eff} = \frac{\langle \sigma_{xy} \rangle}{\dot{\gamma}} \quad (3.4)$$

$\dot{\gamma}$ being the velocity gradient, i.e. the shear rate.

Normal stress differences. A fluid element can be subject to three independent normal stresses, one along each axis direction (x , y or z): these are the components σ_{xx} , σ_{yy} and σ_{zz} . So these three quantities represent how much a fluid element is compressed (or stretched) in a certain direction. The vast majority of liquids are *incompressible* (and also gases are well described by this assumption in many situations), meaning that they can deform but their volume cannot change. This implies that a fluid element does not deform when subject to an isotropic pressure ($\sigma_{xx} = \sigma_{yy} = \sigma_{zz}$). In other words, the diagonal components of the stress tensor are defined modulo a constant, that is the same for all the three. So the relevant quantities to be measured are not the diagonal components alone, but their differences. It is conventional to define *first normal stress difference* $N_1 \equiv \sigma_{xx} - \sigma_{yy}$ and *second normal stress difference* $N_2 \equiv \sigma_{yy} - \sigma_{zz}$. Obviously in dimension two only a normal stress difference exists, and will be denoted in the rest of this work by N . For a Newtonian fluid, the volume average on the whole system of N_1 and N_2 are zero⁴, while for the majority of complex fluids $\langle N_1 \rangle > 0$ and $\langle N_2 \rangle \lesssim 0$ ⁵. The study of a very simple system (a rigid rod in a linear shear flow) is enlightening to understand the origin of normal stress differences in a complex fluid and in general of all the components of the stress tensor. This is proposed in Appendix B.

Other stress components. The stress tensor of a Newtonian fluid is symmetric: $\sigma_{ij} = \sigma_{ji}$. The symmetry of $\boldsymbol{\sigma}$ can be shown to hold also for a mixture of Newtonian fluids containing surfaces of discontinuity of the stress tensor (the proof only requires the conservation of linear and angular momenta). This case includes all suspensions of liquid particles, in particular vesicles and red blood cells, and is then sufficient for our problem.

As a consequence of the symmetry of the stress tensor, the knowledge of the effective viscosity ($\sim \sigma_{xy}$) and of the normal stress difference ($\sim \sigma_{xx} - \sigma_{yy}$) is enough to determine the full tensor in dimension two.

⁴It is indeed possible to find situations in which $\langle N_1 \rangle \neq 0$ or $\langle N_2 \rangle \neq 0$ for a Newtonian fluid, as a divergent channel whose walls move at different velocities.

⁵The symbols $\langle \rangle$ denote a volume average.

In chapter 6 these two rheological quantities will be examined in detail, quantifying the behavior of all the relevant stress components and their link to the parameters governing the microscopic dynamics of a vesicle.

For most materials the stress tensor is symmetric⁶. More generally, an antisymmetric component can be induced in the stress tensor through an external field generating couples on the suspended particles (as for particles with a nonzero electric dipole in an electric field) [Bat70]. The link between the antisymmetry of σ and the torque done on the particles is detailed in Appendix A.

⁶Some examples of non-symmetric stress tensor exist, for instance the one derived for a diffuse interface model for vesicle suspensions [JM08b].

THE MODEL FOR VESICLES

The model used for vesicles, dating back to Canham (1970) and Helfrich (1973), is described. The coupling of the membrane with the surrounding fluid is presented and a basic description of the dynamics of a vesicle in a linear shear flow is given.

Le modèle utilisé pour les vésicules, dû à Canham(1970) et Helfrich (1973) est décrit. Le couplage de la membrane avec le fluide environnant est présenté et une description simple de la dynamique d'une vésicule dans un cisaillement linéaire est donnée.

4.1 Vesicles as a minimal energy configuration

Vesicles, also called *liposomes*, are closed phospholipidic bilayers. The bilayer is the main component of the membrane of living cells, and is formed by two layers of phospholipids, long organic molecules that have two long fatty acid chains and a polar group at an end. Since the fatty chains are not polar while the phosphate group is polar, when phospholipids are in a water solution (which is polar) they organize spontaneously in structures where the lipid chains are not in contact with water (figure 4.1). In fact, this kind of configuration minimizes the surface energy that arises from the interaction between polar and non-polar molecules.

The structures that are formed faster, due to the low number of molecules needed, are *micelles*, which are closed lipid monolayers with no water molecules in the inside. Micelles do not constitute a deep minimum in the energy landscape of the system, since phospholipids occupy a roughly cylindrical volume, while in a micelle a conical shape would be needed to prevent water molecules from penetrating and getting in contact with the fatty acids.

On the other side, the formation of plane bilayer patches is energetically disfavoured due to the free edges exposed to water.

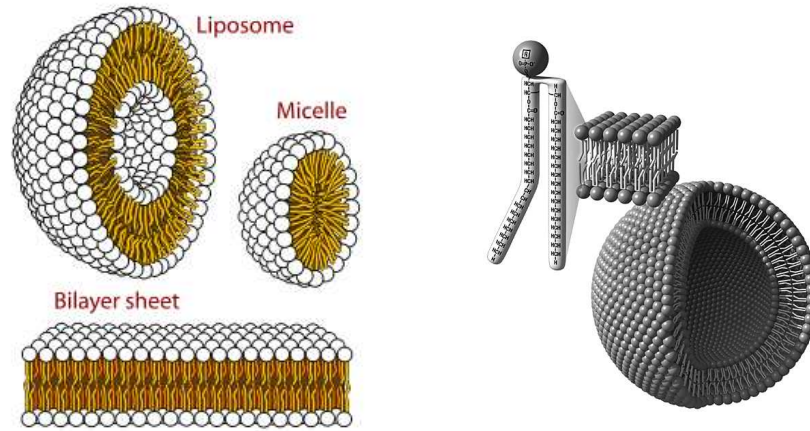


Figure 4.1: Left: three different possibilities of minimization of surface energy of an aqueous solution of phospholipids: liposomes (or vesicles), micelles, and plane bilayer patch. Right: schematic of the structure of a vesicle.

In this sense, the constitution of closed double layers surrounding a water domain (vesicles) is a deeper minimum in the energy of the system. This is why vesicles form spontaneously in a water solution and are stable. Topological changes (division, fusion or pore formation) are possible but rare, since related to processes that are energetically disadvantaged. For this reason in this work they are disregarded.

The physical properties of the membrane can be deduced from the basic chemistry of the phospholipids: (i) since the phospholipidic molecules do not bind with each other, the membrane is *fluid*¹: every molecule is free to move on the surface; (ii) due to the high interaction energy between the fatty chains and the water molecules on one side, and to van der Waals repulsion between neighbors on the other, the phospholipids stay close to each other at an approximately constant density: the membrane is then *inextensible*; (iii) since the bilayer has a finite thickness and the displacement of phospholipids from a monolayer to the other is rare, bending the monolayer has an energy cost (this can be traced back to the inextensibility of the two monolayers on a closed surface): so the membrane has a nonzero bending energy.

The fluid contained inside the vesicle is an aqueous solution (this is required for the stability of the membrane, as discussed in the previous

¹ More precisely, the membrane can also be in a solid (gel) phase, below a critical temperature. The biological conditions to which we refer (human red cells in blood flow) correspond to a fluid membrane, and this is also the usual phase in experiments on the dynamics of vesicles.

paragraph), that is incompressible. Moreover, the membrane is semipermeable to water molecules, but not to bigger ones, as sugars: as a consequence of these two facts, osmotic pressure ensures the conservation of the inner volume.

The bilayer is about $4nm$ thick, while the linear dimension of a vesicle is much larger. We are typically interested in *giant unilamellar vesicles*, whose linear dimension is of the order of $10 \div 100\mu m$, comparable to living cells. This big separation in length scales (4 orders of magnitude) will allow us to approximate the membrane as a two-dimensional surface.

We can then summarize the properties of a vesicle as follows:

- it has a constant volume due to the incompressibility of the enclosed fluid and to osmotic pressure;
- the membrane is inextensible, due to the uniform density of phospholipids;
- the membrane possesses a bending energy, due to its finite thickness.
- the normal component of the velocity of the membrane is equal to that of the adjacent fluid (i.e. the membrane is impermeable), due to the osmotic pressure.

4.2 The model for the curvature

Now that we have described the vesicle as an object with precise physical properties, we can formalize it in a mathematical model. We model then the vesicle as an infinitely thin closed membrane separating two fluids. The membrane is: inextensible (that is, the *local* surface of the vesicle is conserved), endowed with bending energy and impermeable.

In order to characterize the curvature of a surface in three dimensions, we need to introduce the notion of *principal curvatures*. Given a surface embedded in three dimensions, at every point we can define a vector normal to the surface. Every plane containing this vector cuts the surface in a (plane) curve. Rotating the cutting plane around the direction of the normal, different curvatures of the plane curve are obtained. The principal curvatures, denoted (c_1, c_2) , are defined as the minimal and maximal values assumed by this curvature while varying the cutting plane (see figure 4.2). The curvature itself is defined as the inverse of the radius of the osculating circle, that is the circle that fits the best to the curve in the neighborhood of the considered point. In general, a surface embedded in dimension D

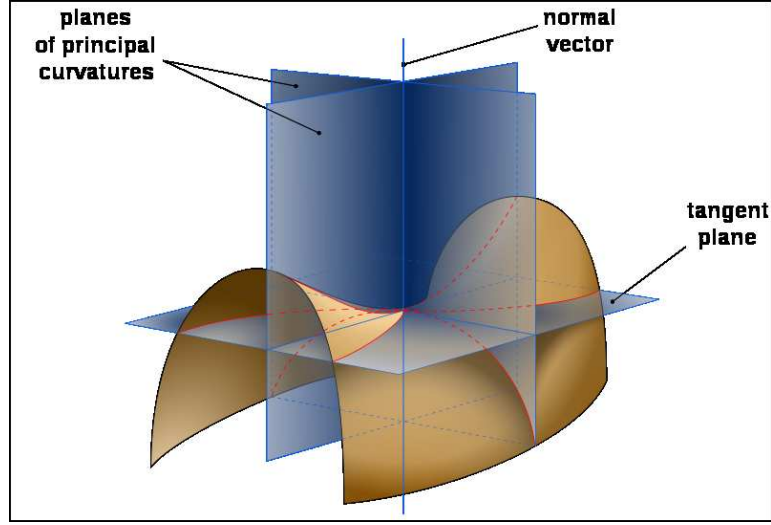


Figure 4.2: Planes defining the principal curvatures of a surface embedded in three dimensions.

has dimension $D - 1$ and the same number of principal curvatures c_i , in particular we have only one if we are in dimension two.

One of the simplest mathematical formulations that takes into account the bending energy of a surface is to assume that bending costs locally an energy [Can70, Hel73]

$$e = \frac{\kappa}{2}c^2 + \kappa_G k \quad (4.1)$$

where

$$c = \sum_{i=1}^{D-1} c_i \quad k = \prod_{i=1}^{D-1} c_i \quad (4.2)$$

are respectively the mean and Gauss curvatures and κ and κ_G the bending moduli corresponding to the two curvatures. Note that in general equation (4.1) should be expressed in the form $e = \frac{\kappa}{2}(c - c_0)^2 + \kappa_G k$, where c_0 is the spontaneous curvature of the membrane. We consider only symmetric bilayers and c_0 is disregarded². This energy density has to be integrated over the whole membrane to obtain the total energy $E = \oint_{\gamma} e ds$, where γ denotes the position of the membrane.

²In two dimensions the spontaneous curvature c_0 plays no role, since its contribution to the energy is a constant. This can be easily seen with a short computation: $\oint_{\gamma} (c - c_0)^2 ds = \oint_{\gamma} c^2 ds + c_0^2 \oint_{\gamma} ds + c_0 \oint_{\gamma} c ds$. The second term is explicitly a constant, and the third can be rewritten using the definition of the curvature (available only in two dimensions) $c \equiv d\theta/ds$, with θ the orientation of the curve, giving $c_0 \oint_{\gamma} d\theta$ which is a constant too.

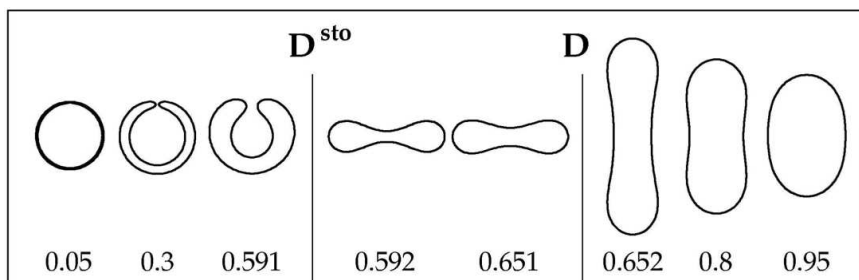


Figure 4.3: Equilibrium shapes in the absence of flow for three-dimensional vesicles (the axis of rotational symmetry is vertical) as a function of the reduced volume [SBL91]. From left to right: stomatocytes, oblates, prolates.

As stated in the previous section, we are not interested in topological changes. The Gauss-Bonnet theorem states that the integral over a closed surface of the Gauss curvature k only depends on the topology of the surface, i.e. it is constant at fixed topology: we can then neglect this term. For a phospholipidic membrane, $\kappa \approx 10^{-19}J$ [DKS90, LLW01].

Equilibrium shapes: importance of the reduced volume

This minimal model allows to compute the equilibrium shapes of the vesicles in the absence of flow. We define a parameter, the *reduced volume* ν , that takes into account the ratio between the surface and the volume of a vesicle. This quantity is a constant of the motion due to the incompressibility of the internal fluid and to the inextensibility of the surface. ν is defined as the ratio between the volume V of the vesicle and the volume of a sphere of same surface A :

$$\nu = \frac{V}{\frac{4}{3}\pi \left(\frac{A}{4\pi}\right)^{\frac{3}{2}}} \quad (4.3)$$

As a consequence, ν can range from 0 (totally deflated vesicle) to 1 (sphere).

The minimization of the total bending energy E (respecting the constraints of constant enclosed volume and constant area) yields the equilibrium shapes. It turns out that for this simple curvature model all the shapes are axisymmetric, and can then be conveniently represented via their section as a function of the reduced volume. This is reported in figure 4.3. In this figure we see that there are three different families of shapes: if we consider a sphere ($\nu = 1$) and deflate it progressively, we first find *prolate* shapes, which are elongated around the rotation axis, which is vertical in the figure (cigar-like shapes). If we swell below $\nu \approx 0.65$, the minimal equi-

librium shape is *oblate*, or discocyte. This kind of shape is the biconcave one assumed by red blood cells. Below $\nu \approx 0.59$ there is a transition towards *stomatocyte*, the vesicle folds on itself and forms a pocket.

In two dimensions a parameter equivalent to the reduced volume is defined: it is the *reduced area* α , which is the surface area A of the vesicle divided by the area of a circle having the same perimeter p :

$$\alpha = \frac{A}{\pi [p/2\pi]^2} \quad (4.4)$$

It must be specified that in two dimensions there is no difference between prolates and oblates, and stomatocytes do not constitute a configuration of minimal energy.

Moreover, minimizing the curvature to obtain the equilibrium shapes corresponds to neglecting Brownian motion for the membrane. This assumption is justified by the dimensions of the vesicles, which are much larger than the amplitude of Brownian fluctuations³ [Sei04].

4.3 Hydrodynamical model

The membrane force

Hitherto we have considered vesicles at rest. Under flow, we observe a large number of nontrivial behaviors, a part of which is the subject of this work.

In order to study the dynamics of a suspension of vesicles we have to introduce the hydrodynamic equations and determine the membrane force from the membrane bending energy (4.1) and the physical constraints.

Let us start from the latter. The membrane is inextensible, i.e. a surface element cannot be dilated or compressed. In the previous paragraph only the conservation of a single parameter, the reduced volume ν , has been imposed: this corresponds to the conservation of the total surface area and is a sufficient condition when the vesicle is at rest (as for an incompressible fluid at rest is sufficient to impose the conservation of the total volume to guarantee its incompressibility). But if the vesicle moves and deforms under the action of the velocity field of the surrounding fluid, we have to take care of the conservation of the *local* surface area. This can be fulfilled through the introduction of a Lagrange multiplier field ζ defined on the surface. This field can be seen as a tension that adjusts locally to preserve

³For a vesicle with a diameter $\sim 10\mu m$, membrane fluctuations can be estimated to be smaller than $1\mu m$.

the local surface area⁴. The membrane energy is then the sum of bending and inextensibility contributions and thus becomes:

$$E = \frac{\kappa}{2} \oint_{\gamma} c^2 ds + \oint_{\gamma} \zeta ds \quad (4.5)$$

The force corresponding to this energy, and representing the force necessary to bend the membrane respecting the inextensibility constraint, is obtained through the functional derivative of E :

$$\mathbf{f}_{mem} = -\frac{1}{\sqrt{g}} \frac{\delta E}{\delta \mathbf{r}} \quad (4.6)$$

where $\delta \mathbf{r}$ is a small displacement of a given point of the membrane and g is the determinant of the metric tensor defining the parametrization used to describe the vesicle surface [Sei99]. The precise form of this force depends on the dimension of the physical space. In three dimensions, it reads [Sei99]:

$$\mathbf{f}_{mem} = \kappa \left[\Delta_s c + c \left(\frac{1}{2} c^2 - 2k \right) \right] \mathbf{n} + \zeta c \mathbf{n} + \nabla_s \zeta \quad \text{in 3D} \quad (4.7)$$

where \mathbf{n} is the unitary outward normal vector and Δ_s is the Laplace-Beltrami operator (i.e. the projection of the Laplacian on the surface). In dimension two this expression becomes [BM02]:

$$\mathbf{f}_{mem} = \kappa \left(\frac{\partial^2 c}{\partial s^2} + \frac{1}{2} c^3 \right) \mathbf{n} + \zeta c \mathbf{n} + \frac{\partial \zeta}{\partial s} \mathbf{t} \quad \text{in 2D} \quad (4.8)$$

where s is the curvilinear coordinate on the membrane and \mathbf{t} is the unitary tangent vector in the direction of increasing s .

The equation for the fluids

In the previous paragraph the expression of the membrane force has been determined. Now the evolution equation for the fluids in the interior and in the exterior of the vesicle has to be considered and coupled with this force and with the various boundary conditions (at the membrane and at the external boundary, if any). From basic fluid mechanics, we know that the equation for the conservation of the momentum can be written as (Cauchy equation):

$$\rho \frac{D\mathbf{u}}{Dt} = \nabla \cdot \boldsymbol{\sigma} \quad (4.9)$$

⁴ The tension field is the equivalent of the pressure, that adjusts locally to preserve the local volume in the bulk.

where ρ is the density of the fluid, \mathbf{u} is the velocity and $\boldsymbol{\sigma}$ the stress tensor, defined in equation (3.1) and representing the forces exerted on the surface of a fluid element by its surroundings. $D/Dt \equiv d/dt + \mathbf{u} \cdot \nabla$ represents the total derivative, i.e. the time derivative computed with respect to a reference that moves with the fluid element. In equation (4.9) the term $\rho D\mathbf{u}/Dt$ represents the inertia of the fluid.

The equation of conservation of mass reads

$$\frac{d\rho}{dt} + \nabla \cdot (\rho\mathbf{u}) = 0 \quad (4.10)$$

and reduces to

$$\nabla \cdot \mathbf{u} = 0 \quad (4.11)$$

if the density is constant in time and uniform in space, as it is generally the case for fluids, provided that the velocity is small compared to the sound speed, a well verified condition in practice.

If the fluid is Newtonian⁵, the expression for the stress tensor is

$$\sigma_{ij} = -p\delta_{ij} + \eta (\partial_i u_j + \partial_j u_i) \quad (4.12)$$

η is the viscosity and p the pressure. As stated at the beginning of the chapter, vesicles are stable in a water solution, so we are mostly interested in studying their behavior in a Newtonian fluid. If we combine (4.9), (4.11) and (4.12), we obtain the Navier-Stokes equation:

$$\rho \frac{D\mathbf{u}}{Dt} = -\nabla p + \eta \nabla^2 \mathbf{u} \quad (4.13)$$

that describes the motion of a Newtonian and incompressible fluid.

Coupling the fluid equation to the membrane force

After obtaining the evolution equation for the fluid and the expression for the membrane force, their coupling is needed in order to determine the evolution equation of the system.

The equation for the fluid applies to the domain occupied by the fluid outside the vesicle and to the domain occupied by the fluid inside. These two fluids can have different material properties, in particular they can have different viscosities.

⁵Newtonian fluids are defined through equation (4.12). They are usually the molecular fluids, that do not present structures at a scale between the molecular one and the macroscopic one. Water is the best example of a Newtonian fluid, but also air, ethanol, honey, glycerol.

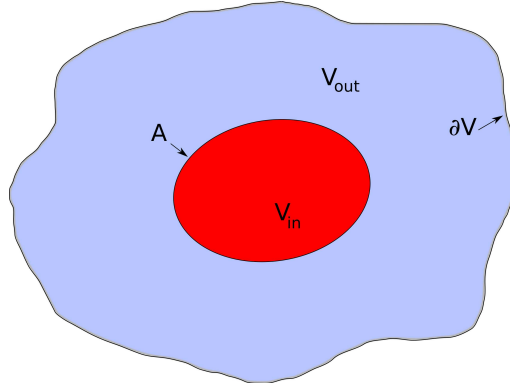


Figure 4.4: The fluid domains and the boundaries of a fluid containing a vesicle.

The membrane force is located at the boundary between these two fluids, then it plays the role of a boundary condition for the stress of the two fluids.

The conservation of mass coupled to the impermeability of the membrane implies that the normal component of the velocity of the two fluids in vicinity of the membrane is equal to the normal velocity of the membrane itself. Moreover, we assume that both fluids adhere to the membrane (this is called assumption of *no-slip* boundary conditions), so that the tangential velocity field is equal to the tangential velocity of the membrane itself. These two conditions guarantee the continuity of the velocity field across the membrane.

It is then possible to write the evolution equation for the system starting from (4.13) and adding the membrane force as follows:

$$\rho(\mathbf{x}) \frac{D\mathbf{u}}{Dt} = -\nabla p(\mathbf{x}) + \eta(\mathbf{x}) \nabla^2 \mathbf{u}(\mathbf{x}) + \mathbf{f}_{mem}(\mathbf{x}) \delta(\mathbf{x} - \mathbf{x}_{mem}) \quad (4.14)$$

where \mathbf{x} is the position vector, $\rho(\mathbf{x})$ and $\eta(\mathbf{x})$ are the material properties of the inner and outer fluids ($\rho(\mathbf{x}) = \rho_{in}$ in V_{in} and so on, see figure 4.4 for the domain labels) and $\delta(\mathbf{x} - \mathbf{x}_{mem})$ is a Dirac Delta function that identifies the position \mathbf{x}_{mem} of the membrane and \mathbf{f}_{mem} is given by equation (4.8).

The dimensionless numbers of the problem

It is useful to write equation (4.14) in a nondimensional form. To do so, the physical quantities are divided by some reference values of relevance in

the problem. We introduce nondimensional quantities as follows:

$$\hat{\mathbf{u}} = \frac{\mathbf{u}}{U} \quad (4.15)$$

$$\hat{\mathbf{x}} = \frac{\mathbf{x}}{R_0} \quad (4.16)$$

$$\hat{t} = \frac{tU}{R_0} = t\dot{\gamma} \quad (4.17)$$

$$\hat{p} = \frac{p - p^\infty}{\eta_{out}U/R_0} = \frac{p - p^\infty}{\eta_{out}\dot{\gamma}} \quad (4.18)$$

$$\hat{\zeta} = \kappa R_0^2 \zeta \quad (4.19)$$

$$\hat{c} = cR_0 \quad (4.20)$$

$$\hat{s} = s/R_0 \quad (4.21)$$

$$\hat{\mathbf{f}} = \frac{R_0^2}{\kappa} \mathbf{f} \quad (4.22)$$

$$\hat{\delta} = \delta R_0 \quad (4.23)$$

where U is a typical velocity (i.e. the velocity of the vesicle), R_0 a typical length (i.e. the radius of the vesicle) p^∞ a reference value for pressure⁶ and $\dot{\gamma} \equiv U/R_0$ is the shear rate, representing the typical velocity gradient in the system⁷. If we substitute these quantities in the equation of motion (4.14), we obtain the dimensionless form:

$$Re \frac{D\hat{\mathbf{u}}}{D\hat{t}} = -\hat{\nabla} \hat{p}(\hat{\mathbf{x}}) + \frac{\eta(\hat{\mathbf{x}})}{\eta_{out}} \hat{\nabla}^2 \hat{\mathbf{u}}(\hat{\mathbf{x}}) + C_a^{-1} \hat{\mathbf{f}}_{mem} \hat{\delta}(\hat{\mathbf{x}} - \hat{\mathbf{x}}_{mem}) \quad (4.24)$$

where the following dimensionless numbers appear:

- the *Reynolds number* Re that represents the relative importance of inertial and viscous effects

$$Re = \frac{\rho U R_0}{\eta_{out}} \quad (4.25)$$

⁶The pressure is a Lagrange multiplier that enforces the incompressibility of the fluid. As a consequence, it doesn't have an intrinsic physical scale, on the contrary it acts on the same scale of the other forces of the problem in order to ensure the fluid incompressibility. This is why it has been made nondimensional using the other force of relevance in the problem, i.e. the viscous force.

⁷ The tension term in the membrane force depends on a Lagrange multiplier: ζ . As stated above for the pressure term, the terms associated to the respect of a constraint are made nondimensional via the other scales in the problem: here we have used the bending force.

- the *viscosity contrast* λ , defined as the ratio between the viscosity of the fluid contained in the vesicle and the viscosity of the outer fluid:

$$\lambda = \frac{\eta_{in}}{\eta_{out}} \quad (4.26)$$

This number arises from the viscosity term: in the outer fluid the value of $\eta(\mathbf{x})/\eta_{out}$ is unity, while inside the vesicle it is λ .

- the *capillary number* C_a , defined as the ratio between the time scale of relaxation of the curvature $\tau_c = \eta_0 R_0^3 / \kappa$ and the time scale of the flow $\tau_f = \dot{\gamma}^{-1}$, giving:

$$C_a = \frac{\tau_c}{\tau_f} = \frac{\eta_{out} \dot{\gamma} R_0^3}{\kappa} \quad (4.27)$$

At the beginning of this chapter a dimensionless number has already been introduced:

- the *reduced volume* (equation 4.3) that compares the volume and the surface of the vesicle, or its two-dimensional equivalent, the *reduced area* (equation 4.4).

The value of the Reynolds number for a flow around a vesicle can be estimated via the material and geometrical parameters. For water they are: $\rho = 10^3 \text{ Kg/m}^3$, $\eta_{out} = 10^{-3} \text{ Pa} \cdot \text{s}$; the typical size of a vesicle is 10^{-5} m and a typical velocity in the available experimental data $10^{-4} \div 10^{-3} \text{ m/s}$, so $Re \approx 10^{-3} \div 10^{-2}$. It follows that the inertial term can safely be disregarded: we will consider in the following that $Re = 0$. We are left with three dimensionless parameters (ν, C_a, λ) that completely determine the dynamics of a vesicle in a linear shear flow⁸. The variation of these parameters generates a rich dynamics and triggers dynamical transitions. This will be the subject of chapter 6, dedicated to the dynamics and rheology of a single vesicle in a linear shear flow. A short summary is presented in the next section.

With the assumption of vanishing Reynolds number, the equation of motion (4.14) for a suspension of vesicles becomes:

$$\boxed{-\nabla p(\mathbf{x}) + \eta(\mathbf{x}) \nabla^2 \mathbf{u}(\mathbf{x}) + \mathbf{f}_{mem}(\mathbf{x}) \delta(\mathbf{x} - \mathbf{x}_{mem}) = 0} \quad (4.28)$$

This equation expresses the *force balance*: the inertial term being negligible, the forces acting on a fluid element sum up to zero.

⁸The limitation of this statement to a linear shear flow is due to the fact that only the velocity gradient $\dot{\gamma}$ enters this set of dimensionless numbers.

The equation above can be restated together with the boundary conditions as follows:

$$-\nabla p + \eta_{in} \nabla^2 \mathbf{u} = 0 \quad \text{in } V_{in} \quad (4.29)$$

$$-\nabla p + \eta_{out} \nabla^2 \mathbf{u} = 0 \quad \text{in } V_{out} \quad (4.30)$$

$$(\boldsymbol{\sigma}_{out} - \boldsymbol{\sigma}_{in}) \cdot \mathbf{n} = \mathbf{f}_{mem} \quad \text{on } A \quad (4.31)$$

$$\mathbf{u} = \mathbf{U}^\infty \quad \text{on } \partial V \quad (4.32)$$

$$\nabla \cdot \mathbf{u} = 0 \quad \text{in } V \quad (4.33)$$

where \mathbf{U}^∞ is an imposed flow on the outer boundary of the system and the subscripts *in* and *out* refer to the inner and outer fluids respectively (see figure 4.4). Depending on the method used to solve the evolution equations, the membrane force term can be kept as a boundary condition or be reformulated as a volume force localized around the membrane.

4.4 Basic dynamics in linear shear

A vesicle immersed in a linear shear flow can show several dynamics depending on the values of the three dimensionless numbers introduced in the previous section (ν, C_a, λ) [KS82, KWSL96, BRS⁺04, KS05, LTV08, KFM09]. The parameter to which the dynamics is more sensitive is the viscosity contrast λ : in fact, if λ is below a critical value λ_c (that depends itself on ν and C_a), the vesicle shape and orientation do not change with time, but the membrane moves around it at constant speed, as the tread of a tank: it is the *tank-treading* motion, first observed on red blood cells in 1978 [FSLSS78] (figure 4.6 A and B). In this motion, the internal fluid is advected by the membrane and is thus sheared. Upon increase of λ (but below λ_c), the inclination angle decreases and approaches zero for $\lambda \rightarrow \lambda_c$. If $\lambda > \lambda_c$ the resulting motion is a quasi-rigid *tumbling*, as a rigid body would do in shear flow (figure 4.6 C and D). In tumbling, the vesicle is weakly deformed and the interior weakly sheared. The value of λ_c is an increasing function of the reduced volume, corresponding to the fact that it is easier to cause tumbling of an elongated vesicle compared to a more rounded one.

This dynamical transition can be interpreted by looking in more detail to the structure of the imposed linear shear flow: it is, in fact, a linear superposition of a rigid rotation and an elongational field along the $\pm\pi/4$ directions, as sketched in figure 4.5. From a tensorial point of view, this can be seen as the decomposition of the tensor of the velocity gradients $\partial_i v_j$ in

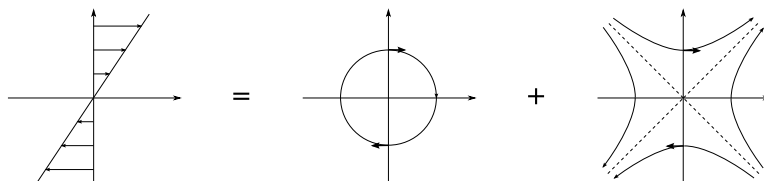


Figure 4.5: Decomposition of the linear shear flow in pure rotation and pure elongation.

its symmetric and antisymmetric parts:

$$\begin{pmatrix} 0 & \dot{\gamma} & 0 \\ 0 & 0 & 0 \\ 0 & 0 & 0 \end{pmatrix} = \left[\begin{pmatrix} 0 & \frac{\dot{\gamma}}{2} & 0 \\ \frac{\dot{\gamma}}{2} & 0 & 0 \\ 0 & 0 & 0 \end{pmatrix} + \begin{pmatrix} 0 & \frac{\dot{\gamma}}{2} & 0 \\ -\frac{\dot{\gamma}}{2} & 0 & 0 \\ 0 & 0 & 0 \end{pmatrix} \right] \quad (4.34)$$

The symmetric part represents the pure elongational flow, while the antisymmetric part represents the pure rotation. The dynamical transition is then a direct consequence of the two components of the shear flow: when the vesicle is soft enough to be sheared ($\lambda < \lambda_c$), the elongational component ‘attracts’ the vesicle towards its elongation direction and the torque applied by the rotational component of the flow can be transmitted to the vesicle through internal shear (tank-treading). On the other side, if $\lambda > \lambda_c$, the vesicle is too stiff to be sheared by the applied flow, then the torque is transmitted to the vesicle in the form of a quasi-rigid rotation (tumbling). In this case, the action of the elongational component is a modulation of the angular velocity of the vesicle, which is higher when its motion is in the same direction of the elongational flow lines and lower when it is in the opposite direction.

The tank-treading to tumbling transition is associated with a critical point, and as a consequence the dynamics is arbitrarily slowed down for $\lambda \rightarrow \lambda_c$.

In two dimensions this is the complete picture of the possible dynamics for the vesicle, as it will be extensively discussed in chapter 6 [BM03, BRS⁺04, NG04, KS05, MVA⁺06]. In three dimensions, the higher number of degrees of freedom allows for more dynamical regimes. In particular, above a critical value of the capillary number C_a , a third regime is present between tank treading and tumbling: close to the transition on the tumbling side, the vesicle dynamics is slow enough to allow relaxation of the shape in the third dimension, making the main section of the vesicle in the shear plane more rounded and then more prone to tank-treading. At this moment tank-treading starts to take place, the vesicle orients more in the direction of the elongational component of the shear, it is then stretched

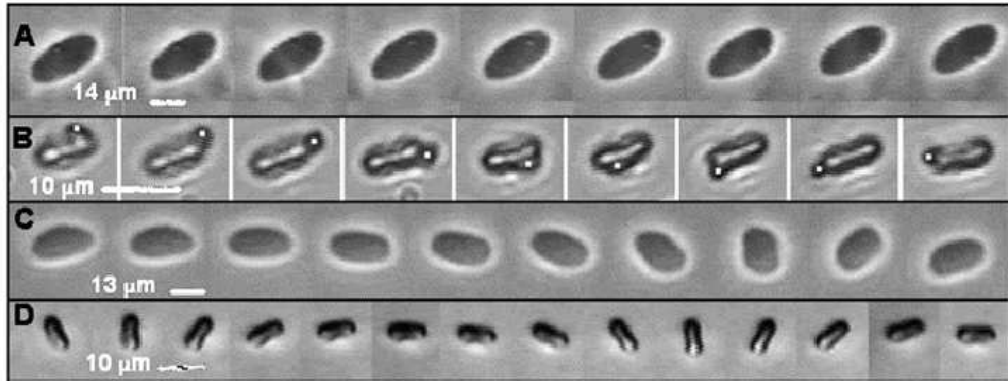


Figure 4.6: Time sequences of tank-treading and tumbling vesicles (A and B, respectively) and red blood cells (C and D, respectively): the two main regimes that characterize vesicle – and RBC – dynamics [AV08].

and becomes thus more prone to tumbling. As a result, the vesicle shows a motion which is composed by a periodic alternation of portions of tumbling and tank-treading. This regime is called *vacillating-breathing* or *swinging* and has been discovered only very recently [Mis06, KS06, DKS09]. Another regime is the so-called *kayaking* or *spinning*, in which the vesicle tumbles but with a main axis that precesses around the vorticity direction (i.e. the direction normal to the shear plane) [LTV08].

The parameter space in three dimensions has not yet completely been explored, so the existence of other regimes is possible. Moreover, in other types of flow the vesicle can show different dynamics. For instance, in Poiseuille (parabolic) flow, a vesicle can assume a ‘parachute’ shape, or an asymmetric ‘slipper’ shape [SB69, VMP04, Poz05, KBM09], both in two and three dimensions. Vesicles in a Poiseuille flow will be presented in chapter 7.

4.5 Vesicles to model red blood cells in two dimensions

The present work is concerned with numerical simulations of vesicles in dimension two, it is then important to discuss the relationship between vesicles (the model) and red blood cells (the biological counterpart) in the particular two-dimensional case.

As stated in section 3.1, the membrane of a red blood cell is submitted, as vesicles, to the constraint of local inextensibility but in addition also to

the elastic restoring force arising from the deformation of the cytoskeleton, that vesicles lack. In three dimensions, these two elements can coexist and both influence the dynamics. But in dimension two the effect of the cytoskeleton, i.e. membrane elasticity, is suppressed by the inextensibility of the membrane, that fixes the distance between neighboring membrane patches.

To be more precise, an effect of the cytoskeleton in two dimensions exists *if the rest configuration is non-circular*. In fact, the cytoskeleton has the mechanical effect of exerting on the membrane an elastic force towards the unstressed configuration. If this configuration is circular, the elastic restoring force does not depend on the membrane patch. But if the rest configuration has a different shape, every membrane patch keeps memory its original curvature, so elastic forces vary from patch to patch. A consequence of the non circular rest configuration is an oscillation of the inclination angle around its average value in the tank-treading regime (observed experimentally for RBCs [AV08]), due to the movement of the membrane around the fixed shape of the particle. In tumbling, the membrane tank-treading is minimal and the effects of elastic forces are then negligible.

In conclusion, in two dimensions the differences between vesicles and red blood cells are reduced to a minimum, due to the inextensibility of the membrane.

THE NUMERICAL METHODS

The boundary integral and the phase field methods to compute the dynamics of vesicles are described. The numerical codes used in this work have been implemented by T. Biben, in our institution, for the single vesicle case. I adapted these codes to the case of multiple vesicles and interfaced the boundary integral code to a fast multipolar solver developed by H. Selmi, and parallelized it on multiple computing cores using the library OpenMP. The boundary Integral code developed by G. Biros is also introduced and compared to ours.

La méthode des intégrales de frontière et la méthode du champ de phase pour calculer la dynamique de vésicules sont décrites. Les codes numériques utilisés dans ce travail ont été développés par T. Biben au sein de notre Laboratoire pour le cas d'une seule vésicule. J'ai adapté ces codes au cas de plusieurs vésicules et aussi interfacé le code intégral à un solveur basé sur la méthode multipolaire rapide développée par H. Selmi. J'ai parallélisé cette méthode sur plusieurs cœurs de calcul à l'aide de la bibliothèque OpenMP. Le code intégral développé par G. Biros est aussi présenté et comparé aux deux codes précédents.

5.1 A moving interface problem

An ensemble of vesicles suspended in a fluid defines several fluid domains, corresponding to the interior of each vesicle and to the suspending medium. Then the dynamical evolution of the system can be seen as the evolution of the fluid domains, connected one to the other through appropriate boundary conditions. While the solution of the fluid motion in a single domain with known boundary conditions is quite simple due to the simplicity of the governing equation (the Stokes equation in our case), the problem is more complicated when the domains are connected one to the other and the boundary conditions themselves (position of the boundary and forces

exerted) depend on the evolution of the system: this is a *moving interface* problem.

From a numerical point of view, moving interfaces are a challenge. The main difficulty arises from the fact that every fluid domain, and then the domain where the solution has to be computed, changes its shape and position with time. This forces in principle to redistribute the ensemble of discretization points (*mesh*) from a time step to another, or to encode somehow in the equations the variations in the domains.

There are several techniques to deal numerically with a moving interface, but they can be regrouped in two general families: (i) the *interface tracking* methods and (ii) the *diffuse interface* methods.

In the interface tracking methods, the interface is tracked directly via a set of discretization points that lie on the interface itself. These points have then to be displaced with the interface during time evolution. This displacement has to be performed in such a way that the distribution of the points continues to represent conveniently the interface, i.e. avoiding the accumulation of points in some areas and big separations between them elsewhere. In fact, these factors usually cause big numerical errors on the computation of the dynamics. Methods that belong to this family are for instance the Boundary Element (or Boundary Integral) Method (BEM / BIM) and the Immersed Boundary Method [Pes02].

The other family of methods to solve moving interface problems is composed by the diffuse interface methods. In these methods, the interface is not tracked directly, on the contrary its position is encoded in an auxiliary field, that assumes a certain value on the location of the interface. The advantage of this technique, which is apparently counterintuitive, is the possibility to use a mesh that does not depend on the position of the interface and thus does not change in time. To this family belong the Phase Field method (PF) and the Level Set method.

We use two different numerical methods to run simulations of vesicles immersed in an external fluid: Boundary Integral and Phase Field methods. The main difference between these two is that with BIM only the membrane of the vesicles is discretized (all the mesh points lie on the interface), while in PF the equations are solved in the *bulk*. We describe both of them in the following paragraphs.

5.2 Boundary Integral Method

The main idea of this method is to solve Stokes equations by means of the Green's function technique. The use of this method yields the velocity

of the membrane, needed for the time evolution of the suspended entities, as a function of integrals over the various boundaries present in the considered fluid domain. For a single vesicle in an unbounded shear flow the only boundary is that of the membrane of the vesicle [Poz92, Poz01]. The computation reduces from a two-dimensional problem (fluid domain) to a one-dimensional problem (the vesicle boundary). This is done, however, at a certain price, non locality: the motion of a given point of the surface of the suspended entity depends on the dynamics of the points which are located elsewhere. The numerical solution of these equations is achieved by a discretization of the vesicle surface, which is a line in two dimensions. Note that this method can only be used to solve linear equations (as Stokes equations) and needs an update of the mesh during the time evolution due to the deformation of the boundaries of the fluid domains [RA78, KWSL96, CM99a]. Moreover, in two dimensions, the constraint of local length incompressibility on the vesicle membrane preserves the distance between neighboring points of the discretization, so the mesh update can be performed with a simple Lagrangian advection.

The equation for the velocity of a point belonging to the membrane (denoted \mathbf{x}_0 hereafter) is [Poz93, KPS94]:

$$\begin{aligned} \mathbf{u}(\mathbf{x}_0) = & \frac{2}{1+\lambda} \mathbf{u}^\infty(\mathbf{x}_0) + \frac{1}{2\pi\eta_{out}(1+\lambda)} \oint_\gamma \mathbf{G}(\mathbf{x} - \mathbf{x}_0) \cdot \mathbf{f}(\mathbf{x}) ds(\mathbf{x}) \\ & + \frac{2(1-\lambda)}{\pi(1+\lambda)} \oint_\gamma \mathbf{u}(\mathbf{x}) \cdot \mathbf{T}(\mathbf{x} - \mathbf{x}_0) \cdot \mathbf{n}(\mathbf{x}) ds(\mathbf{x}) \end{aligned} \quad (5.1)$$

where

$$G_{ij}(\mathbf{x} - \mathbf{x}_0) = -\delta_{ij} \ln |\mathbf{x} - \mathbf{x}_0| + \frac{(\mathbf{x} - \mathbf{x}_0)_i (\mathbf{x} - \mathbf{x}_0)_j}{|\mathbf{x} - \mathbf{x}_0|^2} \quad (5.2)$$

$$T_{ijk}(\mathbf{x} - \mathbf{x}_0) = -4 \frac{(\mathbf{x} - \mathbf{x}_0)_i (\mathbf{x} - \mathbf{x}_0)_j (\mathbf{x} - \mathbf{x}_0)_k}{|\mathbf{x} - \mathbf{x}_0|^4} \quad (5.3)$$

are the Green's functions of the problem (G_{ij} refers to the so-called single layer contribution, while T_{ijk} accounts for the the double layer¹ contribution), \mathbf{u}^∞ represents the imposed flow, γ is the vesicle contour and \mathbf{f} the membrane force, given by equation (4.8):

$$\mathbf{f} = -\kappa \left[\frac{d^2 c}{ds^2} + \frac{1}{2} c^3 \right] \mathbf{n} + \zeta c \mathbf{n} + \frac{d\zeta}{ds} \mathbf{t}$$

¹The names *single layer* and *double layer* come from electrostatics: if f_i is thought of as an electric charge and \mathbf{u} as an electric dipole (i.e. a distribution of opposite charges on two close layers), the integrals containing G and T represent the electric potential generated by these distributions.

For numerical reasons, the numerical scheme which is implemented in the code does not use ζ directly², but rather a tension-like parameter, introduced as a penalty:

$$\mathbf{f} = -\kappa \left[\frac{d^2 c}{ds^2} + \frac{1}{2} c^3 \right] \mathbf{n} + T [(\ell_l - \ell_{l_0}) \boldsymbol{\tau}_l + (\ell_r - \ell_{r_0}) \boldsymbol{\tau}_r] \quad (5.4)$$

where $(\ell_l - \ell_{l_0})$ and $(\ell_r - \ell_{r_0})$ are the differences between the actual distances of a discretization point of the membrane to its left and right neighbors and their initial values. $\boldsymbol{\tau}_l$ and $\boldsymbol{\tau}_r$ are the unit vectors pointing from the considered point to the corresponding neighbors. This tension term accounts for both the tangential and normal components of the membrane incompressibility force which enters via the Lagrange multiplier ζ in (4.8). We can introduce a dimensionless number associated with T , defined as $C_T = \eta_{out} \dot{\gamma} / (r_0 T)$. The elastic constant T is taken quite large, so that the corresponding force is large enough to fulfill quasi conservation of the local length at the time scale imposed by the action of physical forces. This means that the elastic dynamics can be considered as an effective implementation of quasi instantaneous local membrane incompressibility, [CKM03] (in practice, taking $T \approx 10^4$, when the other relevant parameters are of order 1, is sufficient to reach the convergence of this scheme). More precisely if C_a is of order one, then C_T should be chosen small enough (typically 10^{-4} or smaller).

The large separation of time scales between the overall dynamics of the vesicle and the local dynamics of the membrane obliges to choose a small time step. An advantage of the use of the penalization method is that we do not need to solve numerically for a Lagrange multiplier, which should be obtained implicitly from the condition that the surface divergence of the velocity field must vanish (membrane incompressibility).

The membrane velocity is computed by evaluating the right hand side of (5.1): we prescribe an initial vesicle shape as well as an initial velocity on the membrane, so that the right hand side of (5.1) can be evaluated at initial time. The time integration is carried out by means of an explicit Euler scheme, in which the velocity appearing on the right hand side of (5.1) is taken to be the one computed at the previous time step. Each point on the membrane is displaced by a quantity $\mathbf{u} \Delta t$, where Δt is the time step and \mathbf{u} is the membrane velocity, and this yields the new configuration, and so on.

²The simultaneous determination of the velocities of the discretization points \mathbf{x}_0 and of the Lagrange multipliers $\zeta(\mathbf{x}_0)$ is challenging from a numerical point of view, and leads to severe instabilities.

As discussed in chapter 3, the rheological properties correspond to integrals of the stress tensor extended over the whole volume of the system. Within the framework of BIM, it is highly desirable to avoid volume integrals, that would require a specific volume mesh (since the dynamics of the system is completely determined via surface integrals). It is indeed possible to express volume integrals through surface integrals, by using Gauss' theorem. In the case of the integration of the stress tensor, the use of this theorem is nontrivial due to the discontinuities of σ across the membrane of the vesicles, as shown in chapter 4. The calculation, based on the approach of Batchelor [Bat70] (that has been adapted to liquid particles by Kennedy *et al.* [KPS94]) is detailed in Appendix A. This allows us to determine the contribution of the vesicles to the rheology of the system via integrals over the vesicle membrane itself.

The expression used to compute the components of the stress tensor of the composite fluid (solvent + vesicles) reads:

$$\begin{aligned} \langle \sigma_{ij} \rangle = & \frac{1}{S} \left[\eta_{out} \int_S (\partial_i u_j + \partial_j u_i) dA \right. \\ & \left. + \oint_{\gamma} [x_j f_i + \eta_{out}(\lambda - 1) (n_i u_j + n_j u_i)] ds \right] \end{aligned} \quad (5.5)$$

where S denotes the bulk of the system and γ the contour of the vesicle. The first term, which is the average velocity gradient in the system, represents the stress contribution due to the imposed flow [SCB68, Bat70, FA70], while the second term accounts for the presence of the vesicle. The discussion of rheology will thus focus on the latter contribution only.

Numerical implementation and convergence test

BI method is very accurate and thus allows for precise quantitative results. We have studied the numerical convergence of the code upon decreasing the time step and increasing the number of discretization points.

For this test, we consider the simple physical situation of a single vesicle in an unbounded shear flow, that is the case analyzed in detail in chapter 6. We compute both the dynamics and the rheology, in particular we study the inclination angle of the vesicle with respect to the flow lines, the effective viscosity and the normal stress difference.

The method of discretization is described in [CKM03]. It turned out that the convergence with respect to the time step is quite fast, while the convergence with respect to the spatial discretization n is slower: we focused then our attention on the latter. We ran four series of simulations, with

$n \in \{60, 80, 120, 240\}$. For every series we chose a time step for which we can consider that the time convergence is attained: (simulations with a time step three times smaller were giving the same results within an error of 10^{-5}). For this convergence test we consider a vesicle with a reduced area $\alpha = 0.9$ and a capillary number $C_a = 1$.

We have analyzed the behavior of the critical viscosity ratio λ_c beyond which the vesicle undergoes a tumbling transition. It is in general quite difficult to locate with a good enough accuracy a bifurcation point. The results are shown in figure 5.1. The same quantity is also computed for $n = 480$ (in that case we only focus on the critical value λ_c , in that we do not compute the whole curves as in figure 5.1 due to the rather large computing time). In figure 5.2 we report λ_c for different values of n . In order to check the convergence by extrapolation to $n = \infty$, we plot λ_c as a function of $1/n$. It is appealing to fit the data with a parabola (see figure 5.2). Taking a test function $y = ax^2 + d$ (we have omitted the linear term since the figure conveys the impression of a quite small slope at the origin) it is found that the discrepancy between the extrapolated value at $n \rightarrow \infty$ ($d = 5.50$) and the one found by the most refined simulation ran ($n = 240$, $\lambda_c = 5.55$) is about 1%: so we can consider that our discretization is close enough to convergence to be able to discuss the results at a quantitative level. The time step for $n=240$ is $\Delta t = 3 \cdot 10^{-5}$. The perimeter is conserved within a relative error of 10^{-3} , and the surface of 10^{-6} . Cpu time on a desktop processor is of the order of hours or days – depending on the parameter values.

5.3 Phase Field Method

This technique is traced back to van der Waals [vdW79] and has been widely used in the context of critical phenomena [HH77]. The method has then been used for non equilibrium pattern-forming solidification problems [PF90, WSW⁺93, WBM93, Kob93]. It was first introduced for vesicles and membranes in [BM02, BM03, BKM05]. This method is based on the introduction of an auxiliary field, namely the phase field, which assumes two constant values inside and outside the vesicle (in our case -1 and $+1$ respectively), and undergoes a continuous, albeit stiff enough, variation between these values across the membrane position.

Unlike the van der Waals and phase transition problems where the phase field represents a physical quantity (e.g. density), for the vesicle system it can, at first sight, be viewed as a color-like function that delimits the interior of the vesicle from the exterior. Recently a thermodynamical formulation

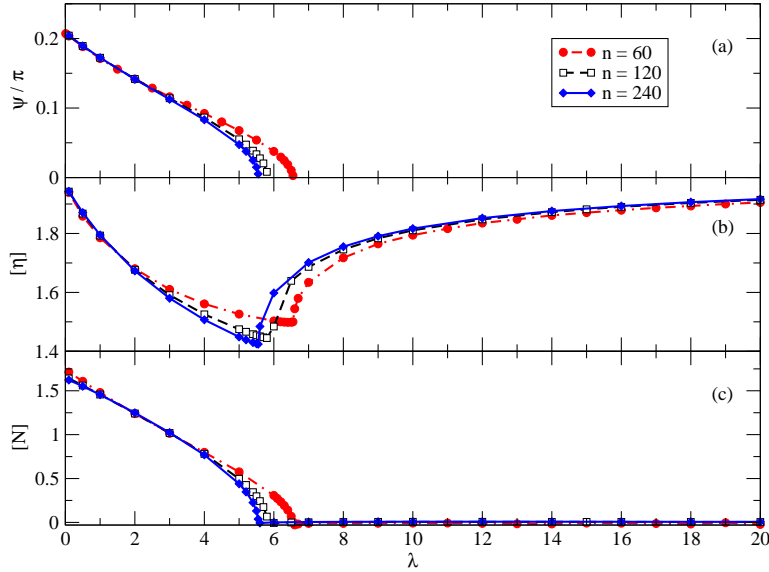


Figure 5.1: Boundary Integral Method: numerical convergence upon increasing n . (a) stationary inclination angle Ψ , measured counterclockwise from the positive x semiaxis (when a stationary solution exists; this is the tank-treading regime), (b) the reduced viscosity $[\eta]$, and (c) the normal stress difference N as a function of the viscosity ratio λ . The reduced area is $\alpha = 0.9$ and the capillary number $C_a = 1.0$. Rheological measurements of (b) and (c) have been averaged over a period in the tumbling regime.

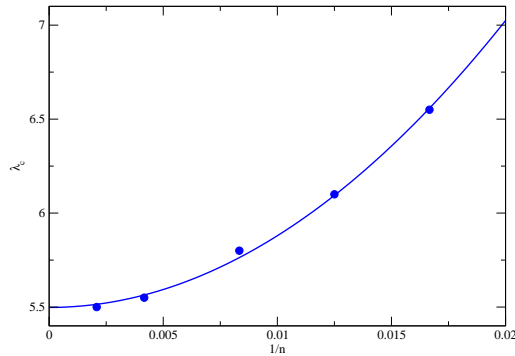


Figure 5.2: Boundary Integral Method: numerical convergence of the parameter λ_c as a function of $1/n$. $n \in \{60, 80, 120, 240, 480\}$. The line represents the fit of the results by the function $y = ax^2 + d$. The value found for the intersection with the y axis is $d = 5.50$, representing the extrapolation for $n \rightarrow \infty$.

of the phase field for membrane dynamics has been proposed, although the notion of thermodynamics associated with a membrane position is a priori not easy to imagine [JM07, JM08a, JM08b]. Here we shall adopt the alternative of a color-like function.

The phase field (PF) behaves as a $\tanh(r/\epsilon)$ profile (where r is the position variable across the membrane). We refer thus to the phase field as a diffuse interface model, since the boundary region is endowed with a certain thickness ϵ , which is not of atomic size (otherwise the problem would be too stiff and could not be handled numerically within a reasonable time), but rather it is required to remain small enough in comparison with the vesicle size and the local radius of curvature. Thus, the thickness of the interface is artificial and does not reflect the physical thickness of the bilayer, since here the phase field is used only for interface tracking. This results in some conceptual and numerical difficulties, the most serious one being the need to extrapolate the results in the limit of vanishing interface thickness [BRS⁺04]. This extrapolation is not always obvious, since the dynamics is sensitive to the value of the interface thickness.

The PF method is a field approach, i.e. the evolution equations are solved everywhere in the bulk regardless of the position of the membrane. The presence of the vesicle in the considered domain is expressed explicitly only in the initial condition. The popularity of the PF approach is due to its various virtues: (i) the possibility to run simulations for any kind of constitutive equation for the ambient fluid (not only linear as is required by the BI method), (ii) the absence of direct tracking of the interface, thanks to which remeshing problems and others due to singularities over the boundaries are avoided and (iii) simulating several vesicles requires only a change in the initial conditions.

Let us recall the model equations initially reported in [BM02, BM03]. The Stokes equations are coupled with an evolution equation for the phase field φ . The latter is derived from a phenomenological free energy (which has the form of a Ginzburg-Landau energy known for phase transition phenomena) having a double well and a wall-like contribution. In addition, the bending force and the inextensibility condition of the membrane (which is a proper problem to vesicles) have to be defined everywhere in the bulk, like the phase-field itself. This is detailed in [BRS⁺04].

The evolution equations of the PF model read:

$$\frac{\partial \mathbf{u}}{\partial t} = \nabla \cdot [\eta(\varphi)(\nabla \mathbf{u} + \nabla \mathbf{u}^T)] - \nabla p + \mathbf{f} \quad (5.6)$$

$$\frac{\partial \varphi}{\partial t} = -\mathbf{u} \cdot \nabla \varphi + \epsilon_\varphi \left[-\frac{\delta F}{\delta \varphi} + c\epsilon^2 |\nabla \varphi| \right] \quad (5.7)$$

$$\frac{\partial \zeta}{\partial t} = -\mathbf{u} \cdot \nabla \zeta + T \nabla_s \cdot \mathbf{u} \quad (5.8)$$

where $\mathbf{n} = \nabla \varphi / |\nabla \varphi|$ is the normal to the iso- φ lines, $c = -\nabla \cdot \mathbf{n}$ is the curvature, $\eta(\varphi) = \eta_{out}(1 + \varphi)/2 + \eta_{in}(1 - \varphi)/2$ is the position-dependent viscosity (this parametrization allows to account for a viscosity contrast between the interior and exterior of the vesicle), p is the pressure, and \mathbf{f} represents the force on the membrane,

$$\mathbf{f} = \left[-\kappa \left[\frac{c^3}{2} + \nabla_s^2 c \right] \mathbf{n} + \zeta c \mathbf{n} + (\mathbf{t} \cdot \nabla \zeta) \mathbf{t} \right] \delta^{interface}(\mathbf{r}) \quad (5.9)$$

and

$$F = \int_S dA \left[\frac{1}{4} (1 - \varphi^2)^2 + \frac{\epsilon^2}{2} |\nabla \varphi|^2 \right] \quad (5.10)$$

is the free energy functional intrinsic to the phase field model. Note that the membrane force is nothing but expression (4.8) written in the phase field spirit. $\delta^{interface}(\mathbf{r}) = |\nabla \varphi|/2$ localizes the force action around the membrane of the vesicle (the interface of the PF) and is a diffuse version of the Dirac function. $\nabla_s \cdot \mathbf{u}$ is the surface divergence of the velocity field, T is similar to the tension-like parameter introduced in (5.4), and has to be large enough in order to enforce the local incompressibility of the membrane, and finally \mathbf{t} denotes the tangent vector to the iso- φ contours.

In (5.7) the term $c\epsilon^2 |\nabla \varphi|$ has been added in order to suppress the surface tension effect arising from the Laplacian $\nabla^2 \varphi$ (that stems from the functional derivative of $|\nabla \varphi|^2$) in the free energy. In fact this term, being a positive contribution to interface energy, acts to reduce the extent of the interface as a surface tension would do. This trick has been introduced by [FCHMRP99], and adopted later for vesicles by [BM03]. Note that this effect can also be suppressed directly from the energy [JM08a], an advantage which may prove useful when using a weak formulation for solving the equations by means of a finite element technique.

The time evolution is implemented after discretizing the space operators by Fourier transforms [Bib05]. This requires periodic boundary conditions. As a consequence, the system simulated is more appropriately an infinite periodic system, with an infinite number of vesicles. To avoid the effect

of interaction between the vesicle and its images, we run simulations at a low volume fraction $\phi \approx 2\%$, corresponding to a squared box whose side is approximately six times the linear dimension of the vesicle. The discretization domain is a squared grid of size 200×200 . The number of points lying in the membrane region (the so-called diffuse interface) is equal roughly to 160.

The effective viscosity is computed by integrating the stress tensor over the sides of the simulation box:

$$\eta_{eff} = \frac{1}{2L\dot{\gamma}} \int_{\partial S} \sigma_{xy} dl = \frac{1}{2L\dot{\gamma}} \int_{\partial S} \eta_{out} (\partial_x u_y + \partial_y u_x) dl \quad (5.11)$$

where ∂S represents the boundary of the simulation box of side L (the two sides parallel to the gradient of the imposed shear flow do not contribute to the result due to periodic boundary conditions.) The above contribution contains both the effect of the imposed flow and the induced contribution due to the presence of the vesicle.

5.4 Comparison between the numerical methods

The results obtained by the two numerical methods are compared in figure 5.3. It is seen that the two methods show the same qualitative behavior. However, the PF method is sensitive to the numerical value of the interface width ϵ , and is expected to provide less precise results, unless a very refined mesh is used. If the mesh is not fine enough the PF method shows a significant quantitative deviation from BI results. However, if a larger mesh size is allowed for the BI method, then the BI and PF methods agree even quantitatively, as shown in figure 5.3. In order to achieve a high enough precision an extrapolation of the PF results to $\epsilon \rightarrow 0$ is needed. Due to the extrapolation, this method predicts a slightly negative inclination angle close to the transition; this should be regarded as a numerical artifact. Note, however, that small negative angles are predicted analytically in three dimensions [LTV08, DBP⁺07], but no support is known in two dimensions. In addition, the presence of a bifurcation makes the task even more serious numerically, since physical properties undergo an *intrinsic* rapid change in the vicinity of the bifurcation point. As a consequence, the computation of the effective viscosity, figure 5.3(b), in the bifurcation region is hardly accessible, and could not so far been determined with a high enough degree of confidence.

5.5 Alternative Boundary Integral implementation

In section 6.7 and chapter 8 a boundary integral code written by G. Biros (*Georgia Institute of Technology, Atlanta, USA*) and collaborators will be used. It is described in detail in [VGZB09]. The motivations of this choice rely on the high precision of this implementation in the computation of the dynamics of a vesicle suspension, and the low number of points necessary in order to discretize rigid boundaries (in fact, in section 6.7 we will study the behavior of highly deflated vesicles and in chapter 8 we will study the behavior of a suspension of vesicles in a bounded geometry, a Taylor-Couette cell).

The code by Biros *et al.* has high accuracy both in space and time. The latter is due to the high-order scheme (2^{nd} or 3^{rd}) used to implement the time evolution, while the precision in space computation is due to the spectral accuracy (i.e. the use of Fourier transforms) to compute derivatives on the surface of the vesicle (we remind that the membrane force contains a fourth derivative, whose precise numerical calculation is challenging).

Moreover, Biros and collaborators implemented contribution to the membrane force arising from inextensibility (see equation 4.8) directly with Lagrange multipliers: this enables to simulate a perfectly circular vesicle. On

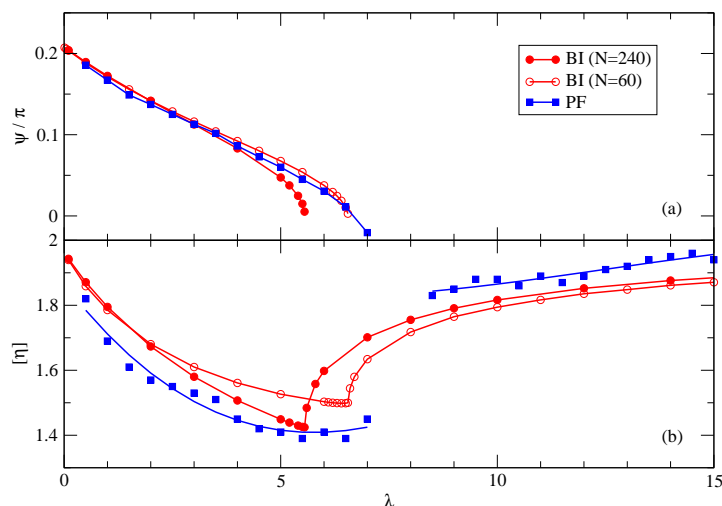


Figure 5.3: Comparison between boundary integral (BI) at two different resolutions, $N = 60$ and $N = 240$, and phase field (PF) results (200×200 grid) extrapolated to $\epsilon \rightarrow 0$.

the contrary, the code written by Biben *et al.* is based on an effective implementation of this force through a penalization method, that would oblige to set the penalty parameter T to infinity in order to preserve the local surface area when approaching the circular shape³ (see equation 5.4). On the contrary, Biros and collaborators succeeded to remove the singularity present in the tension force. Their code is then able to simulate a perfectly circular vesicle.

Convergence tests have been performed passing from $n = 32$ to $n = 64$ discretization points on the membrane and from time steps of order 10^{-2} to 10^{-3} . The results are very satisfactory using the values $n = 64$ and $\Delta t = 10^{-3}$: the perimeter and area of the vesicles are conserved within 1% (1% for the most deformed vesicles, i.e. $\alpha \approx 0.3$). In our experience, the precise conservation of these two quantities is necessary and sufficient to guarantee the convergence of dynamical and rheological measurements.

We compared this code to the boundary integral detailed in section 5.2, written by T. Biben in our institution. The comparison is reported in figure 5.4. The two codes show a very good agreement in the range $0.4 \leq \alpha \leq 0.95$, although small discrepancies are visible in the rheological quantities, especially normal stress difference, for low values of α . The lower limit of the range used for the comparison is dictated by the fact that around $\alpha \approx 0.3$ there is no stationary solution of motion (and simulations become challenging), while the upper limit $\alpha = 0.95$ is determined by the long computing time of the code of Biben *et al.* in the vicinity of $\alpha = 1$ (due to the mentioned singularity in the membrane force).

³ For a circular vesicle the elongational component of the flow (see digram 4.5) is perpendicular to the membrane both at the elongation and compression directions. As a consequence, the tension forces, which are tangent to the membrane, should approach infinity to guarantee a vanishing deformation. This is exactly what happens for an inextensible straight rope, fixed at the two extremities, in the middle of which a normal force acts.

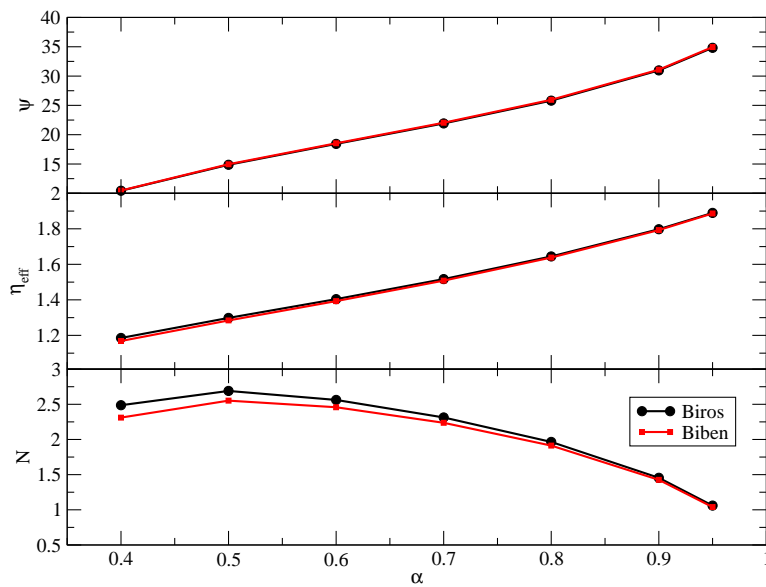


Figure 5.4: Comparison between the code used in this chapter (Biros) and the code developed by T. Biben in our institution. Ψ is the vesicle inclination angle, and $[\eta]$ and N the intrinsic viscosity and the normal stress difference of the suspension.

DILUTE SUSPENSION OF VESICLES

The dynamics of a single vesicle in a linear shear flow and the rheology of a dilute suspension of vesicles are analyzed in detail. While the basic dynamics (tank-treading and tumbling) was already known at the beginning of my thesis, the rheological behavior was still unclear. My work clarifies the subtle links between the microscopic dynamics of the vesicle and the macroscopic behavior of the suspension. The influence of the membrane on rheology is discussed, and its effects are differentiated from the effects due to the bulk of the vesicle. Moreover, low reduced areas are investigated, a case in which the vesicle is highly biconcave. In this case, tumbling is found for a viscosity contrast $\lambda = 1$, a fact that was not expected.

La dynamique d'une vésicule dans un écoulement de cisaillement linéaire et la rhéologie d'une suspension diluée de vésicules sont analysées en détail. Contrairement à la dynamique de base (tank-treading et tumbling), qui était déjà connue au début de ma thèse, le comportement rhéologique n'était pas encore clair. Mon travail clarifie les liens subtils entre la dynamique microscopique de la vésicule et le comportement macroscopique de la suspension. L'influence de la membrane sur la rhéologie est discutée, et ses effets clairement différenciés des effets dus au volume de la vésicule. De plus, des faibles surfaces réduites sont considérées, un cas dans lequel la vésicule est hautement biconcave. Dans ce cas, le mouvement de tumbling est trouvé pour un contraste de viscosité $\lambda = 1$, un fait qui n'était pas attendu.

The main goal of this chapter is to build a solid understanding of the fundamental phenomena linking rheology to microscopic dynamics. We devote then our study to the most simple situation: a single two-dimensional vesicle immersed in an unbounded linear shear flow (figure 6.1). Starting from the isolated vesicle problem, it is possible to extrapolate the rheological results to dilute suspensions, i.e. to a finite concentration, albeit neglecting

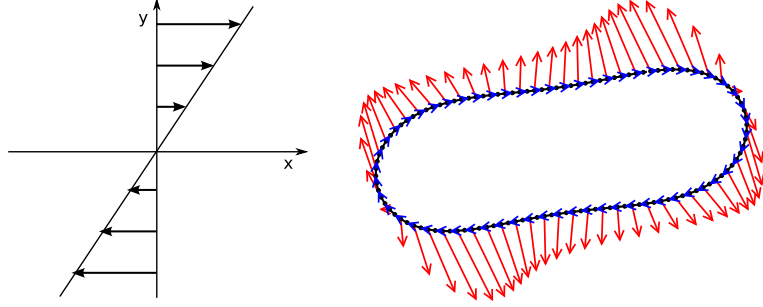


Figure 6.1: Left: The imposed linear shear flow and the coordinate system. Right: A tank-treading vesicle in linear shear flow with a reduced area of $\alpha = 0.7$, a viscosity ratio of $\lambda = 3$ and a capillary number $C_a = 1$. The dots represent a typical mesh (only half of the grid points are shown), the tangential arrows the velocity field and the outward arrows the force exerted by the fluid on the membrane.

hydrodynamical interactions. This is done following Batchelor approach [Bat70], as detailed in Appendix A.

The rheological quantities of interest are the effective viscosity of the solution

$$\eta_{eff} \equiv \frac{\langle \sigma_{xy} \rangle}{\dot{\gamma}} \quad (6.1)$$

and the normal stress difference

$$N \equiv \frac{\langle \sigma_{xx} \rangle - \langle \sigma_{yy} \rangle}{\dot{\gamma}} \quad (6.2)$$

where $\boldsymbol{\sigma}$ is the stress tensor of the suspension – which depends on the still-unknown vesicle conformation – and $\langle \rangle$ denotes volume average. These quantities provide information on the viscous and the non-Newtonian behavior of the fluid, as showed in chapter 3.

It is convenient to subtract the contribution due to the imposed flow and normalize the result by an appropriate factor, which includes the volume fraction ϕ of the suspended entities, following [Bat70]. The imposed linear shear flow trivially yields $\langle \sigma_{xy} \rangle = \eta_0 \dot{\gamma}$ and $N = 0$, so we have the nondimensional reduced quantities:

$$[\eta] \equiv \frac{\langle \sigma_{xy} \rangle - \eta_0 \dot{\gamma}}{\eta_0 \dot{\gamma} \phi} \quad (6.3)$$

and

$$[N] \equiv \frac{\langle \sigma_{xx} \rangle - \langle \sigma_{yy} \rangle}{\eta_0 \dot{\gamma} \phi} \quad (6.4)$$

which will be called respectively *intrinsic viscosity* and *intrinsic normal stress difference*.

The vesicle contribution to the suspension stress is linear in the volume fraction, which expresses the fact that the effects of the vesicles sum up linearly in the absence of hydrodynamic interaction. This kind of approach is expected to provide quantitative results for small enough concentrations (typically $\leq 5\%$, in reference to the experimental validity of Einstein's result for a suspension of spherical rigid particles, see [Lar99]), since, otherwise, we expect that the hydrodynamic interactions can no longer be neglected.

While the volume fraction of the suspension only plays a trivial role in the dilute regime, the non-trivial control parameters are associated to the dynamics of the vesicle itself: the viscosity ratio, $\lambda = \eta_1/\eta_0$, the capillary number $C_a = \eta_0 \dot{\gamma} R_0^3/\kappa$, which expresses the intensity of the flow compared to the bending forces on the membrane, and the reduced area α of the vesicle. Figures 6.2 and 6.3 show the steady angle in the tank-treading regime, the intrinsic viscosity and the intrinsic normal stress difference. A strong dependence of the intrinsic viscosity on λ (varied in the interval $[0.1, 200]$) is observed. At low λ the vesicle motion is of tank-treading type, while at large λ the vesicle tumbles. The minimal suspension viscosity is obtained at the critical value λ_c corresponding to the bifurcation from tank-treading to tumbling. A detailed discussion of these behaviors is provided in 6.1, while in section 6.2 the normal stress difference is analysed. Although we shall mainly consider the λ dependence, the two other parameters α and C_a play a role as well. We show in figures 6.2 and 6.3 the influence of α , by considering values ranging from $\alpha = 0.70$, quite elongated vesicles, to $\alpha = 0.95$ for nearly circular shapes (see figure 6.4). We can see that the influence of α is only quantitative, the qualitative behavior is preserved. Section 6.3 provides a detailed analysis of rheology in the tumbling regime. The influence of C_a will be discussed in section 6.4. In section 6.5 a detailed comparison with drops is drawn. Section 6.6 is devoted to the comparison to three dimensional results, both analytical and experimental, while section 6.7 analyzes in detail the behavior of a suspension formed by highly deflated vesicles.

It is important at this point to stress that these results have been obtained using the BI method for two dimensional vesicles. As a consequence, in principle, these results have to be compared to two dimensional theories¹. In this context, it is interesting to remark that the intrinsic sus-

¹An analytical solution for the velocity field in two dimensions has been provided recently by [FLSG08]. We have used this solution and attempted to derive the effective

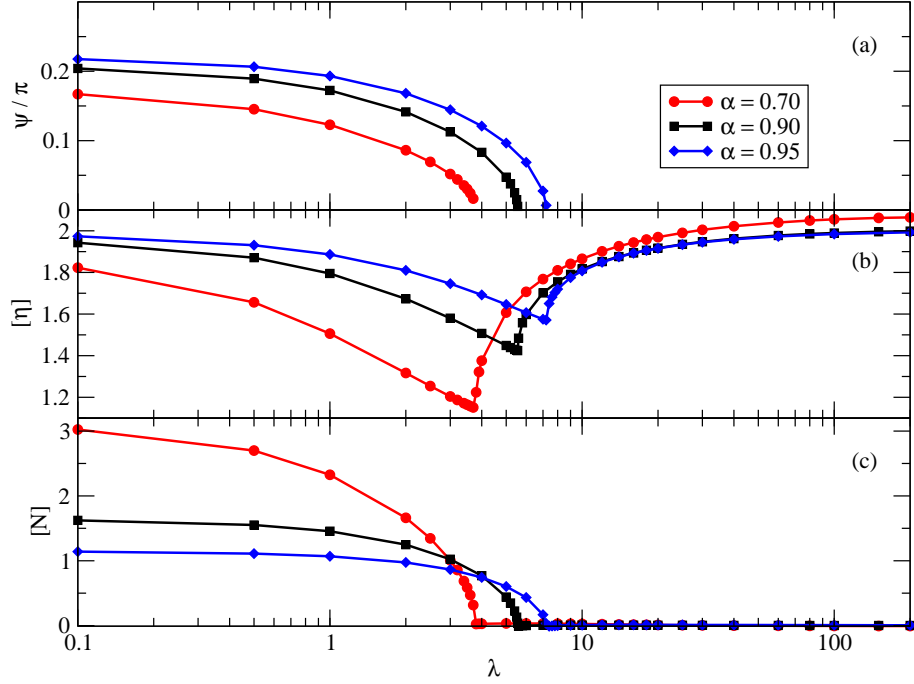


Figure 6.2: Dynamics and rheology of a suspension of vesicles for reduced area $\alpha \in \{0.70, 0.90, 0.95\}$ and a capillary number $C_a = 1.0$. The graphs represent: (a) the stationary inclination angle Ψ (when a stationary solution exists), (b) the intrinsic viscosity $[\eta]$ and (c) the normal stress difference N as a function of the viscosity ratio λ .

pension viscosity of quasi-circular vesicles ($\alpha = 0.95$) approaches the value 2.0 in the two extreme limits, $\lambda \rightarrow 0$ and $\lambda \rightarrow \infty$ as shown in figures 6.2(b) and 6.3(b). The three dimensional analogue approaches the value 2.5 [DM07, DBP⁺07] for quasi-spherical vesicles. These two values turn out to be equal to the Einstein coefficients in two and three dimensions, representing the effective viscosity of a dilute suspension of rigid circles or spheres [Ein06, Ein11, BBBC81, Bra84] respectively. The fact that the effective viscosity of rigid particles quantitatively depends on the spatial dimensions is also manifested by a vesicle suspension. This observation allows us to attempt a quantitative comparison between the results of two and three dimensions thanks to a simple rescaling of the data (section 6.6).

viscosity. However, the result shows a significant difference with the expected intrinsic viscosity in the circular limit (which is equal to 2). Therefore, we suspect that there is either an error in the velocity field provided in [FLSG08] or that the paper suffers from some typing mistakes. The time did not allow me to rederive the velocity field analytically.

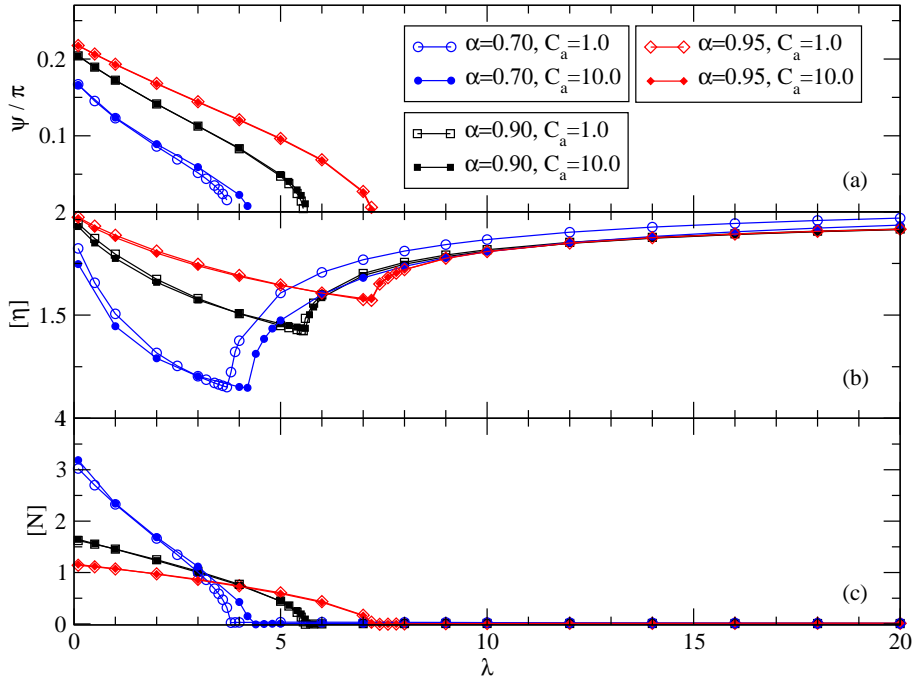


Figure 6.3: Dynamics and rheology of a suspension of vesicles for different reduced areas α and capillary numbers C_a . The three graphs represent: (a) the stationary inclination angle Ψ (when a stationary solution exists), (b) the intrinsic viscosity $[\eta]$ and (c) the normal stress difference N as a function of the viscosity ratio λ .

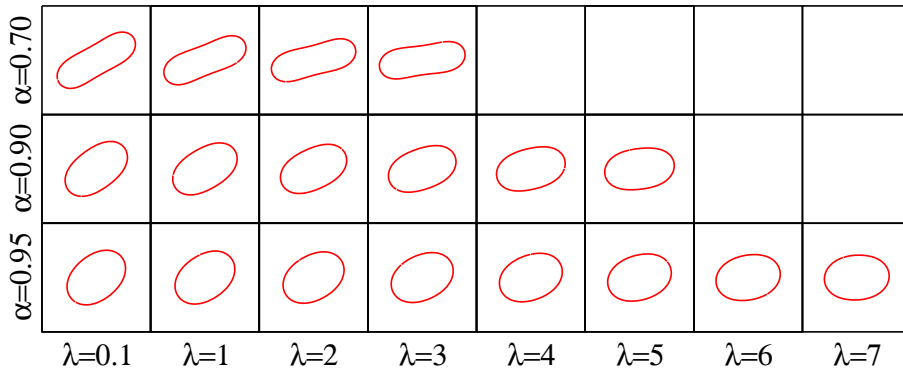


Figure 6.4: Stationary shapes of vesicles for different reduced areas α and a capillary number $C_a = 1.0$. For more elongated vesicles (smaller α) the tumbling to tank-treading transition occurs for smaller values of the viscosity ratio λ .

6.1 The effective viscosity

The effective viscosity of a suspension of vesicles has a complex behavior, strongly dependent on the microscopic dynamics. When plotted as a function of the viscosity ratio, figures 6.2(b) and 6.3(b), $[\eta]$ shows a nonlinear and non monotonic behavior. We shall first consider the two limiting cases $\lambda \rightarrow 0$ (small internal rigidity) and $\lambda \rightarrow \infty$ (high internal rigidity). As already pointed out, the intrinsic viscosity approaches the value of the Einstein coefficient in two dimensions, 2.0, in both limits, provided that the shape is quasi circular ($\alpha=0.95$). For $\lambda \rightarrow 0$ this result is not quite surprising. Indeed, at low values of λ the vesicle performs tank-treading motion, and if its shape is close to a circular one ($\alpha=0.95$) its motion is close to that of a rigid rotation of a circle. The limit $\lambda \rightarrow \infty$ is somehow less trivial at first sight. The vesicle undergoes a periodic tumbling motion and thus changes periodically its orientation. However, for a quasi circular shape, a tumbling motion is quite close to a tank-treading motion (a circle is a degenerate limit where tank-treading and tumbling coincide [RBM04]). In conclusion, the fact that $[\eta]$ approaches the value 2 in both limits (large and small λ) seems to have the same origin.

The limiting values of the effective viscosity (i.e. at $\lambda = 0, \infty$) depend on the reduced area α . For $\lambda = 0$ $[\eta]$ decreases upon decreasing α . This effect is not trivial, since the cross section of the vesicles in the flow, which may be considered as an indicator of flow resistance, does not vary noticeably (actually it even increases slightly, figure 6.4). The key point to explain this effect is that upon reducing α the vesicle has a more elongated shape, a fact which reduces the deformation of the flow lines, and thus lowers dissipation. At large λ this effect is reversed, figure 6.2(b). That is to say the elongation of vesicles (due to a decrease of α) leads to an increase of $[\eta]$. This means that the disturbance of the flow lines, and hence the effect on dissipation, due to the tumbling vesicle on the imposed velocity field is stronger and stronger. A detailed analysis of the intrinsic viscosity in the tumbling regime is provided in section 6.3.

It is interesting to note that the same behavior is obtained analytically in three dimensions: the intrinsic viscosity decreases with Δ , the excess area from a sphere – increasing Δ is equivalent to reducing the reduced volume – in the $\lambda \rightarrow 0$ limit (where it lies below the Einstein value), whereas it increases for $\lambda \rightarrow \infty$, where $[\eta]$ exceeds slightly the Einstein value [DM07, DVM08].

In the tank-treading regime $[\eta]$ is a decreasing function of λ . The reason is as follows: by increasing λ the inclination angle with respect to the flow decreases, and thus the vesicle opposes less resistance to the flow (see figures

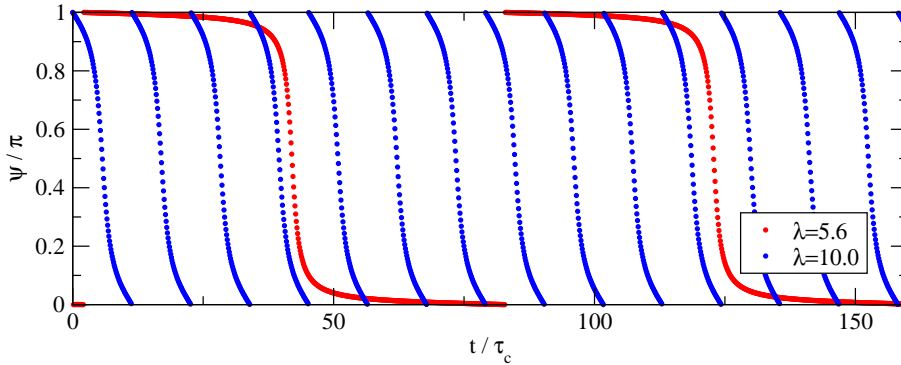


Figure 6.5: Inclination angle as a function of time for vesicles with different λ . $\alpha = 0.90$, $C_a = 1.0$.

6.3(a), 6.3(b) and 6.4). A detailed analysis of this phenomenon is given in section 6.5.

Let us provide further physical explanations to the above results. We have seen that after the transition to tumbling the effective viscosity (averaged over a period) increases with λ (see figure 6.3(b)). The key ingredient is that, on average, in the tumbling regime the vesicle scans a larger cross section against the flow, and this results in an enhanced resistance to flow compared to tank-treading. In addition, despite the existence of a bifurcation, $[\eta]$ is continuous at the TT-TB point and exhibits a minimum. The vesicle spends, close to the transition point, and on the TB side, most of its time aligned with the flow, and makes a rotation by an angle close to π in a small time interval. This is visible in figure 6.5 where we show the inclination angle as a function of time with parameters chosen both close to the tumbling bifurcation point ($\lambda = 5.60$, $\lambda_c = 5.55$) and far away from this point ($\lambda = 10.0$). The continuous decrease of the relative time spent in the flow-aligned position is the main reason why $[\eta]$ increases continuously upon increasing λ in the vicinity of the bifurcation point, i.e. for $\lambda \simeq \lambda_c$. As λ increases beyond λ_c , the TB frequency increases towards the value of a rigid ellipse (figure 6.6), which can be computed analytically [KS82]:

$$\omega_R = \frac{\dot{\gamma}}{\pi} \left(\frac{a}{b} + \frac{b}{a} \right)^{-1} \quad (6.5)$$

where a and b are the lengths of the small and large axes of the ellipse. For an ellipse with a reduced area $\alpha = 0.90$ and for a shear rate $\dot{\gamma} = 1.0$ we have $\omega \cong 0.138$, which is very close to the value found here for a nearly rigid ($\lambda = 200$) vesicle with the same reduced area $\alpha = 0.90$ and at a capillary number $C_a = 1.0$ (see figure 6.6).

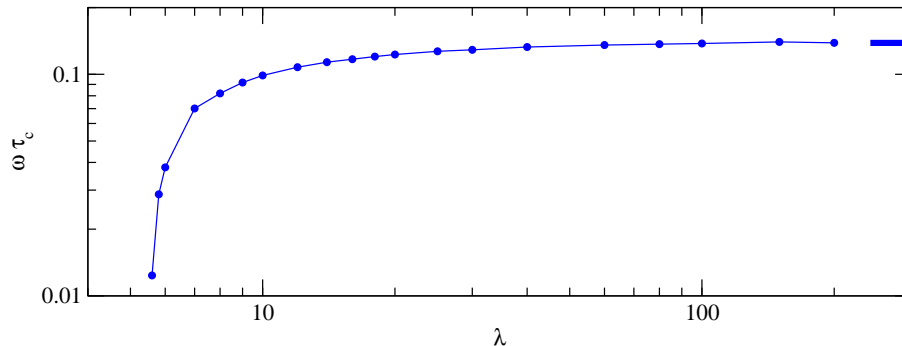


Figure 6.6: Tumbling frequency ω for vesicles with $\alpha = 0.9$ and $C_a = 1.0$ as a function of λ . The results (obtained from BI) have been extrapolated to the limit $n \rightarrow \infty$. The thick horizontal segment on the the extreme right represents the TB frequency for a rigid ellipse having the same α .

More recently, an analytical expression for the intrinsic viscosity in three dimensions in the TB regime has been reported [VMP⁺08]. This expression is valid at small enough C_a where the assumption of a shape-preserving solution is expected to make sense. The analytical expression agrees qualitatively well with the full numerical calculation (figures 6.3 and 6.16), in that it shows a square root singularity at the TT-TB point (on the TB side). To be more precise, a fit of the intrinsic viscosity in the tumbling regime close to the transition with the function $[\eta] = \eta_c + a(\lambda - \lambda_c)^b$ gives an exponent $b \approx 0.4$, which, although slightly different from the theoretical prediction in three dimensions (it is 0.5), is still consistent with a vertical tangent for $\lambda = \lambda_c$.

It is worthwhile to mention that some features of the three dimensional analytical work are not captured by the present simulations, however. Indeed, in three dimensions the cusp singularity exhibited by $[\eta]$ at low enough C_a is smeared out at large enough C_a [DBP⁺07]. In contrast, in the present simulation the cusp is preserved even at high enough C_a . We believe that this behavior is linked with the fact that in three dimensions a third dynamical regime, called vacillating-breathing (or swinging) is observed [Mis06, DBP⁺07, KS06], while in the two-dimensional case there is no support to its existence, at least as long as thermal fluctuations are not taken into account, see [MSNG09]. As a consequence, the inclination angle does not show a square root singularity at the tumbling threshold, in contrast with the present two dimensional simulations where this singularity survives. We believe that the cusp exhibited by $[\eta]$ is directly linked with the behavior of the inclination angle.

A first conclusion that can be drawn is that, besides the VB mode, the dynamics and rheology of a vesicle in two dimensions are qualitatively similar to their three-dimensional analogues. The presence of the VB mode in three dimensions suppresses the cusp singularity in the behavior of the effective viscosity at large enough C_a but does not affect the overall qualitative behavior. These results support the fact that two dimensional simulations are capable of capturing several essential physical properties. When these simulations fail to explain a given feature found in three dimensions (the only situation encountered so far is the suppression of the cusp singularity) it has even been possible to provide a basic reason, and thus to provide to the two dimensional work a robust status.

6.2 The normal stress difference

We have analysed the behavior of the normal stress difference N , and linked it to the vesicle dynamics (figure 6.3). N decreases during tank-treading upon increasing the viscosity ratio. At the critical point N vanishes and remains zero in the tumbling regime, figure 6.2(c). The positivity of the normal stress difference at an inclination angle $0 < \Psi < \pi/4$ is due to the resistance of the vesicle to the elongation imposed by the shear flow (the elongational quadrant of the shear flow is $[0; \pi/2]$, modulo π). $N = 0$ at the transition between tumbling and tank-treading, where a tank-treading vesicle has its main axis parallel to the flow. This is explained through the fact that for $\Psi = 0$ the vesicle is at the boundary between the compression and the elongation of the shear flow (figure 4.5), and is then not stretched. During the tumbling regime, $N = 0$ once averaged over a period due to the restored circular symmetry.

This whole topic is detailed in Appendix B for a rigid filament, which looks to be a very simple model able to offer a clear insight on the origin of stress components in complex fluids.

6.3 Instantaneous stress in the tumbling regime

In the previous sections when referring to vesicles in the tumbling regime we have only presented rheological quantities that have been averaged over a period. We would like to analyse the time dependence of stress, from which we may extract the analogues of effective viscosity (that may be called instantaneous viscosity) and normal stress difference. It must be

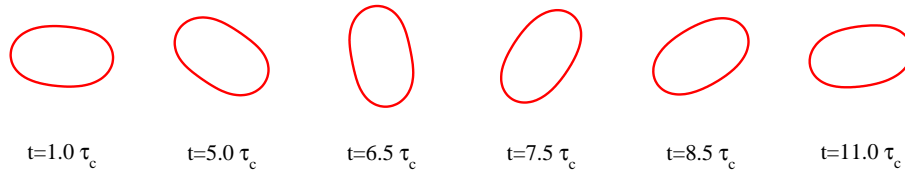


Figure 6.7: Tumbling of a vesicle in a linear shear flow. $\lambda = 8$, $\alpha = 0.9$ and $C_a = 1.0$. Snapshots are taken at irregular time intervals for illustrative purposes.

stressed that, from a theoretical point of view, the way this quantity is defined is similar to the classical definition of the effective viscosity, by using the Batchelor formula (5.5). Thus this definition is not ambiguous, and can be called instantaneous viscosity. Of course, one has to keep in mind that in traditional rheological experiments only an average over time would make sense, due to the uncorrelated dynamics of the vesicles (in the dilute regime) in the sample. Nevertheless, measuring the instantaneous variation of the stress tensor due to a single vesicle can be performed without ambiguity. Moreover, the notion of instantaneous stress is not only of a fundamental interest, but is also experimentally measurable with the advent of microfluidic devices and NEMS (nanoelectromechanical systems). These devices are nowadays capable of measurements with high time resolution on fluid samples with a volume smaller than a microliter [BCMS02, WO07]. Sensing the disturbance of the stress by the presence of a vesicle seems to lie within the precision of experiments. However, the measure would not necessarily reflect the value of an average stress, since the probe sees the medium as a continuum. Nonetheless, the presence of a vesicle will disturb the medium, and should have an effect. This question should deserve an analysis under close scrutiny in the future. Our main objective is basically to draw attention on the fact that measurement on such small scales may become quite feasible in the near future. The question addressed here may help triggering future experimental research along this direction.

Figure 6.7 shows snapshots of a tumbling vesicle and figure 6.8 the time dependence of its inclination angle, intrinsic viscosity and normal stress difference. The capillary number is set to $C_a = 1$, but we have to keep in mind that all the features discussed in the following are also exhibited at $C_a = 10$. The behavior of both effective viscosity and normal stress difference is highly nonlinear and exhibits maxima and minima. This feature, found here numerically, was also briefly reported analytically in three dimensions [DM07]. A surprising feature is that the effective viscosity exhibits two minima within each tumbling period. A convenient representation that

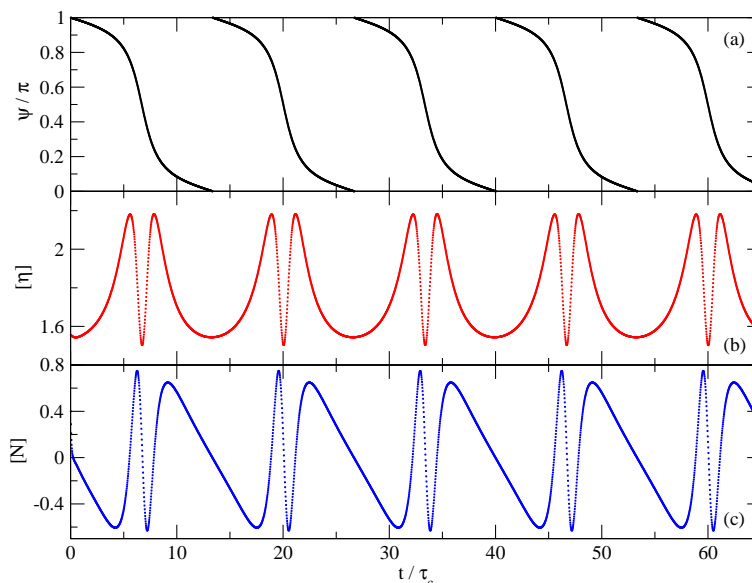


Figure 6.8: Dynamical and rheological quantities in the tumbling regime: (a) inclination angle Ψ , (b) intrinsic viscosity $[\eta]$ and (c) normal stress difference N as a function of time. $\alpha = 0.9$, $\lambda = 8$ and $C_a = 1.0$.

lends itself to a simple interpretation of the results is to plot these quantities as functions of the inclination angle, rather than time, as shown in figure 6.9. Note that the vesicle orientation is defined modulo π (and not 2π), owing to central symmetry. Here we see clearly that the two maxima of dissipation occur at the inclination of $\pm\pi/4$. Let us recall that a linear shear flow can be written as a superposition of pure rotational and elongational components (as shown in section 4.4); elongation is oriented at $\pm\pi/4$ [RBM04] with respect to the imposed flow direction, as sketched in figure 4.5. Only the elongational component (which corresponds to the symmetric part of the shear flow) generates dissipation, while the pure rotation corresponds to rigid-body rotations, which do not involve dissipation. The occurrence of two maxima at the orientation $\pm\pi/4$ is due to the maximal strain efficiency in these directions of the dissipative component of the imposed flow on the vesicle. It must be stressed that these maxima are not due to the deformation of the vesicle itself, since they survive even for nearly rigid vesicles ($\lambda = 200$).

The viscosity is minimal when the vesicle aligns with the flow ($\Psi = 0$), a somehow trivial effect in the light of the previous discussions. Perhaps, the most astonishing and quite counterintuitive effect is the appearance of a minimum of the viscosity for the vertical position (i.e. $\Psi = \pm\pi/2$): our

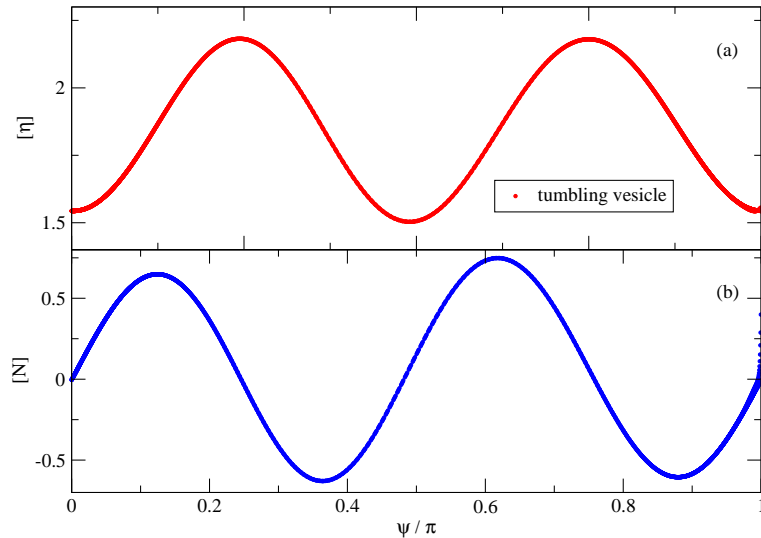


Figure 6.9: Rheological quantities in the tumbling regime: (a) intrinsic viscosity $[\eta]$ and (b) normal stress difference N as a function of the instantaneous inclination angle Ψ . $\alpha = 0.9$ and $\lambda = 8$. Data are shown between $\Psi = 0$ and $\Psi = \pi$, in order to stress that the occurrence of two maxima is not related to the obvious symmetry of the rotation of the vesicle by an angle π .

understanding of this result is that the stream lines of the rotational and elongational components of the flow field are parallel to each other (see figure 4.5), so the competition between the tendency to rotate and strain the vesicle is reduced to a minimum.

The interpretation of the normal stress difference in the periodic regime looks at first sight nontrivial. It turns out that a rigid unidimensional filament in a linear shear flow shows an astonishingly similar rheological behavior, with two maxima and two minima at the same angular positions for both effective viscosity and normal stress difference [TS04]. The computation relative to a rigid rod is detailed in Appendix B. This is a strong argument in favor of the fact that in the tumbling regime, where the vesicle is weakly deformable, the fundamental ingredient to understand rheology is simply its resistance to deformation.

6.4 Dependence on shear rate

We have analysed the behavior of a vesicle suspension upon increasing the shear rate $\dot{\gamma}$. Two series of simulations have been performed, with capillary

numbers $C_a = 1.0$ and $C_a = 10.0$. Vesicles with different reduced area have been considered: $\alpha \in \{0.70, 0.90, 0.95\}$. The results are reported in figure 6.3. It can be seen that the sensitivity on the shear rate depends on the reduced area of the vesicle: in the cases $\alpha \in \{0.90, 0.95\}$ there seems to be no significant dependence upon variation of this parameter. Contrariwise, for smaller α , $\alpha = 0.70$, both dynamics and rheology show significant variations due to shear rate (or to C_a). It is found that upon increasing C_a the transition boundary between tank-treading and tumbling is shifted towards higher values of λ . This effect is traced back to the increase of deformability of the vesicle for significantly deflated vesicles ($\alpha = 0.70$), a fact which is quite invisible for weaker deflation (i.e. for nearly circular shapes), owing to membrane inextensibility (figures 6.10 and 6.11). In addition, a decrease in $[\eta]$ is observed in the tumbling regime.

A vesicle suspension can show then a *shear thinning* behavior if vesicles are sufficiently deflated. In addition, if their viscosity ratio is close to the critical value λ_c , a dynamical transition can occur upon variation of the capillary number C_a , affecting even more the effective viscosity: this is shown in figure 6.12. This complex rheological behavior (shear thinning triggered by deflation and dynamical transition) contrasts with the case of emulsions, which always show shear thinning [KPS94, Pal00]. Drops always deform upon increasing the applied shear but they do not undergo dynamical transitions (except for the possible burst).

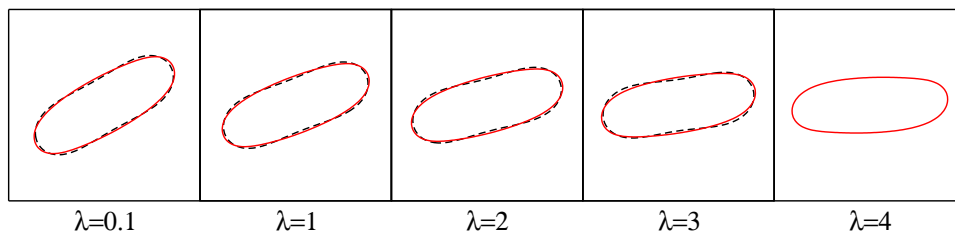


Figure 6.10: Stationary contours of tank-treading vesicles ($\alpha = 0.7$) at $C_a = 10.0$ (solid line) compared with the corresponding ones at $C_a = 1.0$ (dashed line) for different values of the viscosity ratio λ (for $\lambda = 4.0$ and $C_a = 1.0$ there is no tank-treading solution).

Note that the normal stress difference N is normalized in the present work with the factor $\eta_0 \dot{\gamma}$. This contrasts with the conventional notation (used for emulsions, polymer solutions, and so on) $N/\eta_0 \dot{\gamma}^2$. It can be checked that the latter is not dimensionless, and its use in literature is dictated by the fact that for a large variety of suspensions of deformable objects $N \sim \dot{\gamma}^2$. The quadratic behavior is due to the presence in these

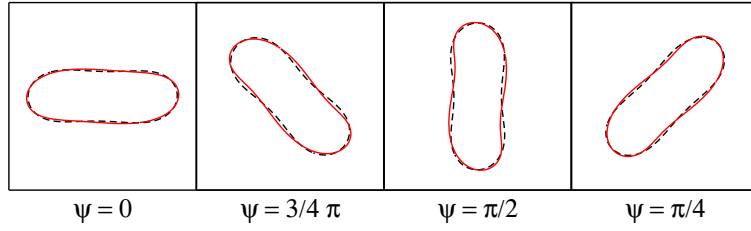


Figure 6.11: Contours of a tumbling vesicle ($\alpha = 0.7$ and $\lambda = 20.0$) at $C_a = 10.0$ (solid line) compared with the corresponding ones at $C_a = 1.0$ (dashed line) for different values of the inclination angle Ψ .

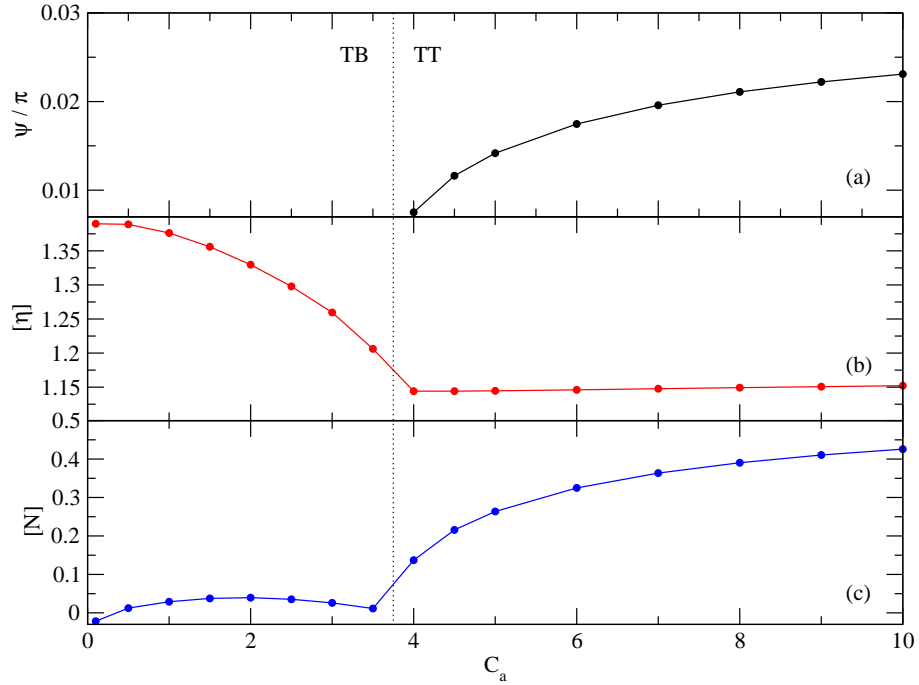


Figure 6.12: Dynamics and rheology of a vesicle with $\alpha = 0.7$, $\lambda = 4.0$ as a function of the capillary number C_a . (a) stationary inclination angle Ψ , (b) intrinsic viscosity $[\eta]$ (showing shear thinning) and (c) normal stress difference N .

systems of an internal (or intrinsic) time scale which depends on $\dot{\gamma}$. This time scale corresponds to the deformation (elongation) of the suspended entities, which is proportional to $\dot{\gamma}$. For vesicles, due to the inextensibility of the membrane, there is a weak dependence of the shape on $\dot{\gamma}$ (see figure 6.10), and the vesicle elongation quickly attains a saturation regime. Thus, we view the absence of an intrinsic time scale proportional to $\dot{\gamma}$ (see

[Lar99], 418-419), to be the source for the linear behavior of N with $\dot{\gamma}$ (see also [DM07] for analytic derivation in the small deformation limit).

6.5 Comparison with drops

Since a vesicle is a droplet enclosed in a phospholipidic membrane, a comparison with emulsion rheology will provide valuable information on the role of the membrane. Drops and vesicles are distinctly different systems: (i) drop interface is governed by tension, which resists area increase, while the vesicle membrane is controlled by resistance to bending, (ii) the drop can change its area, while a vesicle is subject to local membrane inextensibility. The latter property is the most serious ingredient to be emphasized in what follows.

A first difference between vesicle and drop rheology can be obtained by comparing the analytical expressions derived for three-dimensional spherical drops [Tay32, FA70] and quasi-spherical vesicles in the tank-treading regime [Mis06, DM07]:

$$\frac{\eta}{\eta_0} = 1 + \frac{5}{2}\phi \left(1 - \frac{3}{5(\lambda + 1)} \right) \quad \text{for drops} \quad (6.6)$$

$$\frac{\eta}{\eta_0} = 1 + \frac{5}{2}\phi \left(1 - \frac{\Delta}{40\pi}(23\lambda + 32) \right) \quad \text{for vesicles} \quad (6.7)$$

where Δ , a small parameter in (6.7), is the excess area from a sphere, related to the reduced volume ν – the three dimensional analogue of α – via $\Delta = 4\pi(\nu^{-2/3} - 1)$. We recall here that $\nu = [V/(4\pi/3)]/[A/(4\pi)]^{3/2}$ where V is the volume and A the area of the membrane, and $A = r_0^2(4\pi + \Delta)$. While expression (6.6) is an *increasing* function of λ , i.e. the effective viscosity increases with the internal viscosity of the drop, (6.7) is on the contrary a *decreasing* function of λ for tank-treading vesicles. This shows that the phospholipid membrane has a significant effect on the rheology of the suspension. Note that 6.6 is obtained by assuming that the drop is spherical. Of course under shear flow the drop will always deform, but the overall behavior of the viscosity predicted by Taylor remains essentially the same – on the proviso that the deformation is small enough – (see [FA70, KPS94]). Therefore it is reasonable to compare 6.6 with 6.7 which is obtained for a small deformation relative to a sphere (for a sphere a vesicle behaves as a rigid particle due to membrane incompressibility).

An exhaustive analysis of drop dynamics and rheology can be found in [KPS94], here we shall exploit our own simulations in order to present a clear comparison, focusing on the dependence on the viscosity ratio λ . For

this purpose, we have found it more convenient to use the PF model. Indeed, this method delivers directly the velocity field in the whole numerical domain. The analysis of this field will allow us to shed light on the interpretation of the rheological results. Note that the bulk velocity field can be computed within the boundary integral method as well, but this requires some additional numerical treatments.

We define the drop capillary number as $C_{a\gamma} = \eta_0 \dot{\gamma} R / \gamma$, where γ is the surface tension of the drop, and R is its radius of the equivalent circle. We fix the value of the surface tension of a drop in such a way that the drop shape remains as close as possible to that of the vesicle with reduced area $\alpha = 0.9$ (figure 6.14). The estimated value of the surface tension which fulfills this requirement yields $C_{a\gamma} = 0.3$. On the other hand, it has to be kept in mind that drops tend to become more circular upon an increase of λ (figure 6.15). The behavior of the intrinsic viscosity as a function of the viscosity ratio λ for a suspension of vesicles and for an emulsion are quite different (figure 6.13). A comparison of the two behaviors in the range of λ where both the vesicle and the drop exhibit a stationary shape (i.e. within the tank-treading regime of the vesicles; we consider a low capillary number so that drops maintain their integrity), reveals the the same trend difference of (6.6) and (6.7): the intrinsic viscosity increases for emulsions while it decreases for vesicle suspensions upon increasing λ . A key point in order to understand this difference lies in the inspection of the velocity fields around the suspended entities (figure 6.14).

For a two dimensional vesicle, the conservation of the local length of the membrane leads to the constraint of uniform velocity around the membrane itself, while the absence of this constraint for drops allows for a non-uniform velocity.

For a vesicle, the perturbation to the velocity field is enhanced further when it occupies a larger section in the direction of the velocity gradient, that is when the orientation angle ψ is large. Since ψ is a decreasing function of λ , figure 6.13(a), dissipation is also a decreasing function of λ and consequently the effective viscosity too. This explains the decline of the viscosity in the tank-treading regime, figure 6.3(b). Note also that this effect should be more pronounced for more elongated vesicles (smaller reduced area α), because with the same variation of λ the decline of the tank-treading angle (figure 6.3(a)) and of the cross-section of the vesicle in the direction of the gradient of the imposed flow (figure 6.4) are higher. This simple physical interpretation agrees well with the numerical results, which reveal stronger variations of the intrinsic viscosity for smaller α (figure 6.3(b)).

The situation with drops is quite different. Note that both the drop and vesicle orientation angles decrease with λ (see figure 6.13). Nevertheless, in

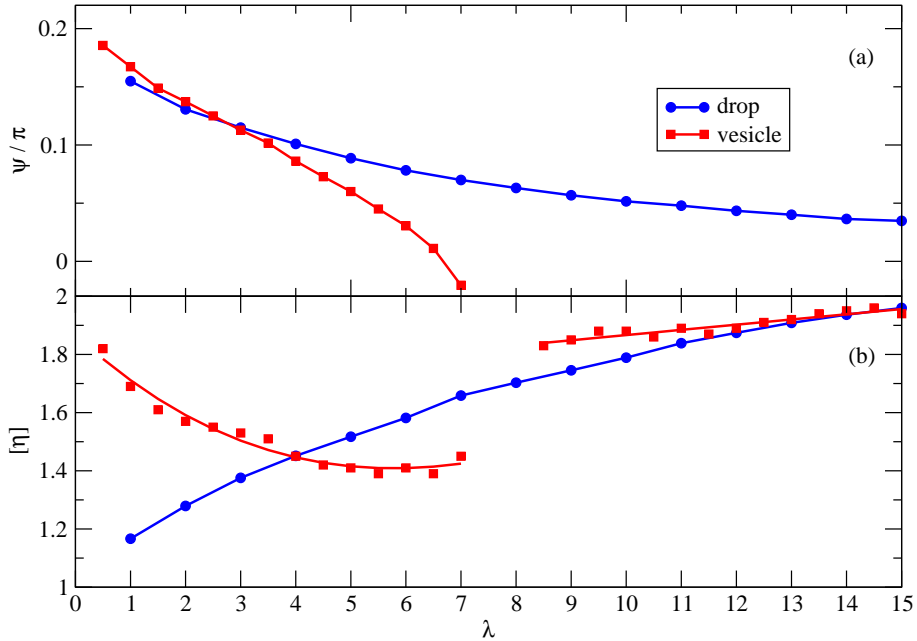


Figure 6.13: Comparison between drop and vesicle suspensions: (a) inclination angle Ψ in the stationary regimes and (b) intrinsic viscosity $[\eta]$ of a suspension of vesicles (data and guideline) and of a suspension of drops. The data refer to a vesicle of a reduced area $\alpha = 0.9$ and to a drop in a flow having a capillary number $C_{a\gamma} = 0.3$.

the former case the viscosity increases with λ while the opposite is found in the latter case. A close inspection of both the velocity field and the precise deformation of the drop will be essential to clarify this difference. The viscosity ratio plays a central role and, unlike vesicles (characterized by membrane inextensibility), no constraint is directly imposed on the velocity field by the drop surface. For a drop, increasing internal viscosity means decreasing its deformability. The consequences are two-fold: (i) the drop assumes a more circular shape (and thus, unlike vesicles, the cross-section in the direction of the flow gradient does not vary noticeably, as it can be appreciated in figure 6.15(a)) and (ii) the perturbations caused by a drop on the imposed flow, which are not limited by any surface incompressibility condition, leads to ample enough velocity gradients (and thus to increase of dissipation) close to the surface. This simple argument highlights the central role played by the membrane of the vesicle: not only is the membrane responsible for the various complex dynamics of the vesicle, but also it induces a peculiar rheological behavior. Finally, let us mention that in the

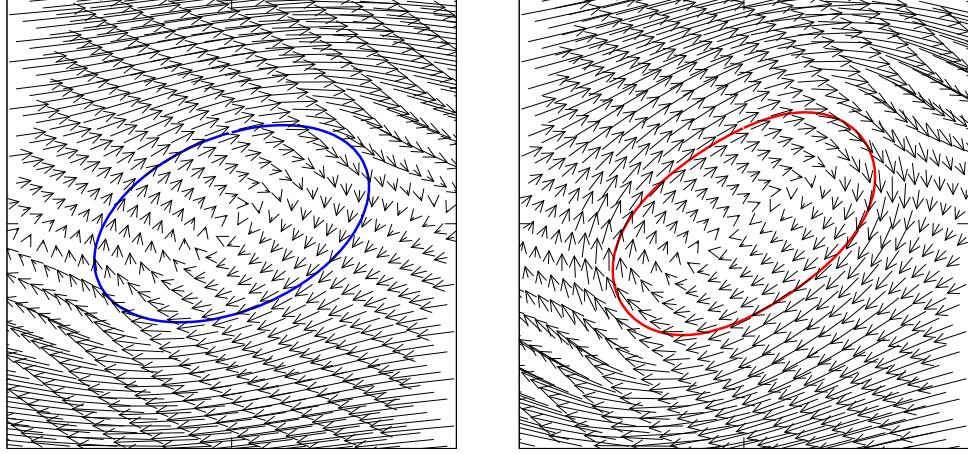


Figure 6.14: This figure shows a drop (left, capillary number $C_{a\gamma} = 0.3$) and a vesicle (right, reduced area $\alpha = 0.9$, capillary number $C_a = 1.0$) and their corresponding velocity fields (we have focused the attention on the central region of the simulation box).

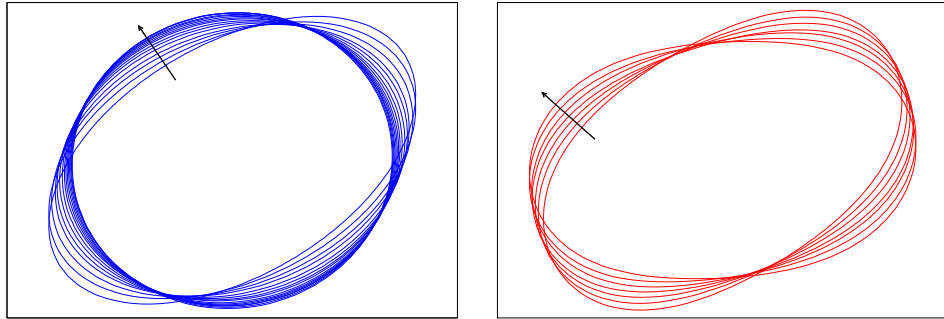


Figure 6.15: Steady contours of (a) drops and (b) vesicles. For the drops the capillary number is $C_{a\gamma} = 0.3$ and the viscosity ratio $1 \leq \lambda \leq 15$ (increasing in the sense of the arrow). For the vesicles the capillary number is $C_a = 1.0$ and the viscosity ratio $1 \leq \lambda \leq 7$ (increasing in the sense of the arrow). Snapshots from the PF method.

analytical theory to leading order, it is the incompressibility condition for the membrane that controls rheology, and not the bending energy [DM07].

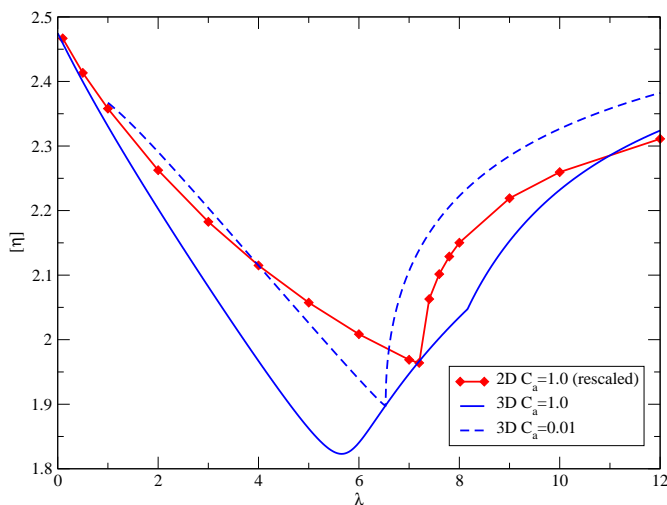


Figure 6.16: Three dimensional theory ($\Delta = 0.25$) from [DBP⁺07] compared with rescaled two dimensional results of the present work ($\alpha = 0.95$). Intrinsic viscosity $[\eta]$ as a function of the viscosity ratio λ .

6.6 Comparison with three dimensional theory and experiments

While the present study is focused to two dimensions, it may be worthwhile to attempt a comparison of our results with the available three dimensional analytical theory and with experiments. It must be remembered that before comparing two and three dimensional intrinsic viscosities a preliminary rescaling has to be performed, as dictated by the different values of the Einstein coefficients in two and three dimensions (i.e. we shall attempt the comparison after multiplying two dimensional data of the intrinsic viscosity by a factor $2.5/2$). In addition, we have to convert a reduced volume ν (corresponding to three dimensions) into a reduced area α (defined in two dimensions). Since a two dimensional vesicle corresponds to a translationally invariant form in the direction perpendicular to the shear plane, a natural choice is to consider the maximum section in the shear plane for the three dimensional vesicle, compute the corresponding reduced area of this section, and then compare it to α . Once the above preliminary rescaling and conversion are made, we compare the results with those obtained analytically by [DBP⁺07], see figure 6.16. We focus on the analytical results with $\Delta = 0.25$ (i.e. $\nu \cong 0.97$ – the value is chosen close to that of a sphere so that the analytical theory is expected to be quantitative), and $C_a = 1.0$. Using the conversion rule discussed above, we find $\nu = 0.97 \leftrightarrow \alpha = 0.95$.

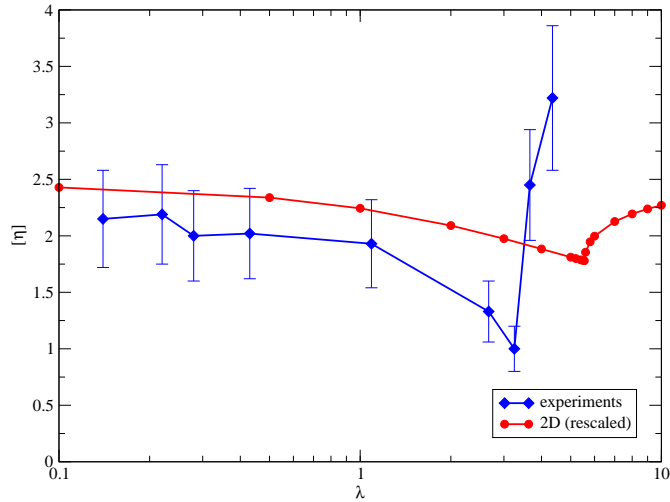


Figure 6.17: Intrinsic viscosity $[\eta]$ as a function of the viscosity ratio λ . Experimental values and a three dimensional theory from [VMP⁺08] compared to the present work.

The quantitative agreement between two dimensional numerical data and three dimensional analytical results is quite satisfactory. It is interesting to note how the numerical results for $C_a = 1.0$ compare surprisingly well with the analytical ones at $C_a = 10^{-2}$. This can be traced back to the fact that the presence of the VB mode in three dimensions can be suppressed for $C_a = 10^{-2}$ and this has the effect of improving the agreement between two and three dimensions. Note that since for such values of α the results are found to be quite insensitive to C_a (figure 6.3), taking a smaller value of C_a has as a main effect the suppression of the VB mode and not insignificant alteration of other quantities.

The comparison with experiments [VMP⁺08] reported in figure 6.17 is somehow difficult, due to vesicle polydispersity ($0.9 \leq \nu \leq 1.0$), and to finite volume concentration ($3\% \leq \phi \leq 12\%$) of the samples. If we take $\alpha = 0.90$ we find the corresponding three dimensional reduced volume to be $\nu = 0.94$ (a value close to the average experimental one). We also rescale our values of the intrinsic viscosity, as explained above. The agreement is partially satisfactory.

6.7 Highly deflated vesicles

In this section the influence of the reduced area α on the dynamics and rheology is discussed. Among the three parameters (α, C_a, λ) that govern

the dynamics of a vesicle in a shear flow, this is the hardest to be scanned extensively. This is because α affects the geometry of the vesicle: both highly circular and highly deflated vesicles are a challenge for numerical simulations, as discussed hereafter.

In order to deal efficiently with this problem, we use an accurate numerical code written by G. Biros *et al.* [VGZB09] and described in section 5.5.

Two reasons motivate the choice of this Boundary Integral implementation for the extensive analysis of the parameter α , from 1 to the lowest attainable. The first one is the ability of this code to simulate nearly spherical (and spherical) vesicles. The second is the spectral accuracy in the computation of surface derivatives. In fact, when considering extreme values of deformation, where the vesicle has such a biconcave shape that approaches self-intersection (see figure 6.18), precision in the derivative computation is crucial². The circular limit, although not very interesting by itself, is important to check the accuracy of the results, since exact analytical solutions exist for the dynamics and rheology of non-interacting disks, as reported in detail in Appendix A [CZM68, BBBC81, Bra84].

In this section we restrict ourself to the case of a vesicle having the same viscosity η of the embedding fluid: $\lambda = 1$. Being interested on the dependence upon the reduced area α , we fix the capillary number C_a for all the simulations presented in this chapter. We set $C_a = 0.1$. The choice of this value is complimentary to the choices of the previous section, where we investigated in detail $C_a = 1$ and $C_a = 10$. At $C_a = 0.1$ membrane bending energy dominates over the forces due to the flow ($C_a \ll 1$).

We have scanned values of α in the interval $\alpha \in [0.3; 1.00]$. In the interval $\alpha \in [0.32; 1.00]$ vesicles show tank-treading (see figure 6.18), while below $\alpha = 0.32$ the vesicle tumbles. In the following paragraphs we detail the dynamics and rheology of tank-treading vesicles and we document the occurrence of tumbling for vesicles with a viscosity contrast $\lambda = 1$.

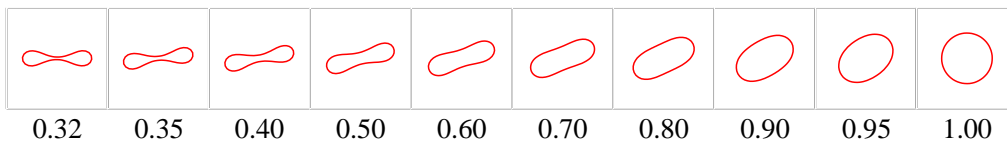


Figure 6.18: Tank-treading vesicle shapes with different reduced areas α under linear shear flow at $C_a = 0.1$. The value of the reduced area α is reported below the corresponding shape.

²We remind that the being force contains the second derivative of the curvature of the membrane, i.e. a fourth derivative, whose numerical computation is challenging.

Dynamics: inclination angle, tank-treading velocity and bending energy

In figure 6.18 we report the equilibrium shapes corresponding to tank-treading vesicles in the interval $0.32 \leq \alpha \leq 1$. In order to characterize the dynamics of the vesicle, we measure the inclination angle of the stationary shape, the tank-treading velocity of the membrane and the bending energy associated with its shape.

In figure 6.19(a) we plot the inclination angle Ψ (measured from the direction of the imposed flow) of a tank-treading vesicle. The angle tends to $\Psi = \pi/4$ for a vesicle having a circular shape (see figure 6.18), as expected analytically [KS82], and numerically [KWSL96, BBM04] and as already seen in chapter 6. The surprising result is that the inclination angle goes to zero for a finite reduced area $\alpha_c = 0.32$. A viscosity contrast bigger than one (i.e. viscosity inside the vesicle bigger than the one of the suspending fluid) is needed for larger α in order to achieve flow alignment. No stationary solution is stable below this limit, and then tank-treading cannot be observed below the critical value of the reduced area α_c : here tumbling takes place.

In figure 6.19(b) we plot the tank-treading velocity of the membrane, i.e. the velocity at which the membrane moves around the stationary shape of the vesicle. Since the membrane is inextensible, the magnitude of this velocity must be the same on all the points of the membrane (in two dimensions). Its value decreases for a smaller reduced area of the vesicle. This is expected due to the fact that with decreasing α the vesicle aligns further with the flow and the torque due to the imposed flow is transferred more to inclination than to tank-treading. For a circular vesicle we obtain the tank-treading velocity $v_{tt} = 0.502 \dot{\gamma}$ in very good agreement with the predicted value $\dot{\gamma}/2$ (see Appendix A, section A.4).

In figure 6.19(c) we plot the total bending energy of the membrane according to (4.1): not surprisingly it increases with the deflation of the vesicle, since the curvature becomes locally higher.

We can compare the results with the value E_B^c for a circle of radius one (i.e. $c = 1$):

$$E_B^c = \kappa \int_0^{2\pi} \frac{c^2}{2} d\phi = \kappa\pi \quad (6.8)$$

and the numerical result obtained for a circular vesicle is $E_B^c = 3.138\kappa$.

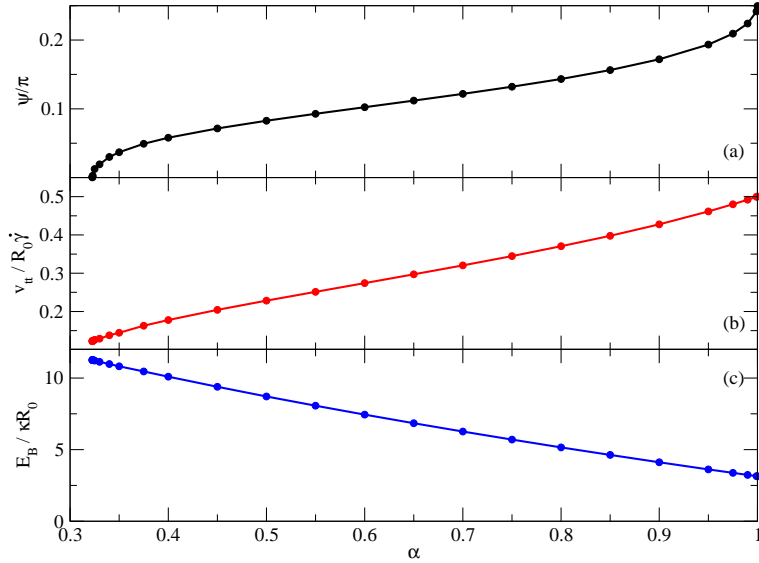


Figure 6.19: Inclination angle Ψ , tank-treading velocity v_{tt} and bending energy E_B of tank-treading vesicles as a function of the reduced area α .

Rheology: effective viscosity and normal stress difference

The rheological quantities that are investigated are the effective shear viscosity η_{eff} of the suspension and the normal stress difference N . We consider the intrinsic effective viscosity and the intrinsic normal stress difference defined in (6.3) and (6.4). Their computation is carried out using equation (5.5), simplified by the fact that $\lambda = 1$. In figure 6.20(b) we represent the intrinsic viscosity, which is maximal for a circular vesicle and decreases for smaller reduced area. This can be explained as follows: the local incompressibility of the membrane ensures, in two dimensions, the uniformity of the velocity along the vesicle contour. So a deflated vesicle, having a smaller cross-section in the shear flow (see figure 6.18), imposes on it smaller constraints, thus resulting in a decrease of dissipation in the embedding fluid. This is the same mechanism already explained in chapter 6 for vesicles with the same reduced area but different viscosity contrast λ .

In the circular limit the intrinsic viscosity coincides with the Einstein coefficient [Ein06, Ein11], representing the intrinsic viscosity of a suspension of non-interacting rigid spheres (or disks in the two-dimensional case). The Einstein coefficient is recovered within an error of 10^{-4} , that is we obtain $[\eta] = 1.9999$ when the analytical result in two dimensions is $[\eta] = 2$ [BBBC81, Bra84] (instead of 2.5 in three dimensions, as computed in Ap-

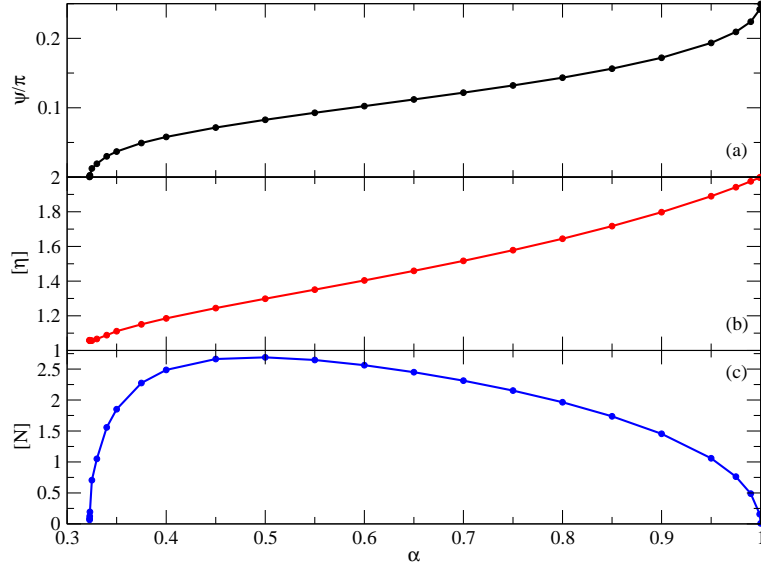


Figure 6.20: Inclination angle Ψ , intrinsic viscosity $[\eta]$ and normal stress difference $[N]$ of a dilute suspension of vesicles as a function of the reduced area α .

pendix A). Note that a circular vesicle, be it fluid inside or not, behaves exactly as a solid particle, since the enclosed fluid undergoes a global solid-like rotation enforced by the vesicle membrane (i.e. this does not hold for a drop).

In figure 6.20(c) we plot the normal stress difference as a function of the reduced area. This rheological observable, normally linked to the elongation of elastic objects, is related here to the orientation of the vesicle in the flow. For a circle ($\alpha = 1$) the analytical solution is $[N] = 0$, while numerically we find $[N] = 0.0245$, providing the order of magnitude of numerical uncertainties on this quantity. We recover this value, $[N] \approx 0$ even at the opposite limit, $\alpha = \alpha_c$. This can be interpreted using a model of unidimensional filament, detailed in Appendix B. Since we obtain $[N] = 0$ at $\alpha = \alpha_c$ (where the vesicle fully aligns with the flow) and at $\alpha = 1$ (where the vesicle is circular), $[N]$ must exhibit an extremum, as shown in figure 6.20(c). This extremum can be expected to be a maximum considering the simple case of a rigid filament in a shear flow, as presented in Appendix B. The precise value of α at which the maximum should be expected ($\alpha = 0.50$ in the simulations) is, at present, not yet completely understood.

Tumbling without viscosity contrast

Simulations have been carried out down to a reduced area $\alpha = 0.3$. Below the critical value λ_c at which the vesicle reaches flow alignment, the vesicle is found to tumble. This fact had not been predicted before³. The nearly self-intersection of the membrane at such a high deflation makes numerical simulations particularly challenging. The required space and time discretization are much finer than those required for tank-treading (the mesh is four times denser and the time step one hundred times smaller), and the dynamics very slow close to this critical point. For this reason we could not scan extensively this regime, and we report here only an example for $\alpha = 0.3$. The contours of the tumbling vesicle are reported in figure 6.21 and the inclination angle as a function of time in figure 6.22. From a physical point of view, the existence of tumbling of a vesicle that does not exhibit viscosity contrast can be explained by looking at the origin of tank-treading. The shear flow exerts a torque on a body immersed in the flow. A vesicle can assume a stationary shape (tank-treading regime) if the torque can be transmitted to the internal fluid, that rotates despite the shape does not change in time. But if this does not occur, the vesicle tumbles. The most often considered cause of impossibility to tank-tread is a high internal viscosity, for which the imposed flow does not succeed in shearing the internal fluid. But another cause can be found in the shape of the vesicle: if it is extremely deflated, the internal fluid should undergo an extremely high shear in the biconcave region in order to allow for tank-treading. This internal shear generates a torque on the membrane, above a certain threshold of which the membrane, and thus the vesicle, starts to tumble. A whole set of simulations close to the tumbling transition would be necessary to quantify this tumbling criterion.

³In [FLSG08] a theoretical curve for vesicles in dimension two for $\lambda = 1$ has actually been traced. A transition to tumbling was found for $\alpha \approx 0.7$ independently of the value of C_a . This value is by far not correct. This is thought to be due to the low order of series expansion (2^{nd} order) of this calculation, which should then only be valid very close to the circular shape, $\alpha \approx 1$.

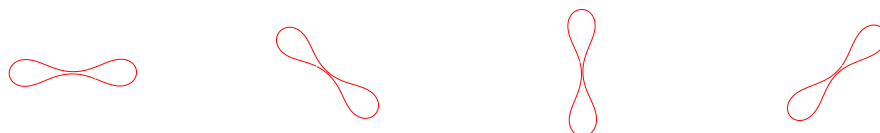


Figure 6.21: Contours of a tumbling vesicle at different inclination angles $\Psi \in \{0, 3\pi/4, \pi/2, \pi/4\}$ ($\alpha = 0.3$, $\lambda = 1$, $C_a = 0.1$).

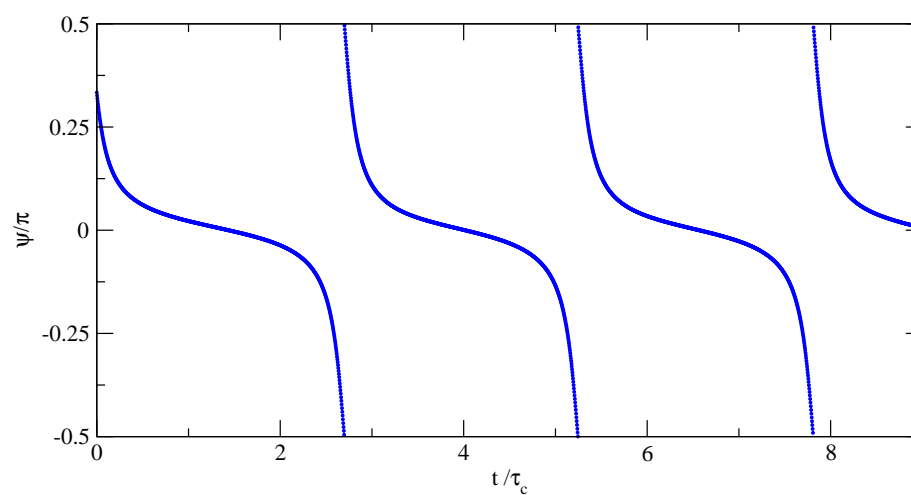


Figure 6.22: Inclination angle Ψ of a tumbling vesicle as a function of time t ($\alpha = 0.3$, $\lambda = 1$, $C_a = 0.1$).

VESICLES IN A POISEUILLE FLOW

Results on unidimensional sets of vesicles in a Poiseuille flow are presented. This situation models the behavior of ensembles of red blood cells in capillaries. It is found that vesicle sets assume a nontrivial spatial organization entirely due to hydrodynamical interactions. Moreover, the existence of a maximal number of vesicles per set is revealed. To my knowledge, no result on this setup exists in the literature. The Fast Multipole Method (FMM), implemented by H. Selmi (*Ecole Polytechnique de Tunisie*, Tunisia) in our collaboration, is presented and used to considerably reduce the computational cost.

Des résultats sur une file de vésicules sont présentés. Cette situation modélise le comportement d'ensembles de globules rouges dans les capillaires. On trouve que les ensembles de vésicules prennent une organisation spatiale complexe entièrement due aux interactions hydrodynamiques. De plus, l'existence d'un nombre maximal de vésicules par ensemble est mis en évidence. A ma connaissance, il n'y a pas dans la littérature de résultats concernant un tel système. La méthode multipolaire rapide (FMM), implémentée par H. Selmi (*Ecole Polytechnique de Tunisie*, Tunisie) dans le cadre d'une collaboration avec nous, est présentée et utilisée pour réduire sensiblement le coût des calculs.

7.1 Introduction

In this chapter we discuss simulations of a series of vesicles in a Poiseuille (parabolic) flow in two dimensions. We consider sets of vesicles aligned along the symmetry axis (x) of the flow, and we restrict ourselves to the case of viscosity ratio $\lambda = 1$. The interest of this configuration is to emulate the behavior of red blood cells in thin capillaries. In our simulations we do not consider walls bounding the fluid domain. Their presence is only modeled via the imposed flow, which is parabolic.

The numerical code used is the Boundary Integral described in section 5.2. Since our simulations involve a large number of vesicles, we have coupled the code with a fast algorithm (the Fast Multipole Method) to compute the integrals appearing in the boundary integral formulation.

7.2 The physical system

We consider sets of vesicles aligned along the symmetry axis of a Poiseuille flow, given by

$$\mathbf{u}(y) = ay^2 \hat{\mathbf{e}}_x \quad (7.1)$$

The local shear rate is

$$\dot{\gamma} = \frac{du_x(y)}{dy} = 2ay \quad (7.2)$$

We define the *capillary number* C_a using the mean value of the shear rate at the vesicle scale ($y = R_0/2$):

$$C_a = \frac{\eta \dot{\gamma} R_0^3}{\kappa} = \frac{\eta a R_0^4}{\kappa} \quad (7.3)$$

The two parameters (C_a, α) determine the dynamics of a single vesicle in a Poiseuille flow, (the viscosity ratio is fixed to $\lambda = 1$).

The behavior of a single vesicle in a Poiseuille flow has already been at the centre of detailed studies, both in bounded and unbounded geometries [NG05, CKPM08, KRC⁺08, KBM09]. The simple study of equilibrium positions and the corresponding vesicle shapes in an unbounded geometry is already a complex task, and has been carried out very recently. In particular, it emerged [CKPM08, KRC⁺08, DVM09] that vesicles in general tend to migrate towards the centreline of a parabolic flow, but for sufficiently small C_a and α , vesicles may reach a stationary position before reaching the center [KBM09].

Other studies focused on the effect of mutual interactions between vesicles in a highly confined geometry, assuming periodic boundary conditions on the inlet and outlet of a short capillary [MNG09], or under the hypothesis of equally spaced vesicles [Poz05].

The study of the dynamics of a dense suspension of vesicles in this flow would be a huge piece of work in the general case. We focus then on the region of the parameter space where a single vesicle migrates to the centreline of the imposed flow: we choose $\alpha = 0.7$ and $C_a = 10$. We initialize the vesicles at the centreline, in order to avoid the transient dynamics corresponding to the migration towards it. This allows us to reduce the complexity of the

system, since a richer dynamics is expected to occur when either the vesicles are not initialized at the centreline or when α and C_a do not correspond to a stable position in the centre of the flow in the single vesicle problem. Although it would be feasible from the numerical point of view, the physical interpretation would need an ample investigation of the parameter space of the multivesicle problem.

7.3 The fast Multipole Method

We use the Boundary Integral method (BIM) detailed in section 5.2 to compute the evolution of the vesicles. This kind of algorithm is intrinsically of order $O(N^2)$, where N is the number of discretization points in the system. In fact, the numerical calculation of the integrals on the surfaces of the vesicles produces a linear system whose solution consumes the majority of the CPU time. A phase of mathematical handling of the matrix containing the physical data of the problem, generated at each time step, allows us to apply the Fast Multipole Method (FMM) [GR87, GR88, Nis02, GD06]. The matrix resulting from BIM is dense and thus difficult to manipulate. A decomposition of the Green's function of the Stokes problem by using the Green's function of the Laplacian operator, as well as variable separation in the Laplacian, enable us to circumvent the problem. Indeed, the action of the Green's function of Stokes problem on the force field is given according to the Laplacian Green's function and its derivative. The matrix arrangement in this well defined form allows us to apply the adequate fast multipolar formulas; indeed FMM is an approximation technique of the matrix-vector product which allows to perform this calculation with optimal efficiency. The use of FMM lowers the computational complexity from $O(N^2)$ to $O(N)$, allowing then for a huge gain in terms of CPU time and memory allocation.

The direct solution of the considered system has until today allowed the precise calculation of dynamics and rheology of one vesicle, but this method is too expensive to be applied to concentrated suspension of vesicles. In this context, FMM offers the possibility to simulate suspensions which count some tens, or even hundreds, of vesicles using a single CPU.

FMM is detailed in Appendix E.

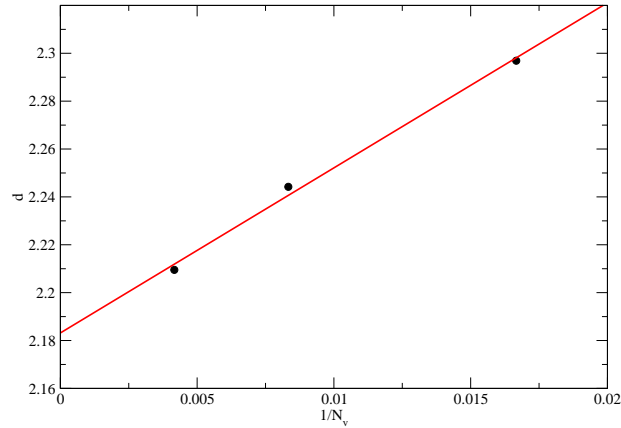


Figure 7.1: Convergence test: distance between two vesicles in the case $n = 2$ as a function of the inverse of the number of discretization points per vesicle N_v .

7.4 Numerical tests

In this section we study the convergence of the code and we analyze the computing time, with special reference to the linear scaling of the FMM with respect to the number of discretization points of the system.

Convergence test

The convergence of the code has been tested. For this purpose, we consider a case with two vesicles, the parameter checked is the distance between the centers of the two vesicles when the system has reached a stationary state. The number of discretization points used is $N_v \in \{60, 120, 240\}$ per vesicle, and the results are shown in figure 7.1 where the distance is plotted as a function of $1/N_v$. A linear fit of the results conveys the idea that already with $N_v = 120$ the error is of the order $2 \div 3\%$, and two times smaller for $N_v = 240$. We consider the first result satisfactory and we proceed to more extensive simulations using $N_v = 120$ discretization points per vesicle. The time step used is $dt = 1 \cdot 10^{-4}$.

Computing times

The CPU time of the code has been studied. Simulations have been run for 10^5 time steps, which is the order of magnitude of the time needed to obtain the equilibrium state for the case with two vesicles. The results are

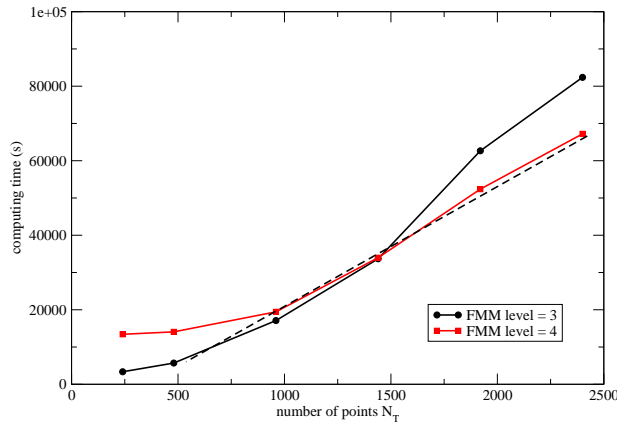


Figure 7.2: CPU time in seconds as a function of the number of discretization points N_T for 10^5 time steps. The dots correspond to simulations with 2, 4, 8, 12, 16, 20 vesicles having 120 points each and using a multipolar development order of 3 and 4. The dashed line shows the linear rescaling of the computing time with respect to N_T , that is retrieved upon the change in the order of the multipolar development.

shown in figure 7.2. Different levels in the recursive decomposition of the computation domain are used for the evaluation of the multipolar moments (see Appendix E): a low level is more convenient for smaller system, while for bigger ones the use of an higher level allows to reach shorter computing times. The linearity of the FMM algorithm with respect to the number of discretization points is retrieved when considering the combination of the lowest computing times among all orders.

7.5 One dimensional vesicle sets

We run simulations for different number of vesicles: the interval $1 \leq n \leq 10$ is extensively studied, moreover few simulations are run with an higher number of vesicles, as it will be detailed in the following. Vesicles are initialized as ellipses elongated in the direction of the velocity gradient (y axis) and the initial spatial separation between them is chosen to be small. The variation of the initial separation, at least below a certain threshold, does not affect the final (equilibrium) state, which can be thus considered as a stable solution with respect to this parameter. The value of this threshold decreases with the increase of the number of vesicles contained in the set. In particular, for $n \leq 6$, a relative distance between vesicle centers equal to four times their average radius is already small enough to let the vesi-

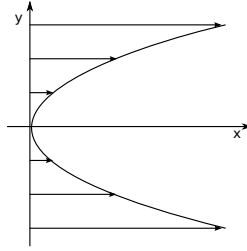


Figure 7.3: The imposed Poiseuille flow. To compare with experiments in a microchannel, the flow should be considered to have the same parabolic profile, but being convex instead of concave, i.e. from the right to the left.

cles approach each other. On the other hand, for $n \geq 7$, this distance is too big and leads to the separation of the set in the course of time. We have decreased the relative distance between vesicles down to a distance between membranes of around 0.5 vesicle radii. The resulting configurations are shown in figure 7.4, the imposed flow in figure 7.3. Simulations for $n \leq 10$ vesicles have been carried out up to the equilibrium state of the system. For bigger ensembles it is found that vesicles detach from the cluster, and simulations have been run up to a reasonable computing time (that is already of several weeks on three CPUs for the biggest sets).

A quantity of interest is the distance between consecutive vesicles as a function of the number of vesicles composing the set. The bigger the number of vesicles in the ensemble is, the more inhomogeneous is the distribution, with a higher density on the rear of the sets (i.e. right side of figure 7.4). This inhomogeneity is not trivial and arises from the complex hydrodynamic interactions between vesicles: the flow pattern established between each pair of consecutive vesicles determines the relative distance at equilibrium.

The relative distances between vesicles are represented in figure 7.5. Here it is shown that the distance between neighboring vesicles increases at the front of the set (that is, on the left in figure 7.4) upon increasing n . For bigger ensembles of vesicles it is eventually found that the leading vesicles detach from the bunch.

In figure 7.6 we represent the velocity of the vesicle sets at equilibrium (all the vesicles in the set move at the same speed). In the following we will always refer to the velocity difference between the imposed flow (computed at the centreline of the parabolic profile, which is zero in our case) and the vesicle sets. This allows to compare the results to what would be experimentally observed in a capillary (where the velocity is nonzero at the centreline) and corresponds to look to the velocity of the sets from the right to the left in figure 7.4. The velocity is found to be a decreasing function

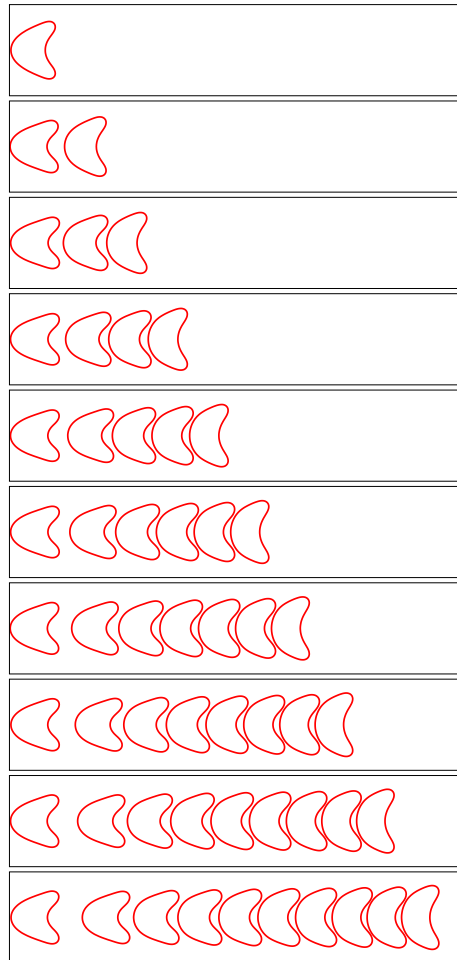


Figure 7.4: Stationary contours of vesicle sets in a Poiseuille flow ($n \in [1 : 10]$). $\alpha = 0.7$, $C_a = 10$: for these parameter values, sets are not stable for $n > 10$.

7. VESICLES IN A POISEUILLE FLOW

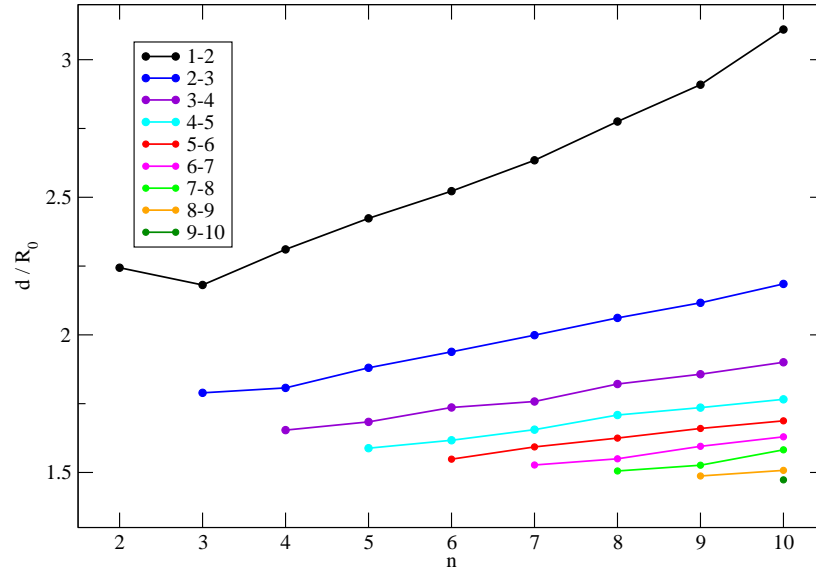


Figure 7.5: Distances between neighboring vesicles as a function of the number of vesicles composing the set. Vesicles are numbered from left to right referring to figure 7.4. The general trend is an increase of relative distances upon increase of the number of vesicles in the set.

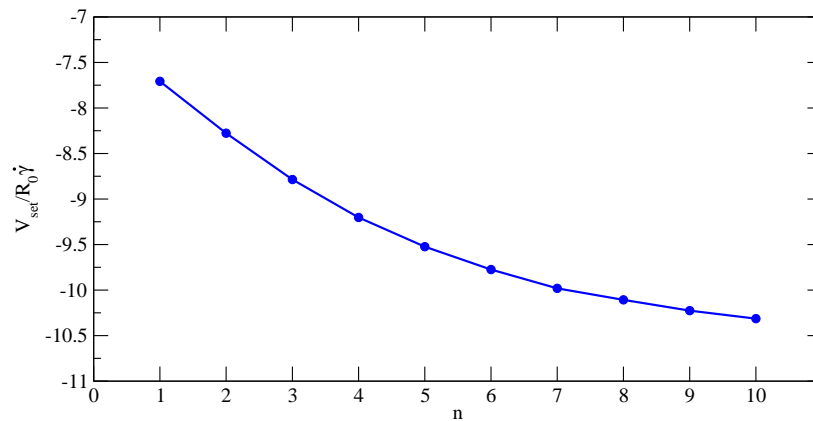


Figure 7.6: Velocity of the vesicle sets as a function of the number of vesicles composing the set (defined as difference between the velocity of the imposed flow at the centreline and the velocity of the sets).

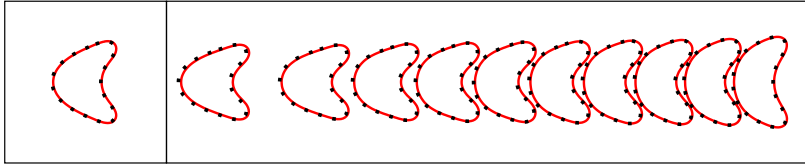


Figure 7.7: Contours for a set with eleven vesicles. The left box contains the first vesicle, that has detached from the others, while in right box the contour of the ten vesicles that remained regrouped. The dotted shapes represent the shapes of a single vesicle and of a set containing ten vesicles from the beginning, respectively (from figure 7.4).

of the number of vesicles in the set. This result is not surprising: vesicles are passively advected by the flow, so being regrouped decreases the drag per vesicle and then the speed.

The whole picture changes when considering ensembles of vesicles of size $n \geq 11$. In fact, sets are found to be unstable above this threshold, and they divide in smaller clusters. In the case studied, this happens in the form of detachment of vesicles from the set, up to the biggest stable configuration, which is $n = 10$ in our case. We detail here the behavior for $n = 11$. In figure 7.7 the contours are reported for $n = 11$. The ten vesicles that remain together organize with the same spatial configuration assumed by a set containing initially only ten vesicles. This does not look surprising, since interactions are not expected when the distance between the bunch and the detached becomes large.

It is interesting to note that even at big distances the velocities of both the detached vesicle and the bunch are remarkably lower than then the velocities of the single vesicle and of the set of ten, respectively. For instance, the configuration reported in figure 7.7 corresponds to a distance between the single vesicle and the bunch of around 100 vesicle radii, and the two velocities corresponding to this configuration are 10.0 and 6.45 (in units of $R_0\dot{\gamma}$), to be compared with 10.3 and 7.7 (data from figure 7.6). This is thought to be due to the long interaction distance in two dimensions.

For $n > 11$ it is found that the leading vesicles detach one at a time from the set, giving rise to an interesting transient dynamics: the first vesicle detaches, followed soon after by the second; they form a doublet, whose speed is lower than the one of a single vesicle. So, when the third vesicles detaches, it joins them to form a triplet, and so on. This dynamics is represented in the graph of figure 7.8, where we represent the inter-distance between the first seven vesicles of a set that initially counts 15 vesicles.

A more exhaustive analysis of this subject is needed. In particular, it

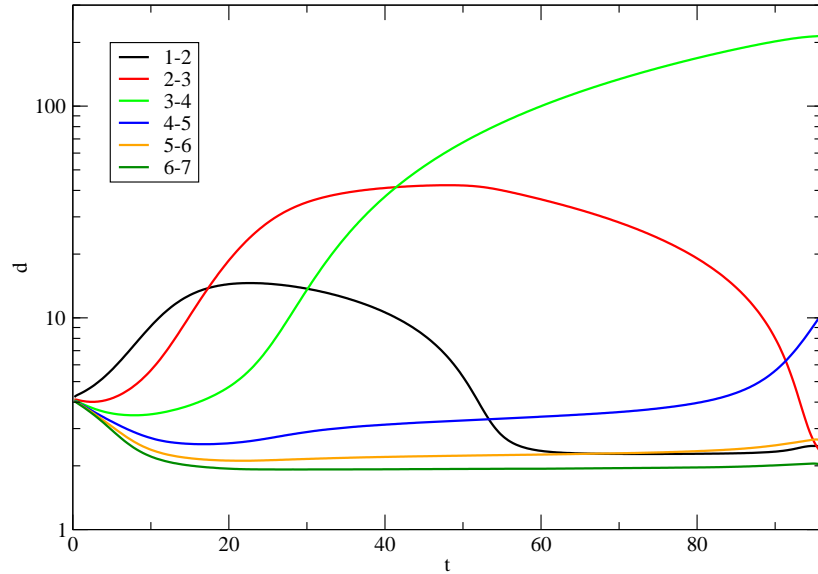


Figure 7.8: Distances between neighboring vesicles for a set with $n = 15$ vesicles as a function of time (measured in units of $\dot{\gamma}^{-1}$). The graph shows the successive detachment of vesicles from the set (the system did not reach an equilibrium state before the end of the simulation).

will be interesting to determine the influence of parameters like the reduced area and the capillary number on the formation of clusters.

An element that deserves more attention is the role of the boundaries: in fact, they are known to reduce the interaction distances between particles in a flow [DCLR05]. Nevertheless, the formation of clusters should be determined by the interactions between neighboring vesicles, and not to long-distance interactions.

The mechanism of cluster breaking intrigues from the point of view of a biological interpretation: it might be seen as a self-regulating mechanism to avoid the formation of big clusters, a fact that might prove useful for red blood cell circulation and oxygen exchange. This is at present a speculation that requires further studies before reaching a more conclusive answer.

VESICLES IN A CURVED FLOW

The motion of vesicles in a curved flow (either an unbounded vortex or a Couette flow) is analyzed. Vesicles are found to migrate inwards. This is contrary to what is usually observed, i.e. migration towards low shear rate regions (which are in the outer part of the considered flows). The result is explained via the coupling of flow curvature and normal stress difference and is believed to be applicable to a vast majority of particle suspensions. The analysis of multiple vesicles in a Couette device reveals self-organization in a rim closer to the inner cylinder, resulting from a subtle interaction among vesicles.

Le mouvement de vésicules dans un écoulement courbe (vortex non borné ou écoulement de Couette) est analysé. On trouve que les vésicules migrent vers l'intérieur. Ceci est le contraire de ce qui est souvent observé, c. à d. une migration vers des zones de faible cisaillement (qui se trouvent vers l'extérieur dans les écoulements considérés). Le résultat est expliqué par le couplage de la courbure des lignes d'écoulement avec la différence des contraintes normales, ce qu'on peut supposer être un résultat généralisable à la majorité des suspensions de particules. L'analyse du comportement de plusieurs vésicules dans un dispositif de Couette montre une auto-organisation des vésicules-mêmes sur un anneau proche du cylindre interne, qui résulte d'une subtile interaction entre les vésicules.

8.1 Cross-streamline migration

In this chapter we deal with the problem of the motion of particles across the streamlines of the imposed flow: this phenomenon is called *cross-streamline migration*. We focus on the case of an imposed flow with curved flow lines.

A single rigid particle immersed in a Newtonian fluid at vanishing Reynolds number Re cannot migrate in the direction transverse to the flow lines

[BG72]. On the contrary, deformable particles have the ability to migrate across the streamlines, even at $Re = 0$, with the proviso that a certain symmetry is broken, such as centro-symmetry in linear shear flow. Symmetries may be broken due to the presence of walls, gradient in shear rate (e.g. Poiseuille flow) [UNH93, MT00, CKPM08, KRC⁺08, KBM09], or the presence of flow line curvature (e.g. cylindrical Couette flow). A prominent example of lateral migration in Poiseuille flow is blood flow in which the cross-streamline migration of red blood cells can result in ample collapse of blood viscosity, reducing thus blood flow resistance in microvasculature (the Fåhræus-Lindqvist effect).

Cross-streamline migration induces an inhomogeneous distribution of the suspended entities and creates thus a microstructure. Microstructures spontaneously arise in many complex fluids, and may have a dramatic impact on rheology [CRB⁺02]. Cross-streamline migration is then an essential factor in different domains, such as industrial polymer processing [Wu79], DNA sorting [SLZ74], drop dynamics [CL79], as well as in biology.

A common belief is that deformable particles have the tendency to migrate towards regions of low shear rates [UBL07, SSRP07, KRC⁺08, DB08, HV10]. In some circumstances, however, the opposite is predicted (the case of drops in a certain range of viscosity contrast between the internal and external fluids [CL79]). There seems to be no clear general answer regarding the determination of the migration direction.

We carry out simulations with vesicles both in an unbounded vortex and in a Taylor-Couette cell. The latter realistic geometry is motivated by the fact that the Taylor-Couette system is widely used as a basic device for the study of rheology of complex fluids, while the more abstract one, the unbounded vortex, will allow the identification of the role of flow lines curvature excluding any migration due to the bounding walls. In fact, the lift produced by the boundaries is a long range effect that is non-negligible even at the centre of the cell [Oll97, CMC⁺08, KCMP09], and is thus difficult to discern from the effects due to flow line curvature [CL81, HJ06].

8.2 Unbounded vortex

In this section we present numerical simulations of single vesicles in an unbounded vortex. Although all the results involve vesicles, the interpretation given seems to be of general validity. This is why we dedicate a short paragraph to the discussion of their application to other systems, typically drop suspensions.

Vesicles

We first consider the idealized situation of an unbounded flow in order to exclude any migration due to bounding walls: this allows us to identify the role of flow lines curvature. The straining component of this unbounded flow is of the Taylor-Couette type: it is an *irrotational vortex*, expressed in cylindrical coordinates (r, θ, z) by $v_\theta(r) = a/r$, $v_r = v_z = 0$, a being a constant. In fact, for a Couette flow $v_\theta(r) = a/r + br$; we drop here the term br , which corresponds to a rigid body rotation and does not affect the shear rate.

It will be seen that vesicle inward migration, or the lack thereof, depends on its dynamical regime (tank-treading vesicles migrate inwards, while tumbling ones do not).

Numerical simulations are carried out using the Boundary Integral code detailed in section 5.2 [GBM10]. We consider a single two-dimensional vesicle immersed in a Newtonian fluid. Vesicles are initialized at a distance of $10R_0$ from the origin, where $R_0 = \sqrt{A/\pi}$, A being the vesicle surface. The length unit is chosen to be R_0 in our simulations. The dimensionless numbers that enter the problem are the reduced vesicle area α , the viscosity contrast λ and the capillary number $C_a = \eta_0 \dot{\gamma} R_0^3 / \kappa$. In the simulations both α and λ are varied. The value of C_a depends on the radial position, while a is fixed to a value $a = -10$ (the dependence of vesicle dynamics on this parameter is weak [GBM10]). We have performed three sets of simulations for different $\alpha \in \{0.7; 0.8; 0.9\}$. For every set the range $\lambda \in [1, 10]$ is explored, a range that covers both tank-treading and tumbling regimes [KS82, BRS⁺04, GBM10].

Typical simulation results are shown in figure 8.2. Tank-treading vesicles migrate towards the center, while tumbling ones show a negligibly small outward migration. Migration strength is found to depend on reduced area

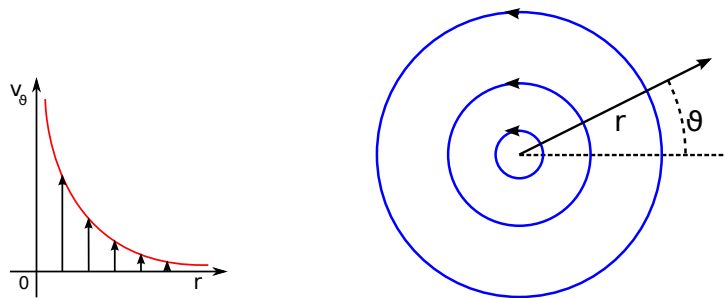


Figure 8.1: Sketch of the imposed velocity field $v_\theta \sim 1/r$: left: the velocity profile; right: the streamlines.

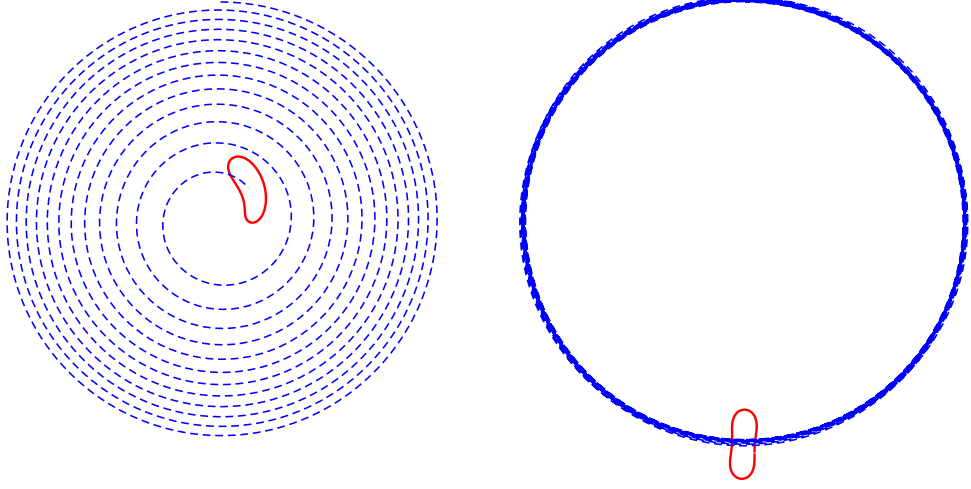


Figure 8.2: Trajectory and contour of a tank-treading vesicle ($\alpha = 0.7$, $\lambda = 1$) migrating towards high shear regions (left) and of a tumbling vesicle ($\alpha = 0.7$, $\lambda = 4$) showing no significant radial migration (after 13 revolutions and 8 tumbling periods, right).

and viscosity contrast in a non trivial way. In figure 8.4 we report the migration velocity v^{mig} for different vesicles at fixed initial radial position $r = 10R_0$. Analogous results are obtained for any distance $3 \leq r/R_0 \leq 10$. In the left panel, the migration velocity is shown as a function of the two independent dimensionless parameters explored in our simulations, namely (α, λ) .

The data do not seem to show a simple trend. For example, the curves in figure 8.4 (left) for migration velocities obtained for different vesicles intersect at some viscosity contrast. This points to the absence of a simple law in this parameter space. We have thus attempted to rationalize these results by evoking basic physical facts that distinguish a simple fluid from a complex one. A particular property of complex fluids is the manifestation of normal stress difference. We have thus represented the data (figure 8.4b), in terms of the normal stress difference N measured in the local (x, y) coordinate system (see figure 8.3 for notations).

We recall that the normal stress difference is defined as $N = \sigma_{xx} - \sigma_{yy}$, where $\boldsymbol{\sigma}$ is the stress tensor of the suspension, computed using equation (5.5) following [Bat70, KPS94] with respect to (x, y) as sketched in figure 8.3, and corresponding to the directions of $(\mathbf{e}_\theta, -\mathbf{e}_r)$ for the centre of mass of the vesicle. The local shear rate in the irrotational vortex is $\dot{\gamma} = -2a/r^2$.

Interestingly enough we observe in figure 8.4 (right) that the data closely

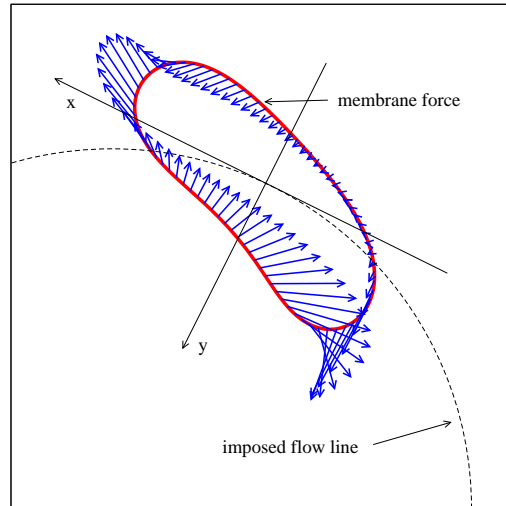


Figure 8.3: Force distribution on vesicle membrane and local coordinate system used for the calculation of N ($\alpha = 0.7$, $\lambda = 1$).

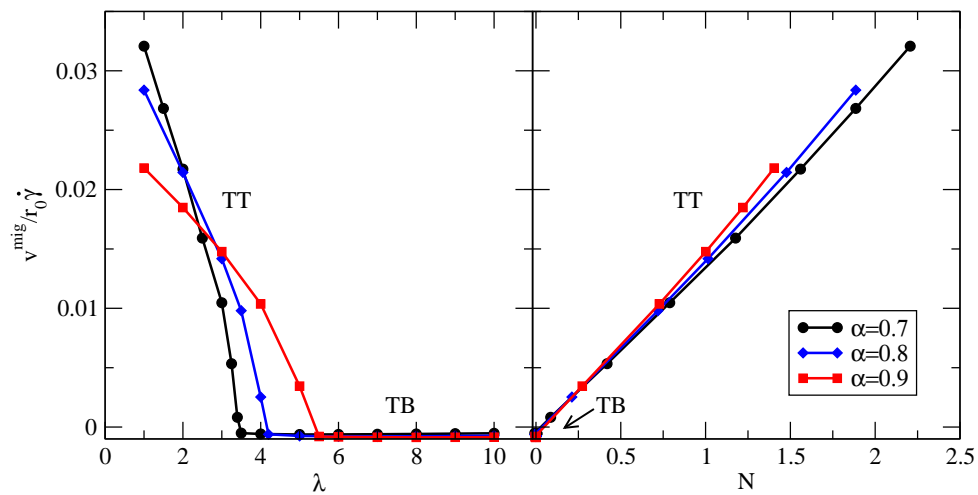


Figure 8.4: Inward migration velocity normalized by $R_0 \dot{\gamma}$ as a function of λ (left) and N (right) for different α at fixed radial position $r = 10R_0$. Every point corresponds to the (λ, N) pair on the abscissae.

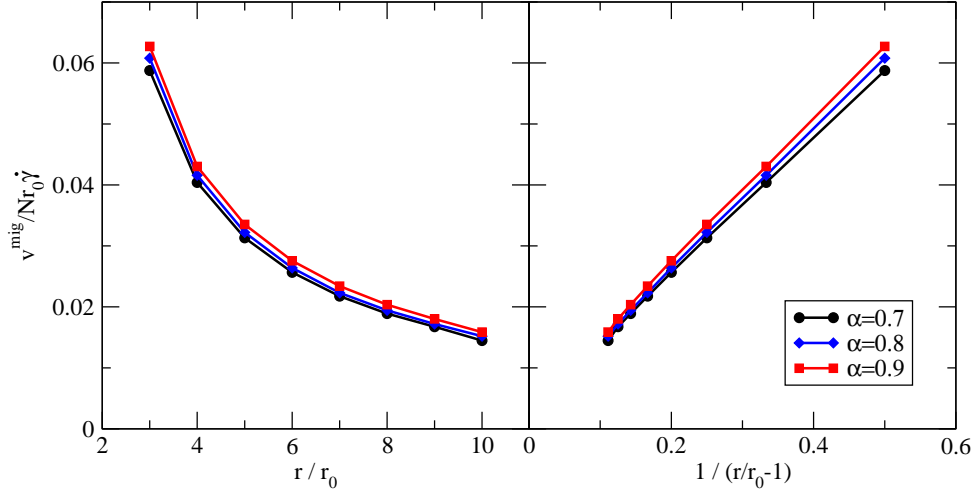


Figure 8.5: Inward migration velocities divided by $NR_0\dot{\gamma}$ as a function of r (left) and $1/(r/R_0 - 1)$ (right) for different α . Every point corresponds to the (λ, N) pair on the abscissae.

collapse on a single master curve, showing that the dynamics does not depend on the control parameters (α, λ) independently, but rather on their combination embedded in the function $N(\alpha, \lambda)$. Figure 8.4 (right) shows, moreover, that $v^{mig}/R_0\dot{\gamma}$ is simply proportional to N . This result holds for all the radial positions explored so far, $3 \leq r/R_0 \leq 10$: data collapse is manifested within an error of 10% (or less), and the results are represented with a universal straight line passing through the origin. The small discrepancies are believed to be due to the details of the flow around vesicles with different shapes and orientations.

To gain further insight we have examined the migration velocity as a function of the curvature of the flow. Figure 8.5 (left) shows $v^{mig}/NR_0\dot{\gamma}$ as a function of the radial position. This dependence on r is nonlinear. Expressing the results with the help of an appropriate rescaling (figure 8.5, right) reveals that $v^{mig}/Nr_0\dot{\gamma}$ is a simple linear function of $C_0 \equiv 1/(r/R_0 - 1)$. Note that C_0 is approximately the flow curvature on the innermost part of the vesicle, which is also the highest among the flow lines passing through the vesicle. The relevance of the innermost flow line, which has the highest shear gradient among the streamlines passing through the vesicle, is considered to be due to membrane incompressibility, that propagates stresses along the membrane. From the above results we infer the following scaling relation for migration

$$v^{mig} \sim R_0\dot{\gamma}C_0N \quad (8.1)$$

This is a central result: a macroscopic measure of N (which may be a very complex function of various parameters) directly leads to the determination of the (microscopic) migration velocity. The relevance of normal stress difference for the migration of particles was already pointed out in [SL91], although in the case of migration due to the presence of a wall in a parallel flow.

One might ask why should migration in a curved flow be dictated by normal stress difference at all. To answer this question, one may consider the composite fluid and denote its spatial and temporal averaged stress by σ (very much like the definition of the classical stress, as used in equation (5.5)). Let us assume stationary, circular motion, enjoying symmetry with respect to the angle θ . Using momentum conservation in polar coordinates one can show that [BAH87] (the calculation and the arguments are detailed in Appendix C):

$$\frac{\partial \sigma_{rr}}{\partial r} = \frac{1}{r} [-\rho v_\theta^2 + N] \quad (8.2)$$

where ρ is the fluid density, $N = \sigma_{\theta\theta} - \sigma_{rr}$ and $1/r$ the flow line curvature. $-\rho v_\theta^2/r$ is the inertia term, absent in our case. If $N \neq 0$, a radial stress gradient takes place. It results in an inward force pushing the fluid towards the center if $N > 0$: the force sign can be easily deduced by the comparison with the inertia term, which is always directed outwards. No such simple result holds in flows which do not exhibit flow line curvature. This result shows that the coupling between the normal stress difference and the curvature is the direct motor for inward motion. This is in agreement with equation (8.1), that has been derived directly from simulations of a suspension of vesicles, without making any *ad hoc* assumption.

Moreover, we have performed simulations in a parallel flow having the same velocity profile as the irrotational vortex – i.e. $v_x(y) = 1/y$ in cartesian coordinates (x, y) . Contrarily to the vortex flow, vesicles show in this case migration towards regions of low shear rate, despite the fact that $N > 0$. This points to the nontrivial fact that inward migration in the vortex (and also in the Couette set-up) is due to the curvature of the flow lines rather than to a shear gradient.

Tank-treading vesicles show positive normal stresses (see figures 6.2 and 6.3) and they migrate inwards. In the tumbling regime, we have found $N \simeq 0$ (averaged over a tumbling period), and a negligibly small migration. Moreover, N vanishes for tank-treading vesicles when approaching the transition to tumbling or when the shape is close to a sphere (as described in sections 6.2 and 6.7) [DM07, GBM10]. This is consistent with the fact that $v_{mig} \rightarrow 0$ with increasing λ or α (figure 8.4).

Drops and other particles

In view of the generality of the arguments presented for migration, it is natural to attempt a generalization to other types of complex fluids. For example, experimental measurements of migration are known for soft entities in Taylor-Couette and cone-plate rheometers: drops [CL79, CL81, HJ06] and polymers in dilute suspensions [Bru84, AMB02] either migrate towards the center (cone-plate) or adopt an equilibrium position that lies between the gap centreline and the inner cylinder (Taylor-Couette), which corresponds to high shear rate regions. Because drops, polymers, and vesicles have quite different properties, their similar behavior with respect to migration supports our conjecture that the basic mechanisms governing migration are independent of the mechanical details of the suspended entity and depend only on the flow curvature and N , as it is the case for a suspension of polymers (the Weissenberg, or rod-climbing, effect [Wei47]).

8.3 Couette flow

Having identified the basic ingredient for migration of a single vesicle in a curved flow, we switch now to the more realistic situation of a Taylor-Couette cell, formed by two coaxial cylinders (circles in two dimensions) rotating at different angular velocities in order to generate shear in the region between them, which is occupied by the fluid.

In the following we first explore the case of a cell containing a single vesicle, and we pass then to the more complex case of a suspension composed by several vesicles.

The numerical code used in this section is a Boundary Integral written by Biroš *et al.* [RVB10] and already used in section 6.7 for a single vesicle.

In the following we define the geometry and give the relative values. The velocity field in a Taylor-Couette cell is tangential and of the form

$$u_{\theta}(r) = \frac{a}{r} + br \quad (8.3)$$

where the two coefficients a and b depend on the geometry of the cell and on the angular velocities of the walls:

$$a = \frac{R_i^2 R_o^2 (\omega_i - \omega_o)}{R_o^2 - R_i^2} \quad b = \frac{R_o^2 \omega_o - R_i^2 \omega_i}{R_o^2 - R_i^2} \quad (8.4)$$

with R denoting the radii of the walls, ω the angular velocities and the subscripts i and o refer to the internal and to the external walls, respectively.

In this geometry, it is possible to compute the effective viscosity of the fluid in the gap between the two cylinders, that is related to the shear stress $\sigma_{r\theta}$. The derivation of such expression is based on the conservation of angular momentum within the two cylinders, and on the assumption of a linear relation between stress and strain, as is the case for a Newtonian fluid¹. The derivation is detailed in Appendix D. We obtain:

$$\eta_{eff} = \frac{R_i}{4\pi(\omega_i - \omega_o)} \left[\frac{1}{R_i^2} - \frac{1}{R_o^2} \right] \oint_{\Gamma_i} f_\theta(r) dr \quad (8.5)$$

where Γ_i is the surface of the internal cylinder and $f_\theta(r)$ the tangential component of the force exerted by this boundary to shear the fluid. This expression is valid for any value of the two cylinder radii R_i and R_o . The reduced effective viscosity is retrieved from the effective viscosity by using equation (6.3).

The radii are set to $R_i = 10R_0$ and $R_o = 20R_0$ (if not differently specified), r_0 being the mean radius of a vesicle as already defined in the previous section. The angular velocities are set to $\omega_i = 1$ and $\omega_o = 0$, measured in units of the inverse of the relaxation time of the curvature of the membrane.

Vesicles are chosen with different reduced area α , between 0.5 and 0.95. For simplicity, we set the viscosity contrast λ to unity.

In the code, the vesicles are discretized with 64 points and the boundaries with $1/10^{th}$ of the corresponding density. The time step is 10^{-2} . The space and time discretization chosen allow for a conservation of the vesicle area within 10^{-4} and local perimeter within 10^{-3} .

Single vesicle

First, we focus on the more academic case of a single vesicle in a Taylor-Couette cell, that will constitute a precious step for the understanding of the dynamics of a collection of cells in the same geometry.

We run several simulations with different reduced areas, $0.5 \leq \alpha \leq 0.95$ and we measure both the rheology of the suspension while observing the dynamics of the system. For every value of α we run two simulations, initializing the vesicle either close to the external wall or close to the internal one. The goal of this procedure is to check whether the vesicles, that are expected to show cross-streamline migration as discussed in section 8.2, exhibit a single equilibrium position or not.

¹ This should not be regarded as an unjustified hypothesis: the effective viscosity is defined as the viscosity of a Newtonian fluid that corresponds to the measured stress and strain (see section 3.2).

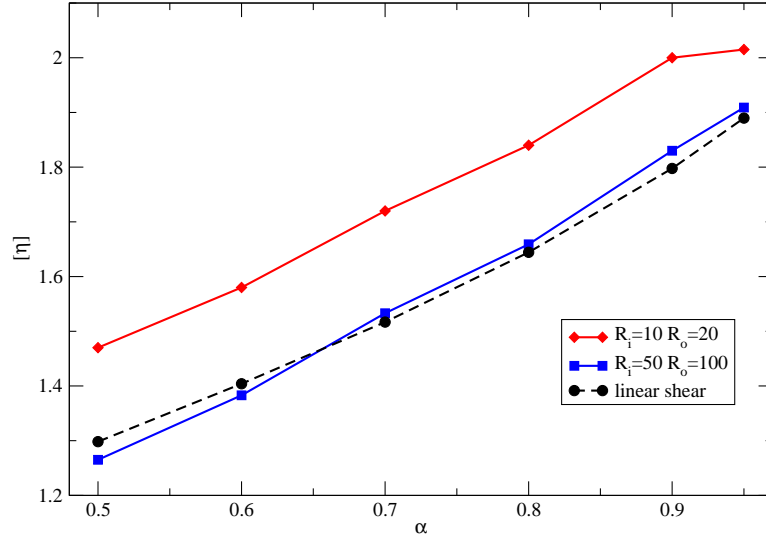


Figure 8.6: The intrinsic viscosity in a Taylor-Couette cell with a single vesicle (red and blue lines, for two different geometries as indicated). The data relative to an unbounded linear shear flow are represented via the dashed line (from figure 6.20).

The first interesting result is that all vesicles, regardless of their reduced area or starting position, migrate to the same radial position which is located between the inner cylinder ($r = 10$) and the flow centreline ($r = 15$) at $r \simeq 14.3^2$ (figure 8.7, left). This indicates that the force driving inward migration (due to the normal stress difference as discussed in section 8.2) rescales with α as does the lift force due to the walls [BBM04].

The intrinsic viscosity of the suspension is reported in figure 8.6, where we compare it to the same quantity measured in section 6.7 (in that case, the flow lines were straight and the system unbounded). A quantitative difference exists between the two curves. This difference can be due to the confinement and to the curvature of the flow lines that also produces a non-homogeneous shear rate. In the limit of a wide gap ($|R_o - R_i| \gg R_0$) and of negligible curvature of the flow lines ($|R_o - R_i| \ll R_i$), the effective viscosity computed in a Taylor-Couette cell must coincide with the one computed in the unbounded case. It is then interesting to quantify these inequalities by finding the smallest geometry that allows to retrieve the macroscopic values. After several tests, varying both the gap³ (i.e. $|R_o - R_i|$) and R_i between

²If the two curvature radii would tend to infinity, the equilibrium position would be the centre of the channel.

³While varying the size of the system, the angular velocity of the inner cylinder is

$10R_0$ and $200R_0$, we could determine that the minimal size necessary to recover a reasonable agreement with the macroscopic rheology is $R_i \approx 50$, $R_o \approx 100$. The intrinsic viscosity computed for this geometry is reported in figure 8.6.

Although in this geometry the effective viscosity is in quantitative agreement with the macroscopic limit, in which the flow curvature is negligible, the dynamics is still affected. In fact, the equilibrium position of the vesicles is $r_{eq} \approx 70.5R_0$, instead of the gap centreline $r_{centre} = 75$ that would be retrieved in the case of vanishing curvature of the flow lines.

Multiple vesicles

Having identified the basic phenomena causing the migration of a single vesicle in a Taylor-Couette cell, we are now in a position to address the question of the impact of these features on the organization of a collection of vesicles. We have first addressed the problem of a dilute enough suspension. We ran simulations for low volume fraction $\phi \approx 1\%$ and $\phi \approx 2\%$ with $R_i = 10R_0$, $R_o = 20R_0$. The number of vesicles corresponding to these two volume fractions is 4 and 7, respectively. The vesicles, that are chosen to have a swelling ratio $\alpha = 0.9$, are initialized in a random configuration. Despite the very low volume fraction, vesicles organize in an ordered phase: they migrate to the same flow line selected as equilibrium radial position by a single vesicle in the same geometry, and here they organize themselves in a rim by keeping the same interdistance (figure 8.7, right). The variation of the initial configuration doesn't seem to have any influence on the final equilibrium state. The organization in a rim which has the same radius as that dictated by the final position of a single vesicle is not obvious: indeed, the fact that the vesicles select the same interdistance is a clear indication for their significant mutual interactions, and despite this effect the terminal position does not seem to be affected.

For a better understanding, we have analyzed the behaviour of the flow lines. A single vesicle creates two vortices (figure 8.7, left). The size of the vortices is, in our geometry, of about a quarter of the circumference: we thus expect vesicles to interact significantly when their number M reaches 4. This is confirmed by our simulations that show disorder for $M < 4$ and order for $M \geq 4$. For $M \geq 4$ vesicles keep order because deviations would cause restoring forces due to vortex interactions. For all explored volume fractions we found persistence of order, as in figure 8.7 (right).

adapted in order to have a constant mean shear in the gap.

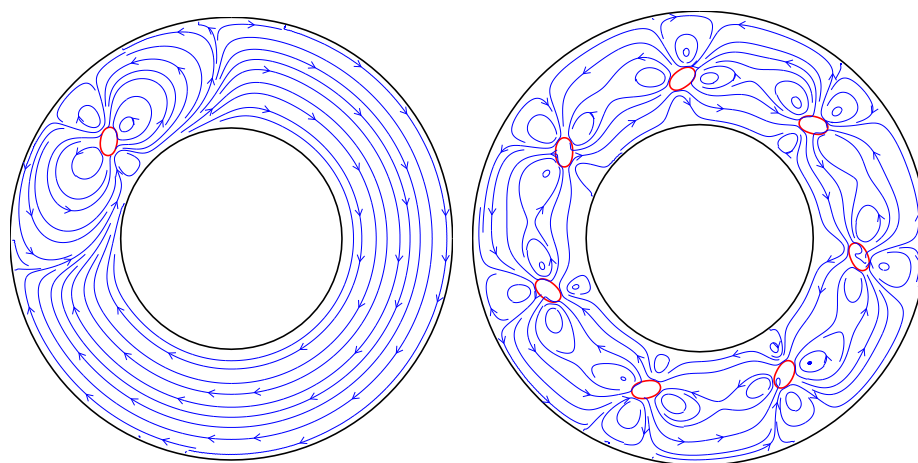


Figure 8.7: Equilibrium configurations in a Taylor-Couette device for a single vesicle (left) and several vesicles (right, volume fraction $\approx 2\%$). The lines represent the induced flow. On the right, spontaneous organization is due to inward migration and vortex interaction.

CONCLUSIONS AND PERSPECTIVES

The main findings of this thesis are summarized and some perspectives outlined. The transposition of the results to red blood cells is discussed.

Concluding remarks

In this thesis an analysis of different dynamical and rheological behaviors of a suspension of vesicles by means of two-dimensional numerical simulations is presented.

The contributions concern the dynamics of a single vesicle in linear and curved shear flow, the rheology of a dilute suspension of vesicles and the self-organization of sets of vesicles both in an unbounded Poiseuille flow and in a Couette device.

Three major results have followed:

- The rheology of a dilute suspension of vesicles has been detailed and understood; the role played by the membrane has been differentiated from the effects due to the bulk of the vesicle.
- The cross-streamline dynamics of a vesicle immersed in a curved flow has been linked to the normal stress difference that the vesicle itself creates. The mechanism that has been unveiled is supposed to be quite general and thus transferable to other deformable particles, like drops, capsules, polymers.
- An intricate mechanism of self-organization in Poiseuille flow has been observed, by which vesicles organize in sets of finite size, respecting a maximum number of vesicles per set.

Two-dimensional simulations have shown their strength offering a simple method to understand the fundamental physical behaviors.

Perspectives

The present work opens a set of perspectives:

- *the effect of interactions on rheology* – While the present work details the rheological properties of a suspension of vesicles neglecting hydrodynamical interactions, considering the full dynamics of several vesicles and retrieving the rheology is still an open issue.
- *effect of boundaries on vesicles in Poiseuille flow* – The complex dynamics in an unbounded Poiseuille flow revealed by the present work could be affected by the presence of boundaries close to the vesicles, that is also the physiological condition for red blood cells.
- *the simulation of red blood cells in two dimensions by including the elasticity due to the cytoskeleton* – The effect of the cytoskeleton is nevertheless believed to be minor, due to the very small difference between vesicles and red blood cells in two dimensions.
- *Phase transitions in microscopic Couette flow* – The present work brings evidence of the self-organization of vesicles at the microscale: an ordered phase is found even at very low concentration. This study needs to be continued in order to understand the dependence of the ordered state upon the dynamical parameters of the system.

Contributions transposable to RBCs

As already stated in section 4.5, vesicles and red blood cells are extremely similar in dimension two. The results listed above are contributions to vesicle dynamics and rheology, and a significant part of this work can be transposed to red blood cells, in particular:

- rheology of a dilute suspension, behavior in a curved flow and in a microscopic Couette device: the role played by the elasticity of the membrane of red blood cells is a slight modification of some dynamical regimes, in particular tank-treading, but the main results are believed to remain unaltered. Probably a renormalization of the bending rigidity of the vesicle is enough to account for the contribution arising from the elasticity.
- spatial organization in Poiseuille flow: in this case the membrane does not tank-tread and so the elasticity arising from the cytoskeleton is thought to play a very minor role, and results should remain unaltered.

CONCLUSIONS ET PERSPECTIVES

Ce chapitre résume les principaux apports de cette thèse et propose quelques perspectives. La transposition des résultats aux globules rouges est discutée.

Remarques conclusives

Dans cette thèse une analyse des différents comportements dynamiques et rhéologiques d'une suspension de vésicules est présentée, et effectuée grâce à des simulations numériques à deux dimensions.

Les contributions concernent la dynamique d'une vésicule dans des écoulements de cisaillement linéaires et courbes, la rhéologie d'une suspension diluée de vésicules et l'auto-organisation d'ensembles de vésicules à la fois dans un écoulement de Poiseuille non borné et dans une cellule de Taylor-Couette.

Trois résultats majeurs ont suivi :

- la rhéologie d'une suspension diluée de vésicules a été détaillée et comprise. Le rôle joué par la membrane a été différencié des effets dus au volume de la vésicule ;
- la dynamique de migration d'une vésicule à travers les lignes d'un écoulement courbe a été reliée à la différence des contraintes normales que la vésicule elle-même génère. Il a été argumenté que le mécanisme mis en évidence est général et donc applicable à d'autres particules déformables, comme des gouttes, capsules, polymères ;
- un mécanisme complexe d'auto-organisation en écoulement de Poiseuille a été observé, selon lequel les vésicules s'organisent en paquets de taille finie, en respectant un nombre maximum de vésicules par paquet.

Les simulations à deux dimensions ont démontré leur puissance en offrant une méthode simple pour comprendre les comportements physiques fondamentaux.

Perspectives

Le travail présenté ouvre un certain nombre de perspectives :

- *effet des interactions sur la rhéologie* – Ce travail détaille les propriétés rhéologiques d’une suspension de vésicules en négligeant les interactions hydrodynamiques. La dynamique complète d’une suspension, qui prendrait en compte ces interactions, est encore une question ouverte ;
- *effet des parois sur les vésicules dans un écoulement de Poiseuille* – La dynamique complexe dans un écoulement de Poiseuille non borné illustrée par ce travail pourrait être affectée par la présence de parois proches des vésicules, présence qui est aussi la condition physiologique des globules rouges ;
- *simulations de globules rouges à deux dimensions en incluant l’élasticité due au cytosquelette* – Du fait de la faible différence entre vésicules et globules rouges à deux dimensions, l’effet du cytosquelette est estimé être mineur ;
- *transitions de phase dans un écoulement de Couette microscopique* – Ce travail montre l’auto-organisation des vésicules à la microéchelle : un état ordonné est observé même à très faible concentration. Cette étude demande d’être poursuivie pour comprendre la dépendance de cet état ordonné aux paramètres dynamiques du système.

Contributions transposables aux globules rouges

Comme cela a déjà été dit en section 4.5, les vésicules et les globules rouges à deux dimensions sont très similaires. Les résultats ci-dessus sont des contributions à la dynamique et à la rhéologie des vésicules, et une partie significative de ce travail peut être transposé aux globules rouges, en particulier :

- *rhéologie d’une suspension diluée, comportement dans un écoulement courbe et dans une cellule de Couette microscopique* – l’élasticité de la membrane des globules rouges modifie faiblement les régimes dynamiques, en particulier le tank-treading, mais les résultats principaux sont estimés devoir rester inchangés. Une renormalisation du module de courbure de la membrane est probablement suffisante pour prendre en considération la contribution due à l’élasticité ;

-
- *organisation spatiale dans un écoulement de Poiseuille* – dans ce cas la membrane ne présente pas de tank-treading, donc l'élasticité du cytosquelette est estimée devoir jouer un rôle négligeable, et les résultats ne devraient pas en dépendre.

Appendices

THE STRESS TENSOR OF A DILUTE SUSPENSION OF PARTICLES

A detailed derivation of the mean stress tensor of a suspension of particles following Batchelor approach [Bat70] is presented. Attention is paid to singularities that this formulation introduces on the particle surfaces. An expression for a suspension of liquid particles (as drops, capsules, vesicles) is derived. These results are illustrated by computing analytically the effective viscosity of a dilute suspension of rigid disks in two dimensions (i.e. the two-dimensional Einstein coefficient).

On présente un calcul détaillé pour obtenir la moyenne du tenseur des contraintes d'une suspension de vésicules en suivant l'approche de Batchelor [Bat70]. Une grande attention est prêtée aux singularités que cette formulation introduit sur les surfaces des particules. Une expression pour une suspension de particules liquides (comme des gouttes, capsules, vésicules) est déduite. Les résultats sont illustrés en calculant analytiquement la viscosité effective d'une suspension diluée de disques rigides en deux dimensions (c. à d. le coefficient d'Einstein à deux dimensions).

In this Appendix we derive the expression of the mean stress tensor of a suspension.

We first consider the general case of a suspension of particles whose stress tensor is unknown. Then we specify the calculation for the case where the particles are liquid drops with arbitrary forces at the interface, so that the expression is valid for systems like droplets, vesicles, capsules.

A special care is taken for inspecting the role of the interface between the particle and the embedding fluid: in fact on this surface we can have discontinuities and singularities that have to be taken properly into account.

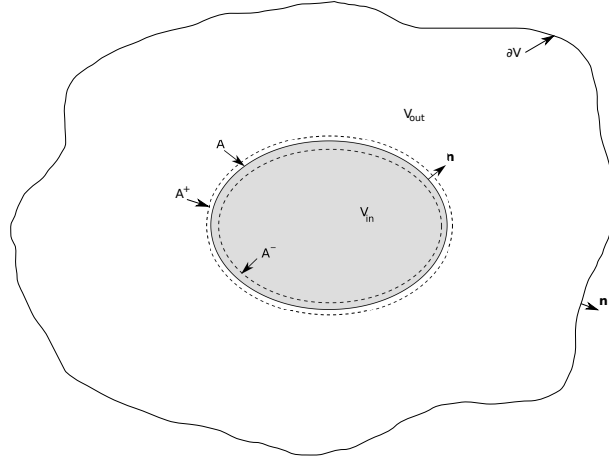


Figure A.1: The domains and their boundaries. The system is composed by the embedding fluid, the interior of the suspended particle and the separation surface. We define V_{out} the volume occupied by the embedding fluid, V_{in} the volume occupied by the suspended particle (gray in the figure) and A the interface between them. The whole system is delimited by a boundary ∂V , the inner volume of the particle by A^- (dashed line *inside* the particle) and the outer volume by A^+ (dashed line *outside* the particle) and ∂V . The normal vectors \mathbf{n} to the boundaries are chosen to point outwards.

A.1 Mean stress tensor for a particle suspension

We consider a model suspension which contains a single particle embedded in a Newtonian fluid. Even though the Stokes approximation is usually valid at the scale of the particle, we proceed in total generality and we do not make at this stage any simplification coming from the small Reynolds number limit $Re \rightarrow 0$.

The stress tensor is defined as:

$$\sigma_{ij} = f_i n_j \tag{A.1}$$

where \mathbf{f} is the (surface) force density exerted on the surface of a fluid element and \mathbf{n} the normal vector in the considered direction.

With this definition, $\nabla \cdot \boldsymbol{\sigma} = \partial_j \sigma_{ij}$ represents the volume density of forces.

The mean stress tensor of the suspension is defined via the volume average:

$$\langle \sigma_{ij} \rangle \equiv \frac{1}{V} \int_V \sigma_{ij} dV \quad (\text{A.2})$$

$$= \frac{1}{V} \int_{V_{out}} \sigma_{ij} dV + \frac{1}{V} \int_{V-V_{out}} \sigma_{ij} dV \quad (\text{A.3})$$

where V is the total volume of the system, V_{out} denotes the volume occupied by the suspending fluid and $V - V_{out}$ its complementary.

We can pass from bulk to surface integrals, exploiting the following identity:

$$\partial_k(x_j \sigma_{ik}) = \delta_{kj} \sigma_{ik} + x_j \partial_k \sigma_{ik} \quad (\text{A.4})$$

from which

$$\sigma_{ij} = \partial_k(x_j \sigma_{ik}) - x_j \partial_k \sigma_{ik} \quad (\text{A.5})$$

then:

$$\langle \sigma_{ij} \rangle = \frac{1}{V} \left[\int_{V_{out}} \sigma_{ij} dV + \int_{V-V_{out}} \sigma_{ij} dV \right] \quad (\text{A.6})$$

$$= \frac{1}{V} \left[\int_{V_{out}} \sigma_{ij} dV + \int_{V-V_{out}} \partial_k(x_j \sigma_{ik}) dV - \int_{V-V_{out}} x_j \partial_k \sigma_{ik} dV \right] \quad (\text{A.7})$$

The last two terms are volume integrals extended to the region of the system complementary to the region occupied by the fluid, which means that the region $V - V_{out} = V_{in} + A$ contains all possible complications coming from the interface between the fluid and the suspended particle. A priori this surface can contain a discontinuity in the stress tensor, due to the presence of surface forces. This means that, if one wants to apply the divergence theorem to the second integral of (A.7), one has to consider derivatives in the sense of distributions, i.e. to take into account terms coming from the derivative of a discontinuity.

It is worth noting that no singularity is present in the definition of the mean stress tensor as a volume integral (A.2), but the use of identity (A.4) introduces derivatives and then singularities, since the stress tensor is at most discontinuous in the integration domain.

Then,

$$\int_{V-V_{out}} \partial_k(x_j \sigma_{ik}) dV = \int_{A^+} x_j \sigma_{ik} n_k dA + \int_{V-V_{out}} \delta_{interface} x_j \Delta(\sigma_{ik}) n_k dV \quad (\text{A.8})$$

The function $\delta_{interface}$ is a Dirac delta function which represents all the possible surfaces of discontinuity enclosed in the volume ($V - V_{out}$), and

$\Delta(\sigma_{ik})$ the stress tensor jump across these interfaces (positive if the external stress is larger than the internal one, due to the sign of the normal vector, that points outwards). If one assumes that the only discontinuity surface is the particle surface A , equation (A.7) becomes:

$$\langle \sigma_{ij} \rangle = \frac{1}{V} \left[\int_{V_{out}} \sigma_{ij} dV + \int_{A^+} x_j \sigma_{ik} n_k dA + \int_A x_j \Delta(\sigma_{ik}) dA - \int_{V-V_{out}} x_j \partial_k \sigma_{ik} dV \right] \quad (\text{A.9})$$

where the stress tensor in the second integral is taken *outside* the surface of the particle. Then the singularity present in the last integral (which contains the surface of discontinuity A) exactly cancels out with the jump $\Delta(\sigma)$ considered in the surface integral: this is coherent with the fact that no singularity is present in the very first formulation $\int_V \sigma_{ij} dV$: they arise only from the introduction of derivatives. We obtain then the simplified result:

$$\langle \sigma_{ij} \rangle = \frac{1}{V} \left[\int_{V_{out}} \sigma_{ij} dV + \int_{A^+} x_j \sigma_{ik} n_k dA - \int_{V_{in}} x_j \partial_k \sigma_{ik} dV \right] \quad (\text{A.10})$$

where the second integral is computed using the stress tensor *outside* the surface of the particle and the last integral does not contain the surface of discontinuity A .

The stress tensor in the particle and on its surface ($V - V_{out}$) is *a priori* unknown, while in the fluid (V_{out}) its expression reads:

$$\sigma_{ij}^F = -p\delta_{ij} + \eta_{out} (\partial_i u_j + \partial_j u_i) \quad (\text{A.11})$$

where η_{out} is the viscosity of the embedding fluid.

We can write then:

$$\langle \sigma_{ij} \rangle = \frac{1}{V} \left[\int_{V_{out}} \sigma_{ij}^F dV + \int_A x_j \sigma_{ik}^F n_k dA - \int_{V_{in}} x_j \partial_k \sigma_{ik} dV \right] \quad (\text{A.12})$$

For computational convenience we can extend the anisotropic term of the first integral to the whole volume V of the system, subtracting then the contribution coming from the volume of the particle:

$$\begin{aligned} \int_{V_{out}} \sigma_{ij}^F dV &= \int_{V_{out}} [-p\delta_{ij} + \eta_{out}(\partial_i u_j + \partial_j u_i)] dV \\ &= \int_{V_{out}} -p\delta_{ij} dV + \eta_{out} \int_V (\partial_i u_j + \partial_j u_i) dV \\ &\quad - \eta_{out} \int_{V-V_{out}} (\partial_i u_j + \partial_j u_i) dV \end{aligned} \quad (\text{A.13})$$

The last integral is computed on $V - V_{out}$, which means the particle and its surface. The integrand is at most discontinuous on the interface, since the velocity field is continuous (due to no-slip boundary conditions). It is then *not singular* on A , so there is no contribution arising directly from this surface. Then the only contribution of this integral comes from the bulk (V_{in}), and can be expressed through a surface integral:

$$\int_{V_{out}} \sigma_{ij}^F dV = \int_{V_{out}} -p\delta_{ij} dV + \eta_{out} \int_V (\partial_i u_j + \partial_j u_i) dV - \eta_{out} \int_A (n_i u_j + n_j u_i) dA \quad (\text{A.14})$$

So, equation (A.12) becomes:

$$\langle \sigma_{ij} \rangle = \frac{1}{V} \left\{ \int_{V_{out}} -p\delta_{ij} dV + \eta_{out} \int_V (\partial_i u_j + \partial_j u_i) dV + \int_A [x_j \sigma_{ik}^F n_k - \eta_{out} (n_i u_j + n_j u_i)] dA - \int_{V_{in}} x_j \partial_k \sigma_{ik} dV \right\} \quad (\text{A.15})$$

This is the result obtained by Batchelor in 1970 [Bat70]. We can interpret the terms in the following way:

- the first term is an isotropic contribution, the mean pressure of the embedding fluid;
- the second term is the mean velocity gradient of the suspension, multiplied by the viscosity of the embedding fluid. It can be interpreted as the stress that would exist in the absence of the particle and with the same average velocity gradient;
- the third term represents the contributions coming from the forces acting on the surface of the particle and from the velocity field inside the particle, expressed as a surface integral;
- the last term represents the integral over the particle of the body forces ($f_{body} = \nabla \cdot \boldsymbol{\sigma}$). However, body forces will not be considered. In addition, inertia is not accounted for (Stokes limit), so that this term can be ignored.

This result can be expressed in a slightly different form with the conversion of the volume integral of the velocity gradient into a surface integral.

This is done by splitting the integral into the two domains of continuity of the velocity gradient and by using the divergence theorem:

$$\begin{aligned}
\int_V (\partial_i u_j + \partial_j u_i) dV &= \int_{V_{in}} (\partial_i u_j + \partial_j u_i) dV + \int_{V_{out}} (\partial_i u_j + \partial_j u_i) dV \\
&= \int_{A^-} (n_i u_j + n_j u_i) dA - \int_{A^+} (n_i u_j + n_j u_i) dA + \int_{\partial V} (n_i u_j + n_j u_i) dA \\
&= \int_{\partial V} (n_i u_j + n_j u_i) dA
\end{aligned} \tag{A.16}$$

where the last simplification is possible due to the continuity of the velocity \mathbf{u} across the interface A (assumption of no-slip conditions).

These few lines show that if the velocity is imposed to the suspension through the external boundaries, the mean velocity gradient of the system is the one of the imposed flow.

So equation (A.15) can be rewritten as

$$\boxed{
\begin{aligned}
\langle \sigma_{ij} \rangle &= \frac{1}{V} \left\{ \int_{V_{out}} -p \delta_{ij} dV + \eta_{out} \int_{\partial V} (n_i u_j + n_j u_i) dA \right. \\
&\quad + \int_A [x_j \sigma_{ik}^F n_k - \eta_{out} (n_i u_j + n_j u_i)] dA \\
&\quad \left. - \int_{V_{in}} x_j \partial_k \sigma_{ik} dV \right\}
\end{aligned} \tag{A.17}$$

A.2 Suspension of liquid particles

We consider now the determination of the mean stress tensor of a suspension formed by a Newtonian fluid containing drops of another Newtonian fluid. The calculation is general enough to be valid for any kind of forces exerted at the surface of the drops, like surface tension, bending or elastic forces. The following discussion is then valid for drops, vesicles, capsules and any other system that can be described as a liquid drop and some interfacial force. A difference in the viscosities of the internal and external fluids (η_{in} and η_{out} , respectively) is taken into account through the parameter $\lambda = \eta_{in}/\eta_{out}$, the viscosity contrast.

By proceeding as done in section A.1, we express the mean stress tensor through an integral extended over the whole volume. Contrarily to section A.1, the stress tensor is known in this case not only in the outer volume V_{out} occupied by the suspending fluid, but also in the internal volume of

the drop V_{in} . This symmetry allows us to derive two equivalent expressions for the mean stress tensor, applying respectively the divergence theorem to compute: (i) the integral over the internal volume V_{in} and (ii) the integral over the external one V_{out} . Finally, the combination of these two formulas will allow us to express $\langle \sigma_{ij} \rangle$ as a function of the interfacial forces and the viscosity contrast. In the two following subsections we derive the two equivalent expressions for the mean stress tensor of the suspension.

The inner region

We apply here, as in section A.1, the divergence theorem to the region occupied by the particle: it is then possible to take advantage of a part of the computations already done in that section, whose validity is general (in fact, no hypotheses were done on the nature of the stress tensor of the particle). We restart from (A.12):

$$\langle \sigma_{ij} \rangle = \frac{1}{V} \left[\int_{V_{out}} \sigma_{ij}^{out} dV + \int_{A^+} x_j \sigma_{ik}^{out} n_k dA - \int_{V_{in}} x_j \partial_k \sigma_{ik}^{in} dV \right] \quad (\text{A.18})$$

where V_{in} represents the internal volume of the drop (excluding the membrane), V_{out} the external one (excluding the membrane too), A^+ the external side of the membrane and $\boldsymbol{\sigma}^{in}$, $\boldsymbol{\sigma}^{out}$ the stress tensor of the inner and outer fluids. We reformulate now the integral over V_{out} of the stress tensor appearing in (A.18), by adding and subtracting the integration over V_{in} and writing explicitly its expression:

$$\begin{aligned} \int_{V_{out}} \sigma_{ij}^{out} dV &= \int_{V_{out}} -p \delta_{ij} dV + \int_V \eta(\mathbf{x}) (\partial_i u_j + \partial_j u_i) dV \\ &\quad - \int_{V-V_{out}} \eta(\mathbf{x}) (\partial_i u_j + \partial_j u_i) dV \end{aligned} \quad (\text{A.19})$$

The symbol $\eta(\mathbf{x})$ represents the local viscosity: $\eta(\mathbf{x}) \equiv \eta_{in}$ inside the drop and $\eta(\mathbf{x}) \equiv \eta_{out}$ outside. It is worth noting that we extend the external stress tensor to V_{in} using the value of the internal one $\boldsymbol{\sigma}^{in}$, while in section A.1 the external stress tensor has been extended to V_{in} using $\boldsymbol{\sigma}^{out}$ (the real stress tensor of the particle being unknown). This passage is at the origin of the differences that will arise hereafter.

On the surface A , $\boldsymbol{\sigma}$ can be at maximum discontinuous (due to the interfacial forces and the viscosity contrast), then the last integral of (A.19) does not contain contributions coming from the membrane. Then, it is possible to substitute the integration over $(V - V_{out})$ with one over V_{in} and

(A.19) becomes:

$$\begin{aligned} \int_{V_{out}} \sigma_{ij}^F dV &= \int_{V_{out}} -p\delta_{ij} dV + \int_V \eta(\mathbf{x}) (\partial_i u_j + \partial_j u_i) dV \\ &\quad - \eta_{in} \int_{V_{in}} (\partial_i u_j + \partial_j u_i) dV \end{aligned} \quad (\text{A.20})$$

The last integral can now be computed by means of the divergence theorem:

$$\begin{aligned} \int_{V_{out}} \sigma_{ij}^F dV &= \int_{V_{out}} -p\delta_{ij} dV + \int_V \eta(\mathbf{x}) (\partial_i u_j + \partial_j u_i) dV \\ &\quad - \eta_{in} \int_A (n_i u_j + n_j u_i) dA \end{aligned} \quad (\text{A.21})$$

Substituting this expression in equation (A.18), we obtain:

$$\begin{aligned} \langle \sigma_{ij} \rangle &= \frac{1}{V} \left[\int_{V_{out}} -p\delta_{ij} dV + \int_V \eta(\mathbf{x}) (\partial_i u_j + \partial_j u_i) dV \right. \\ &\quad \left. - \eta_{in} \int_A (n_i u_j + n_j u_i) dA + \int_{A^+} x_j \sigma_{ik}^{out} n_k dA \right. \\ &\quad \left. - \int_{V_{in}} x_j \partial_k \sigma_{ik}^{in} dV \right] \end{aligned} \quad (\text{A.22})$$

that is the first expression for the average stress tensor of the suspension mentioned at the beginning of this section A.2.

The outer region

We repeat now the same calculation, but exchanging the role of internal and external fluids (i.e. we apply the divergence theorem to compute the integral over the external volume). The calculations are analogous to those used to retrieve equation (A.22), but the use of the divergence theorem for the stress tensor in the outer fluid will cause the appearance of surface integrals extended to the outer boundary ∂V . Then for clarity we restart from the very beginning, the definition of $\langle \sigma_{ij} \rangle$, as in section A.1:

$$\langle \sigma_{ij} \rangle \equiv \frac{1}{V} \int_V \sigma_{ij} dV \quad (\text{A.23})$$

$$= \frac{1}{V} \int_{V_{in}} \sigma_{ij} dV + \frac{1}{V} \int_{V-V_{in}} \sigma_{ij} dV \quad (\text{A.24})$$

$$= \frac{1}{V} \int_{V_{in}} \sigma_{ij} dV + \frac{1}{V} \int_{V-V_{in}} [\partial_k (x_j \sigma_{ik}) - x_j \partial_k \sigma_{ik}] dV \quad (\text{A.25})$$

Now we analyze in detail the first term of the second integral:

$$\begin{aligned} \int_{V-V_{in}} \partial_k(x_j \sigma_{ik}) dV &= \\ &= \int_{\partial(V-V_{in})} x_j \sigma_{ik} n_k dA + \int_{V-V_{in}} \delta_{interface} x_j \Delta(\sigma_{ik}) n_k dV \end{aligned} \quad (\text{A.26})$$

$$= - \int_{A^-} x_j \sigma_{ik} n_k dA + \int_{\partial V} x_j \sigma_{ik} n_k dA + \int_A x_j \Delta(\sigma_{ik}) n_k dA \quad (\text{A.27})$$

where it has been taken into account that on the surface A the normal vector \mathbf{n} points into the integration domain (giving a minus sign), then equation (A.25) becomes:

$$\begin{aligned} \langle \sigma_{ij} \rangle &= \frac{1}{V} \left[\int_{V_{in}} \sigma_{ij} dV - \int_{A^-} x_j \sigma_{ik} n_k dA + \int_{\partial V} x_j \sigma_{ik} n_k dA \right. \\ &\quad \left. + \int_A x_j \Delta(\sigma_{ik}) n_k dA - \int_{V-V_{in}} x_j \partial_k \sigma_{ik} dV \right] \end{aligned} \quad (\text{A.28})$$

The integral of the stress discontinuity on A cancels out with the singularity present in the last term, which is extended to the external volume V_{out} and the surface A . Then,

$$\begin{aligned} \langle \sigma_{ij} \rangle &= \frac{1}{V} \left[\int_{V_{in}} \sigma_{ij}^{in} dV - \int_{A^-} x_j \sigma_{ik}^{in} n_k dA + \int_{\partial V} x_j \sigma_{ik}^{out} n_k dA \right. \\ &\quad \left. - \int_{V_{out}} x_j \partial_k \sigma_{ik}^{out} dV \right] \end{aligned} \quad (\text{A.29})$$

which is the equivalent of (A.18) but computed applying the divergence theorem at the outer region V_{out} .

Following the same technique applied above (equation A.19), we re-write the volume integral over V_{in} as:

$$\begin{aligned} \int_{V_{in}} \sigma_{ij}^{in} dV &= \int_{V_{in}} -p \delta_{ij} dV + \int_V \eta(\mathbf{x}) (\partial_i u_j + \partial_j u_i) dV \\ &\quad - \int_{V-V_{in}} \eta(\mathbf{x}) (\partial_i u_j + \partial_j u_i) dV \\ &= \int_{V_{in}} -p \delta_{ij} dV + \int_V \eta(\mathbf{x}) (\partial_i u_j + \partial_j u_i) dV \\ &\quad - \eta_{out} \int_{V_{out}} (\partial_i u_j + \partial_j u_i) dV \end{aligned} \quad (\text{A.30})$$

The last integral can be computed by means of the divergence theorem, so equation (A.30) becomes:

$$\begin{aligned} \int_{V_{in}} \sigma_{ij}^{in} dV &= \int_{V_{in}} -p\delta_{ij} dV + \int_V \eta(\mathbf{x}) (\partial_i u_j + \partial_j u_i) dV \\ &+ \eta_{out} \int_{A^+} (n_i u_j + n_j u_i) dA - \eta_{out} \int_{\partial V} (n_i u_j + n_j u_i) dA \end{aligned} \quad (\text{A.31})$$

(remind that the normal vector \mathbf{n} on the drop surface A points in the integration domain, as sketched in figure A.1).

Substituting expression (A.31) in equation (A.29) we obtain:

$$\begin{aligned} \langle \sigma_{ij} \rangle &= \frac{1}{V} \left[\int_{V_{in}} -p\delta_{ij} dV + \int_V \eta(\mathbf{x}) (\partial_i u_j + \partial_j u_i) dV \right. \\ &+ \eta_{out} \int_A (n_i u_j + n_j u_i) dA - \int_{A^-} x_j \sigma_{ik}^{in} n_k dA \\ &- \eta_{out} \int_{\partial V} (n_i u_j + n_j u_i) dA + \int_{\partial V} x_j \sigma_{ik}^{out} n_k dA \\ &\left. - \int_{V_{out}} x_j \partial_k \sigma_{ik}^{out} dV \right] \end{aligned} \quad (\text{A.32})$$

that is the second equivalent expression for the average value of the stress tensor of the suspension, the first one being (A.22).

Summing up the two results

We have now two equations, (A.22) and (A.32), which express the mean stress tensor. With the aim of recovering a compact formulation, we sum now these two results and divide by two:

$$\begin{aligned} \langle \sigma_{ij} \rangle &= \frac{1}{2V} \left[\int_{V_{in}+V_{out}} -p\delta_{ij} dV + 2 \int_V \eta(\mathbf{x}) (\partial_i u_j + \partial_j u_i) dV \right. \\ &- \eta_{out}(\lambda - 1) \int_A (n_i u_j + n_j u_i) dA + \int_A x_j f_i^{mem} dA \\ &- \int_{V_{in}+V_{out}} x_j \partial_k \sigma_{ik} dV - \eta_{out} \int_{\partial V} (n_i u_j + n_j u_i) dA \\ &\left. + \int_{\partial V} x_j \sigma_{ik}^{out} n_k dA \right] \end{aligned} \quad (\text{A.33})$$

where $\mathbf{f}^{mem} = [\boldsymbol{\sigma} \cdot \mathbf{n}]^{A^+} - [\boldsymbol{\sigma} \cdot \mathbf{n}]^{A^-}$ is the membrane force, corresponding to the jump in the stress tensor across the membrane.

Now several terms can be re-written:

$$\int_{V_{in}+V_{out}} -p\delta_{ij}dV = \int_V -p\delta_{ij}dV \quad (\text{A.34})$$

since the integration over the membrane does not contribute. For the same reason and remembering the definition of λ

$$\begin{aligned} & \int_V \eta(\mathbf{x}) (\partial_i u_j + \partial_j u_i) dV \\ &= \eta_{in} \int_{V_{in}} (\partial_i u_j + \partial_j u_i) dV + \eta_{out} \int_{V_{out}} (\partial_i u_j + \partial_j u_i) dV \\ &= \eta_{in} \int_A (n_i u_j + n_j u_i) dA - \eta_{out} \int_A (n_i u_j + n_j u_i) dA \\ & \quad + \eta_{out} \int_{\partial V} (n_i u_j + n_j u_i) dA \\ &= \eta_{out}(\lambda - 1) \int_A (n_i u_j + n_j u_i) dA + \eta_{out} \int_{\partial V} (n_i u_j + n_j u_i) dA \end{aligned} \quad (\text{A.35})$$

Using (A.34) and (A.35), equation (A.33) becomes, after the recombination of few terms:

$$\begin{aligned} \langle \sigma_{ij} \rangle &= \frac{1}{2V} \left[\int_V -p\delta_{ij}dV + \eta_{out}(\lambda - 1) \int_A (n_i u_j + n_j u_i) dA \right. \\ & \quad + \int_A x_j f_i^{mem} dA - \int_{V_{in}+V_{out}} x_j \partial_k \sigma_{ik} dV \\ & \quad \left. + \eta_{out} \int_{\partial V} (n_i u_j + n_j u_i) dA + \int_{\partial V} x_j \sigma_{ik}^{out} n_k dA \right] \end{aligned} \quad (\text{A.36})$$

In the Stokes limit $\nabla \cdot \boldsymbol{\sigma} = 0$ in the fluids, then the fourth integral is zero. The last term contains the forces on the external boundary. Integrating the identity (A.4) over the volume V we obtain

$$\int_V \partial_k (x_j \sigma_{ik}) dV = \int_V \sigma_{ij} dV + \int_V x_j \partial_k \sigma_{ik} dV \quad (\text{A.37})$$

and by means of the divergence theorem, taking care of the singularities, we can re-write the previous equality as:

$$\int_{\partial V} x_j \sigma_{ik}^{out} n_k dA + \int_A x_j \Delta(\sigma_{ik}) n_k dA = \int_V \sigma_{ij} dV + \int_A x_j \Delta(\sigma_{ik}) n_k dA \quad (\text{A.38})$$

where in the first integral $\boldsymbol{\sigma} \equiv \boldsymbol{\sigma}^{out}$ since we are in the outer fluid. The expression becomes

$$\int_{\partial V} x_j \sigma_{ik}^{out} n_k dA = \int_V \sigma_{ij} dV = V \langle \sigma_{ij} \rangle \quad (\text{A.39})$$

which gives us an expression¹ equivalent to the last integral of (A.36), that becomes then:

$$\langle \sigma_{ij} \rangle = \frac{1}{V} \left[\int_V -p \delta_{ij} dV + \eta_{out} \int_{\partial V} (n_i u_j + n_j u_i) dA + \eta_{out} (\lambda - 1) \int_A (n_i u_j + n_j u_i) dA + \int_A x_j f_i^{mem} dA \right] \quad (\text{A.40})$$

This formula is very useful: the contributions to the rheology of the imposed flow and of the suspended drop are clearly separated, except for the mean pressure term. The interpretation of the terms is the following:

- the first term is the mean pressure of the suspension;
- the second represents the mean shear gradient of the flow. If the flow is imposed on the boundaries, this term, that is determined by the velocity on the external boundaries ∂V , represents the mean stress of the imposed flow;
- the third term adds a stress contribution if the internal viscosity is different from the external one ($\lambda \neq 1$). To gain a deeper insight on the origin of this term, it is useful to look at the surface integral as deriving from a volume integral of the stress tensor of the fluid constituting the drop;
- the fourth term represents the contribution to the mean stress tensor of the forces exerted on the surface of the drop.

Shortcut

There is a shortcut for the derivation of the mean stress tensor for a suspension of liquid particles (equation A.40). The calculations are much shorter, but the physical interpretation of the calculation itself is less evident. For simplicity, we drop from the beginning all the terms which are zero in the Stokes limit, i.e. every term containing $\nabla \cdot \boldsymbol{\sigma}$.

Restarting from Batchelor result, equation (A.15):

$$\langle \sigma_{ij} \rangle = \frac{1}{V} \left[\int_{V_{out}} -p \delta_{ij} dV + \eta_{out} \int_V (\partial_i u_j + \partial_j u_i) dV + \int_A [x_j \sigma_{ik}^{out} n_k - \eta_{out} (n_i u_j + n_j u_i)] dA \right] \quad (\text{A.41})$$

¹The last equivalence of equation (A.39) states that we can measure the mean stress tensor of a suspension by measuring the forces on the boundaries of the system, as usually done experimentally.

Adding and subtracting the equivalent of the surface term of the previous equation, but computed with σ^{in} and η_{in} , (A.41) becomes (remembering that $\eta_{in} = \lambda\eta_{out}$):

$$\begin{aligned} \langle \sigma_{ij} \rangle = & \frac{1}{V} \left[\int_{V_{out}} -p\delta_{ij}dV + \eta_{out} \int_V (\partial_i u_j + \partial_j u_i) dV \right. \\ & + \int_A [x_j (\sigma_{ik}^{out} n_k - \sigma_{ik}^{in} n_k) + \eta_{out}(\lambda - 1) (n_i u_j + n_j u_i)] dA \\ & \left. + \int_A [x_j \sigma_{ik}^{in} n_k - \eta_{in} (n_i u_j + n_j u_i)] dA \right] \end{aligned} \quad (\text{A.42})$$

The last integral is equivalent to the integral of the pressure inside the drop, as can be easily shown:

$$\begin{aligned} \int_A [x_j \sigma_{ik}^{in} n_k - \eta_{in} (n_i u_j + n_j u_i)] dA = \\ = \int_{V_{in}} [\partial_k (x_j \sigma_{ik}^{in}) - \eta_{in} (\partial_i u_j + \partial_j u_i)] dV \end{aligned} \quad (\text{A.43})$$

$$= \int_{V_{in}} [\partial_k (x_j \sigma_{ik}^{in}) - \sigma_{ij}^{in} - p\delta_{ij}] dV \quad (\text{A.44})$$

$$= \int_{V_{in}} [x_j \partial_k \sigma_{ik}^{in} - p\delta_{ij}] dV \quad (\text{A.45})$$

$$= \int_{V_{in}} -p\delta_{ij} dV \quad (\text{A.46})$$

So, substituting this expression in equation (A.42), we obtain:

$$\begin{aligned} \langle \sigma_{ij} \rangle = & \frac{1}{V} \left[\int_V -p\delta_{ij}dV + \eta_{out} \int_V (\partial_i u_j + \partial_j u_i) dV \right. \\ & \left. + \int_A [x_j f_i + \eta_{out}(\lambda - 1) (n_i u_j + n_j u_i)] dA \right] \end{aligned} \quad (\text{A.47})$$

which is the result reported by Kennedy *et al.* in [KPS94].

Equation (A.47) is equivalent to equation (A.40), thanks to equation (A.16).

A.3 Loss of symmetry of the mean stress tensor

The various expressions derived above for the mean stress tensor of a suspension ((A.15), (A.17), (A.40), (A.47)), are not symmetric, contrarily to

the one of the suspending Newtonian fluid. The terms that are not explicitly symmetric are the force term on the interface of the suspended particles and the volume integral of the divergence of the stress tensor, that is zero in the Stokes limit.

Let us consider equation (A.17) (for the other expressions, the calculations are analogous), then we extract the non-symmetric part of the mean stress tensor by multiplying it by the totally antisymmetric Levi-Civita tensor ϵ :

$$\epsilon_{ijk} \langle \sigma_{jk} \rangle = \epsilon_{ijk} \int_A [x_k \sigma_{jl} n_l] dA - \epsilon_{ijk} \int_{V_{in}} x_k \partial_l \sigma_{jl} dV \quad (\text{A.48})$$

since all the other terms are explicitly symmetric and then vanish when multiplied by ϵ .

The total torque \mathbf{L} which acts on a particle in the suspension is defined as

$$L_i \equiv \epsilon_{ijk} \int_{V_{in+A}} x_j f_k dV \quad (\text{A.49})$$

$$= \epsilon_{ijk} \int_{V_{in+A}} x_j \partial_l \sigma_{kl} dV \quad (\text{A.50})$$

$$= \epsilon_{ijk} \int_{V_{in+A}} [\partial_l (x_j \sigma_{kl}) - \sigma_{kj}] dV \quad (\text{A.51})$$

where \mathbf{f} is the volume density of force and in the last passage the identity (A.4) has been used. Newton's second law states that:

$$\partial_j \sigma_{kj} = \rho a_k \quad \Rightarrow \quad \sigma_{kj} = \rho a_k x_j \quad (\text{A.52})$$

ρ being the mass density.

Then combining the two equations (A.52) we obtain:

$$\sigma_{kj} = x_j \rho a_k = x_j \partial_l \sigma_{kl} \quad (\text{A.53})$$

Then we can write the total torque as:

$$L_i = \epsilon_{ijk} \int_{V_{in+A}} [\partial_l (x_j \sigma_{kl}) - x_j \partial_l \sigma_{kl}] dV \quad (\text{A.54})$$

$$= \epsilon_{ijk} \left[\int_A x_j \sigma_{kl} n_l dA - \int_{V_{in}} x_j \partial_l \sigma_{kl} dV \right] \quad (\text{A.55})$$

where in the last passage we used the same considerations on the singularities adopted for equation (A.7). Using the antisymmetry properties of ϵ ,

we recover an alternative form:

$$L_i = \epsilon_{ijk} \left[\int_A x_j \sigma_{kl} n_l dA - \int_{V_{in}} x_j \partial_l \sigma_{kl} dV \right] \quad (\text{A.56})$$

$$= -\epsilon_{ikj} \left[\int_A x_j \sigma_{kl} n_l dA - \int_{V_{in}} x_j \partial_l \sigma_{kl} dV \right] \quad (\text{A.57})$$

$$= -\epsilon_{ijk} \left[\int_A x_k \sigma_{jl} n_l dA - \int_{V_{in}} x_k \partial_l \sigma_{jl} dV \right] \quad (\text{A.58})$$

where in the last passage we only exchanged the dummy subscripts $j \leftrightarrow k$. We can recognize in this term the non-symmetric part of the mean stress tensor (A.48), up to a minus sign: then we can say that the non-symmetric part of the mean stress tensor is due to the torque with which the particle acts on the suspending fluid:

$$\boxed{L_i = -\epsilon_{ijk} \langle \sigma_{jk} \rangle} \quad (\text{A.59})$$

We can draw the conclusion that the non-symmetric part of the stress tensor of the suspension is due to the *torque* that the suspended particle exerts on the fluid. This torque can be due to an external field, as for particles with a nonzero electric dipole in an electric field.

A.4 Two-dimensional Einstein coefficient

In this section we exploit equation (A.15) to compute the effective viscosity of a two-dimensional dilute suspension of rigid disks immersed in a linear shear flow of a Newtonian fluid. We start from considering a single circular particle immersed in an infinite fluid. We consider the limit of vanishing Reynolds number $Re \rightarrow 0$, so that the evolution equation in the fluid is the Stokes equation:

$$\nabla \cdot \boldsymbol{\sigma}^F = 0 \quad (\text{A.60})$$

where $\sigma_{ij}^F = -p\delta_{ij} + \eta(\partial_i u_j + \partial_j u_i)$ is the stress tensor of the fluid.

The velocity field \mathbf{u} around a circular particle embedded in a linear shear flow of shear rate $\dot{\gamma}$ can be computed analytically in the Stokes regime. We use polar coordinates (r, θ) centered on the center of the particle to follow the geometry of the system.

As boundary conditions of the problem, we require linear shear flow at infinity and no-slip conditions on the surface of the particle, which is considered a fixed (non-rotating²) disk of unit radius. Here below the boundary

²The results will be extended to a freely-rotating particle.

conditions that we require, expressed in polar coordinates:

$$\begin{aligned}
u_r(r = \infty, \theta) &= \frac{\dot{\gamma}}{2} r \sin 2\theta \\
u_\theta(r = \infty, \theta) &= -\frac{\dot{\gamma}}{2} r (1 - \cos 2\theta) \\
u_r(r = 1, \theta) &= 0 \\
u_\theta(r = 1, \theta) &= 0
\end{aligned} \tag{A.61}$$

The following set of u_r, u_θ, p is a solution of the problem satisfying the above boundary conditions:

$$\begin{aligned}
u_r(r, \theta) &= \dot{\gamma} \left[\frac{r}{2} - \frac{1}{r} + \frac{1}{2r^3} \right] \sin 2\theta \\
u_\theta(r, \theta) &= \dot{\gamma} \left[\left(\frac{r}{2} - \frac{1}{2r^3} \right) \cos 2\theta - \left(\frac{r}{2} - \frac{1}{2r} \right) \right] \\
p(r, \theta) &= -\dot{\gamma} \frac{2}{r^2} \sin 2\theta
\end{aligned} \tag{A.62}$$

In addition, removing the term $-\frac{\dot{\gamma}}{2r}$ from the expression of u_θ gives the solution for the problem where the particle is freely rotating, which is the appropriate assumption to describe a suspension of free particles. In this case, the appropriate boundary conditions at the surface of the particle are:

$$\begin{aligned}
u_r(r = 1, \theta) &= 0 \\
\frac{\partial u_\theta}{\partial \theta}(r = 1, \theta) &= 0
\end{aligned} \tag{A.63}$$

The first condition expresses the impermeability of the particle and the second one its rigid motion.

We want to determine now the *effective viscosity* of the solution containing a rigid and freely-rotating disk. The average of the xy component of the stress tensor of the imposed linear shear flow will be denoted σ_{xy}^{shear} , whose value is:

$$\sigma_{xy}^{shear} = \eta (\partial_x v_y^{shear} + \partial_y v_x^{shear}) = \eta \dot{\gamma} \tag{A.64}$$

The mean xy component of the stress tensor of the suspension (i.e. the whole system) will be denoted σ_{xy} . By definition we have:

$$\eta_{eff} \equiv \eta \frac{\langle \sigma_{xy} \rangle}{\langle \sigma_{xy}^{shear} \rangle} \tag{A.65}$$

and the contribution due to the particle:

$$\langle \sigma_{xy}^{part} \rangle \equiv \langle \sigma_{xy} \rangle - \langle \sigma_{xy}^{shear} \rangle \tag{A.66}$$

entailing that

$$\langle \sigma_{xy} \rangle = \langle \sigma_{xy}^{shear} \rangle + \langle \sigma_{xy}^{part} \rangle \quad (\text{A.67})$$

thus

$$\eta_{eff} = \eta \frac{\langle \sigma_{xy} \rangle}{\eta \dot{\gamma}} = \eta \frac{\eta \dot{\gamma} + \langle \sigma_{xy}^{part} \rangle}{\eta \dot{\gamma}} = \eta \left[1 + \frac{\langle \sigma_{xy}^{part} \rangle}{\eta \dot{\gamma}} \right] \quad (\text{A.68})$$

In this expression we identify clearly the contribution to the effective viscosity due to the imposed flow and the one due to the presence of the particle.

Once the velocity field is known, we can compute the effective viscosity. Recalling equation (A.17) and specifying it for the xy component of the stress tensor σ gives:

$$\begin{aligned} \langle \sigma_{xy} \rangle = \frac{1}{V} \left\{ \int_{\partial V} \eta (n_x u_y + n_y u_x) dA \right. \\ \left. + \int_{A^+} [y \sigma_{xk} n_k - \eta (n_x u_y + n_y u_x)] dA \right\} \end{aligned} \quad (\text{A.69})$$

As already discussed, the first term represents the imposed shear flow. We identify the second integral with $\langle \sigma_{xy}^{part} \rangle$:

$$\langle \sigma_{xy}^{part} \rangle = \frac{1}{V} \int_A [y \sigma_{xk}^F n_k - \eta (n_x u_y + n_y u_x)] dA \quad (\text{A.70})$$

Using the solutions presented above for a non-rotating or freely-rotating circular particle, the integral can be calculated analytically. We obtain the results:

$$\langle \sigma_{xy}^{part} \rangle = \frac{1}{V} 3\pi \eta \dot{\gamma} \quad \text{for a non-rotating particle} \quad (\text{A.71})$$

$$\langle \sigma_{xy}^{part} \rangle = \frac{1}{V} 2\pi \eta \dot{\gamma} \quad \text{for a freely rotating particle} \quad (\text{A.72})$$

The prefactor $\frac{1}{V}$ can be interpreted as the number concentration of particles, then $\frac{\pi}{V}$ can be seen as the volume (or area, in 2D) fraction of particles (π is the area of a disk having a unit radius).

Thus, in the framework of a linear theory where interactions between particles are neglected, we can infer a rheological law valid for small concentrations:

$$\eta_{eff} = \eta [1 + 3\phi] \quad (\text{A.73})$$

for a non-rotating particle, and:

$$\boxed{\eta_{eff} = \eta [1 + 2\phi]} \quad (\text{A.74})$$

for a freely rotating particle.

The latter extends to the two-dimensional case Einstein's famous result $\eta_{eff} = \eta [1 + \frac{5}{2}\phi]$ valid for a suspension of rigid spheres in three dimensions [Ein06, Ein11], while the former becomes in three dimensions $\eta_{eff} = \eta [1 + 4\phi]$.

RHEOLOGY OF A TUMBLING FILAMENT

The rheology of a suspension of non-interacting rigid filaments is studied analytically. This very simple system offers a deep insight on the rheology of tumbling particles (including vesicles) in dilute suspensions. The basic ideas have been first suggested in [TS04].

On étudie analytiquement la rhéologie d'une suspension de fibres rigides sans considérer les interactions entre elles. Ce système très simple permet d'éclairer la rhéologie de suspensions diluées de particules faisant un mouvement de bascule (y compris les vésicules). Les idées de base ont été suggérées dans [TS04].

We consider a one dimensional rigid filament immersed in a two dimensional linear shear flow of a Newtonian fluid in the Stokes regime. We further suppose that the inertia of the filament can be neglected. The initial orientation angle θ_0 of the filament with respect to the flow lines is $\theta_0 \leq \pi/2$, as in figure B.1.

The rigidity of the filament implies that it has to rotate with a uniform angular velocity. The rotational component of the shear flow is a rigid rotation, so this constraint does not need to be imposed explicitly in our case.

If the filament is infinitely extensible, it cannot generate any force on the fluid and each material point of the filament is advected following the flow line on which it initially lies, and the filament will initially undergo a compression (for $\pi/2 \leq \theta \leq \pi$) and finally an unbounded extension (for $0 \leq \theta \leq \pi/2$).

If the filament is *inextensible*, it acts back on the fluid in such a way to preserve its length. The force generated will oppose compression and extension, and will then be oriented in the direction of the filament. When $\pi/2 \leq \theta \leq \pi$, the filament has to resist compression, so the force exerted by it will be outward. On the contrary, when $0 \leq \theta \leq \pi/2$, the filament has to resist extension, so the force exerted by it will be inward.

These very few and simple ingredients are enough to understand *quali-*

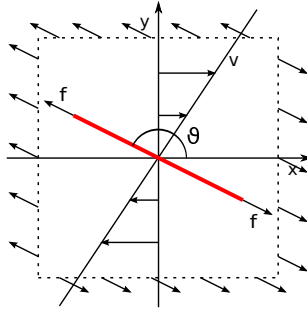


Figure B.1: A rigid and inextensible filament in a linear shear flow. f denotes the forces done by the filament on the fluid. The dashed line is the contour used to compute the stress contribution of the filament in section B.1. The arrows on the contour represent a rough approximation of the force distribution due to the presence of the filament.

tatively and *quantitatively* the rheology of a dilute suspension of rigid filaments. In the two following sections we give both an intuitive explanation and a precise computation of the behavior of the effective viscosity and the normal stress difference.

B.1 Qualitative interpretation

In order to compute the contribution of the filament to the stress (represented by the stress tensor) we consider a squared box that contains the filament. We can estimate the contribution of the filament by considering the force density due to the filament on the contour of the box. We make the rough assumption that this force density is uniform on each side of the box, and has the same direction and sign of the force f acting on the closest half of filament. The stress tensor is then proportional to this force:

$$\sigma_{ij} \sim -f_i n_j \quad (\text{B.1})$$

where the minus sign is due to the fact that the stress tensor represents the force surface density applied *on* a fluid element, and f represents the force *exerted by the fluid element* (to which the filament belongs) on the neighboring fluid. Now we integrate the components of the stress tensor on the contour of the box: a simple evaluation of the sign and the relative magnitude of the components of the stress tensor¹ provides the angle

¹This evaluation is simply done by looking at the sine and cosine of the angle that the filament forms with the flow.

dependence of the intrinsic viscosity $\eta \sim \langle \sigma_{xy} \rangle$ and intrinsic normal stress difference $N \sim \langle \sigma_{xx} - \sigma_{yy} \rangle$. The results are summarized in tables B.1 and B.2 for $\theta \in [0, \pi]$ in which the angle θ is defined (remember that the system has a central symmetry).

$\pi/2 < \theta < \pi$	$\sigma_{xy} > 0$	$[\eta] > 0$
$\theta = \pi/2$	$\sigma_{xy} = 0$	$[\eta] = 0$
$0 < \theta < \pi/2$	$\sigma_{xy} > 0$	$[\eta] > 0$
$\theta = 0$	$\sigma_{xy} = 0$	$[\eta] = 0$

Table B.1: Signs of the xy component of the stress tensor and value of the intrinsic viscosity as a function of the inclination angle of the filament.

$3\pi/4 < \theta < \pi$	$\sigma_{xx} < 0, \sigma_{yy} < 0$	$ \sigma_{xx} > \sigma_{yy} $	$[N] < 0$
$\pi/2 < \theta < 3\pi/4$	$\sigma_{xx} < 0, \sigma_{yy} < 0$	$ \sigma_{xx} < \sigma_{yy} $	$[N] > 0$
$\pi/4 < \theta < \pi/2$	$\sigma_{xx} > 0, \sigma_{yy} > 0$	$ \sigma_{xx} < \sigma_{yy} $	$[N] < 0$
$0 < \theta < \pi/4$	$\sigma_{xx} > 0, \sigma_{yy} > 0$	$ \sigma_{xx} > \sigma_{yy} $	$[N] > 0$

Table B.2: Signs of the normal components of the stress tensor and value of the intrinsic normal stress difference as a function of the inclination angle of the filament.

The intrinsic viscosity is always non-negative because so is σ_{xy} , due to the simultaneous change in sign of \mathbf{f} and of the projection direction on the x axis for $\theta = \pi/2$. It exhibits then two minima coinciding with its zeros and two maxima can be deduced from the hypothesis of continuity of $[\eta]$ with respect to θ .

The intrinsic normal stress difference is positive or negative depending on the relative magnitudes of the normal stress components, that are directly linked to the projection of the force vector on the x and y axes, that's why $[N]$ changes sign at $\theta = \pi/4$ and $\theta = 3\pi/4$.

B.2 Rigorous argument

To compute *quantitatively* the contribution of the filament to the effective viscosity and normal stress difference of the suspension we use Batchelor formula that allows to compute this quantity via an integral on the surface of the particle [Bat70]:

$$\langle \sigma_{ij} \rangle = \frac{1}{V} \left[\int_{-L/2}^{+L/2} [-f_i x_j] dl - \eta \int_{-L/2}^{+L/2} [n_i u_j + n_j u_i] dl \right] \quad (\text{B.2})$$

where \mathbf{f} is the force density with which the filament acts on the fluid, V the volume of the system and \mathbf{n} is the normal to the surface of the filament. The second integral vanishes for a quasi one-dimensional filament, since at every point there are two contributions with same velocity but opposite normal vector.

The force density can be evaluated assuming it to be equal to the Stokes drag (i.e. proportional to the velocity gradient) [RBM04]. Since the force opposes elongation, we consider the velocity component in the θ direction. Under the assumption of *passive* filament we can then compute this force

$$\mathbf{v}_r = \frac{\dot{\gamma}}{2} r \sin(2\theta) \hat{\mathbf{r}} \quad \Rightarrow \quad \mathbf{f} = -\eta \frac{\dot{\gamma}}{2} \sin(2\theta) \hat{\mathbf{r}} \quad (\text{B.3})$$

To compute the effective viscosity, equation (B.2) becomes, passing from l to the radial coordinate r

$$\langle \sigma_{xy} \rangle = \frac{\eta \dot{\gamma}}{V} \int_0^{L/2} \sin(\theta) \cos(\theta) r \sin(2\theta) dr \quad (\text{B.4})$$

$$= \frac{\eta \dot{\gamma}}{2V} \sin(2\theta) \sin(2\theta) \frac{L^2}{8} \quad (\text{B.5})$$

$$= \frac{\eta \dot{\gamma} L^2}{16V} \sin^2(2\theta) \quad (\text{B.6})$$

We can compute then the contribution of the filament to the effective viscosity, i.e. the intrinsic viscosity $[\eta] = \langle \sigma_{xy} \rangle / \eta \dot{\gamma} \phi$. ϕ is the volume fraction occupied by the filament in the suspension and it is zero if the system is unbounded and contains only one filament. We perform a linear extrapolation to finite concentration, as done in Appendix A. The volume (surface in two dimensions) occupied by the filament is $A = \epsilon L^2$, being $\epsilon < 1$ its aspect ratio. Then $\phi = A/V = \epsilon L^2/V$, and we have

$$[\eta] = \frac{1}{16\epsilon} \overline{\sin^2(2\theta)} \quad (\text{B.7})$$

The function $\sin^2(2\theta)$ is always non-negative and has two maxima and two minima (which are also zeros) in the interval $[0, \pi]$, in agreement with the qualitative argument of the previous paragraph.

To compute the normal stress difference, equation (B.2) becomes, pass-

ing from l to the radial coordinate r

$$\langle \sigma_{xx} - \sigma_{yy} \rangle = \frac{\eta\dot{\gamma}}{V} \int_0^{L/2} [\cos^2(\theta) - \sin^2(\theta)] r \sin(2\theta) dr \quad (\text{B.8})$$

$$= \frac{\eta\dot{\gamma}}{V} \cos(2\theta) \sin(2\theta) \frac{L^2}{8} \quad (\text{B.9})$$

$$= \frac{\eta\dot{\gamma}L^2}{16V} \sin(4\theta) \quad (\text{B.10})$$

We can compute then the intrinsic normal stress difference $[N] = \langle \sigma_{xx} - \sigma_{yy} \rangle / \eta\dot{\gamma}\phi$: we have

$$[N] = \frac{1}{16\epsilon} \sin(4\theta) \quad (\text{B.11})$$

The function $\sin(4\theta)$ has a period of $\pi/2$ and then exhibits two maxima, two minima and four zeros in the interval $[0, \pi]$, agreeing with what seen in the previous paragraph.

Finally, it is enlightening to remark that the angular dependence of both the intrinsic viscosity and the normal stress difference of a suspension of filaments is the same as found analytically for vesicles in three dimensions [DM07]. Moreover, also the numerical results presented in section 6.2, figure 6.9, confirm this behavior. This shows as during its tumbling motion a vesicle is, from a rheological point of view, very similar to a rigid filament.

MIGRATION DRIVEN BY NORMAL STRESS
DIFFERENCE

It is shown how the normal stress difference in a fluid undergoing circular motion generates a force on the fluid itself. Forces due to normal stresses are at the origin of non-Newtonian effects as the Weissenberg effect. This derivation does not make any assumption on the constitutive equation of the fluid. An intuitive argument is given to explain the migration of deformable particles in a curved flow of a Newtonian fluid.

On montre comme la différence des contraintes normales dans un fluide en mouvement circulaire génère une force sur le fluide-même. Les forces dues aux contraintes normales sont à l'origine d'effets non newtoniens comme l'effet Weissenberg. Cette dérivation ne fait aucune hypothèse sur l'équation constitutive du fluide. Un argument intuitif est utilisé pour expliquer la migration de particules déformables dans un écoulement courbe d'un fluide newtonien.

We consider *Cauchy's equation of motion* valid for any continuous medium, solid or fluid:

$$\frac{\partial}{\partial t} [\rho \mathbf{v}] + \nabla \cdot [\rho \mathbf{v} \mathbf{v}] = \nabla \cdot \boldsymbol{\sigma} + \rho \mathbf{g} \quad (\text{C.1})$$

where ρ is the density of the material, $\boldsymbol{\sigma}$ its stress tensor, \mathbf{v} the velocity field, \mathbf{g} the volume forces, such as gravity, acting on the fluid.

We consider now the case of a fluid of uniform density undergoing a steady circular motion. We assume that no body force \mathbf{g} is acting on the fluid. Remembering that the divergence of a tensor \mathbf{T} in polar coordinates (r, θ) is

$$\nabla \cdot \mathbf{T} = \frac{1}{r} \left(\frac{\partial}{\partial r} (r T_{rr}) + \frac{\partial}{\partial \theta} T_{\theta r} - T_{\theta \theta}, \frac{\partial}{\partial r} (r T_{r\theta}) + \frac{\partial}{\partial \theta} T_{\theta \theta} - T_{\theta r} \right) \quad (\text{C.2})$$

the radial component of Cauchy's motion equation reads

$$\frac{\partial}{\partial t} [\rho \mathbf{v}] + \frac{1}{r} \rho \left[\frac{\partial}{\partial r} (r v_r^2) + \frac{\partial}{\partial \theta} v_\theta v_r - v_\theta^2 \right] = \frac{1}{r} \left[\frac{\partial}{\partial r} (r \sigma_{rr}) + \frac{\partial}{\partial \theta} \sigma_{\theta r} - \sigma_{\theta\theta} \right] \quad (\text{C.3})$$

This expression can be simplified using the assumptions of steady ($\partial \mathbf{v} / \partial t = 0$) and circular ($v_r = 0$, $\partial \cdot / \partial \theta = 0$) flow:

$$-\frac{1}{r} \rho v_\theta^2 = \frac{1}{r} \left[\sigma_{rr} + r \frac{\partial \sigma_{rr}}{\partial r} - \sigma_{\theta\theta} \right] \quad (\text{C.4})$$

We define now the *normal stress difference* as $N = \sigma_{\theta\theta} - \sigma_{rr}$ (the component with the positive sign is commonly chosen to be the one in the flow direction, θ in our case), then equation (C.4) becomes

$$\frac{\partial \sigma_{rr}}{\partial r} = \frac{1}{r} [-\rho v_\theta^2 + N] \quad (\text{C.5})$$

The first term on the right hand side represents the inertia of the fluid. This term is never positive ($-\rho v_\theta^2 / r \leq 0$), then from (C.5) it contributes to a radial decrease of the normal stress σ_{rr} . So, if we integrate it on the surface of a fluid element, it will account for a net outward contribution. In the same way, *if the normal stress difference N is positive*, it will generate a net inward contribution.

If a Newtonian fluid is considered, $N = 0$ everywhere and no inward force is present. If a non-Newtonian fluid is taken instead (with positive N), a centripetal force is generated in the fluid. Due to its incompressibility, it cannot migrate towards the centre¹. On the other hand, a small drop of a complex fluid inserted in a Newtonian matrix would be the only part of the system experiencing an inward force, so it would start to move towards the centre. This shows as in general a positive normal stress difference is a motor for *inward* movement of fluids.

¹This is indeed the case if the fluid has a free surface, as shown in figure 3.2.

THE COMPUTATION OF EFFECTIVE VISCOSITY IN A COUETTE CELL

An expression for the computation of the effective viscosity in a Taylor-Couette cell is derived. This formula, based on the conservation of angular momentum in the cell, allows to compute the effective viscosity by measuring the torque done by either of the cylinders on the fluid sample.

On dérive une expression pour le calcul de la viscosité effective dans un dispositif de Taylor-Couette. Cette formule, basée sur la conservation du moment angulaire dans le dispositif, permet de calculer la viscosité effective en mesurant le couple exercé par les cylindres sur l'échantillon de fluide.

A Taylor-Couette cell is an experimental apparatus used to shear fluid samples. It consists of two coaxial cylinders, one of which (at least) has a nonzero angular velocity around the axis, and imposes thus a torque on the fluid sample contained in the gap between the two cylinders.

In experiments, technological solutions as lubricated lids often allow to neglect the forces exerted between the fluid and the two plane surfaces delimiting the gap volume in the axial direction. Moreover, in our two-dimensional numerical simulations the fluid is only delimited by the two cylindrical (circular) surfaces. We shall then consider in the following a two-dimensional situation. We recall that the effective viscosity is defined as the viscosity that would be measured if the fluid sample were Newtonian (see section 3.2). This is why in the computations we will pretend that the fluid in the device is Newtonian, even if this is not the case in general.

The conservation of the angular momentum applied to the fluid sample implies that the torque M (which is a scalar in two dimensions) made by the surface forces on the inner cylinder is equal in value, but opposite in sign, to the torque made by the surface forces $\mathbf{f}(\theta)$ on the outer cylinder:

$$M = \oint_{\gamma_1} R_1 f_\theta(\theta) d\theta = - \oint_{\gamma_2} R_2 f_\theta(\theta) d\theta \quad (\text{D.1})$$

More precisely, the conservation of the angular momentum applied to a

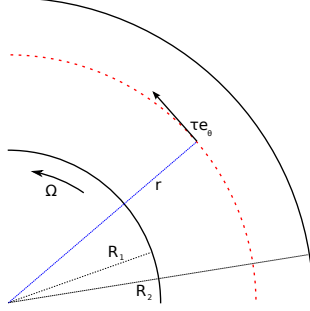


Figure D.1: Schematic of a section of the Taylor-Couette cell. The dashed line represent an arbitrary circular line in the fluid sample.

fluid region delimited on one side by the inner cylinder and on the other by an arbitrary circle of radius r in the gap ($R_1 < r < R_2$, see figure D.1) implies that the torque M is equal to the torque done by the shear force $\tau(r)\hat{\mathbf{e}}_\theta \equiv \boldsymbol{\sigma}_{\theta r}(r) \cdot \hat{\mathbf{e}}_r$ on the circle of radius r :

$$M = 2\pi r^2 \tau(r) \quad (\text{D.2})$$

that leads to an expression for τ :

$$\tau(r) = \frac{M}{2\pi r^2} \quad (\text{D.3})$$

For a Newtonian fluid, the shear rate $\dot{\gamma}$ does not depend on the angular position θ , but only on r : $\dot{\gamma} = \dot{\gamma}(r)$. It can be defined as

$$\dot{\gamma}(r) = -r \frac{d\omega}{dr} \quad (\text{D.4})$$

where ω is the angular velocity in the fluid sample. This formula takes in account the fact that a rigid rotation (uniform angular velocity) does not contribute to shear. From equation (D.4) we can express the difference in angular velocity of the boundaries, denoted Ω , as an integral of the shear rate:

$$\Omega \equiv \omega(R_1) - \omega(R_2) = \int_{R_2}^{R_1} -\frac{\dot{\gamma}(r)}{r} dr \quad (\text{D.5})$$

This integral can be computed by means of a change of variable from r to τ using equation (D.3), that gives us:

$$r = \sqrt{\frac{M}{2\pi}} \tau^{-\frac{1}{2}} \quad dr = -\frac{1}{2} \sqrt{\frac{M}{2\pi}} \tau^{-\frac{3}{2}} d\tau \quad (\text{D.6})$$

So equation (D.5) becomes:

$$\Omega = \frac{1}{2} \int_{\tau(R_2)}^{\tau(R_1)} \frac{\dot{\gamma}(\tau)}{\tau} d\tau \quad (\text{D.7})$$

For a Newtonian fluid, the shear stress τ is linked to the shear rate $\dot{\gamma}$ through the viscosity η :

$$\dot{\gamma}(\tau) = \frac{\tau}{\eta} \quad (\text{D.8})$$

that substituted in equation (D.7) leads to a trivial integral and then to

$$\Omega = \frac{1}{2\eta} [\tau(R_1) - \tau(R_2)] \quad (\text{D.9})$$

Substituting in equation (D.9) the expression (D.3) and solving it for η , we obtain the wanted relationship between viscosity (that should be regarded in general as *effective* viscosity), stress and strain:

$$\eta_{eff} = \frac{M}{4\pi\Omega} \left[\frac{1}{R_1^2} - \frac{1}{R_2^2} \right] \quad (\text{D.10})$$

where the torque M can be evaluated via either expression in (D.1). It is important to remark that in the derivation of this formula the assumption of narrow gap (i.e. $|R_2 - R_1| \ll R_1$) has not been used, and then expression (D.10) is valid for any value of (R_1, R_2) .

The correct definition of the shear rate and application of the formulas for the derivation of the effective viscosity is particularly important for the study of yield stress materials (these materials do not flow below a critical value of the shear stress, so in a Taylor-Couette cell it might happen that a part of the sample is sheared, while the rest does not deform at all). For this reason, discussions on this topic can be found in the literature about this kind of materials, as in [ELP08].

 THE FAST MULTIPOLE METHOD

The fast multipole method is detailed and the formulas upon which it is based are introduced. This work is due to H. Selmi, applied mathematician at *Ecole Polytechnique de Tunisie* (Tunisia), with whom we have closely collaborated.

On détaille la méthode multipolaire rapide et les formules sur lesquelles elle est basée. Ce travail est dû à H. Selmi, mathématicien appliqué à l'*Ecole Polytechnique de Tunisie* (Tunisie), avec lequel nous avons collaboré étroitement.

The Fast Multipole Method (FMM) is a technique to compute efficiently the product between a matrix and a vector. If the dimension of the vector is N and the matrix is square, the matrix-vector product is classically a N^2 problem, in the sense that the number of operation needed to make the computation is proportional to N^2 . Then, if N is big, the computing time is large and so is the required memory.

The matrix produced by the boundary integral method (BIM) can be large and is dense, so its storage and direct manipulation become difficult tasks. The aim of FMM is the evaluation of far-field interactions. This problem is not trivial since the kernels involved vanish only asymptotically for $r \rightarrow \infty$, r being the distance between two points of the system.

In fact the Green function of the Stokes problem may be written as the Laplacian kernel and its derivatives:

$$G(\mathbf{x} - \mathbf{x}_0) = G_l(\mathbf{x} - \mathbf{x}_0)\mathbb{1} + \frac{(\mathbf{x} - \mathbf{x}_0) \otimes (\mathbf{x} - \mathbf{x}_0)}{|\mathbf{x} - \mathbf{x}_0|^2} \quad (\text{E.1})$$

where

$$G_l(\mathbf{x} - \mathbf{x}_0) = -\ln |\mathbf{x} - \mathbf{x}_0| \quad (\text{E.2})$$

The effect of the second part of the kernel on a given force field \mathbf{f} can be written as:

$$\frac{(\mathbf{x} - \mathbf{x}_0) \otimes (\mathbf{x} - \mathbf{x}_0)}{|\mathbf{x} - \mathbf{x}_0|^2} \mathbf{f}(\mathbf{x}) = -\nabla_x G_l(\mathbf{x} - \mathbf{x}_0) \langle \mathbf{f}(\mathbf{x}) \cdot (\mathbf{x} - \mathbf{x}_0) \rangle \quad (\text{E.3})$$

The elements of the matrix are not stored, thanks to the use of a formula that expresses the velocity in terms of multipole moments, which are computed browsing a tree defined by recursive decomposition of the domain. Notice that the computation of those moments are based on the variable separation of the Laplacian kernel G_l and given by the following lemma. In the following we use complex analysis in order to simplify the notation, even though we are interested only in the real part. With the representation of the point $\mathbf{x}(x, y)$ by the complex number z , we have $G_l(\mathbf{x} - \mathbf{x}_0) = \Re(G_l(z - z_0))$.

Lemma 1. For every z, z_0 and z_{c_1} complex numbers such that $|z_{c_1} - z| < |z_{c_1} - z_0|$, and a given scalar force field $q(z)$, we have the following equality:

$$q(z)G_l(z - z_0) = -q(z)\ln(z_0 - z_{c_1}) + \sum_{k=0}^{\infty} \frac{a_k}{(z_0 - z_{c_1})^k} \quad (\text{E.4})$$

where

$$a_k = \frac{q(z)(z - z_{c_1})^k}{k} \quad (\text{E.5})$$

Proof. The intercalation of the complex number z_{c_1} in the Green function G_l gives:

$$q(z)\ln(z - z_0) = q(z)\ln(z_0 - z_{c_1}) - q(z)\ln\left(1 - \frac{z - z_{c_1}}{z_0 - z_{c_1}}\right) \quad (\text{E.6})$$

finally we use the following expansion:

$$\ln(1 - u) = \sum_{k=0}^{\infty} \frac{u^k}{k} \quad \text{for } |u| < 1 \quad (\text{E.7})$$

□

E.1 Multipole expansion

The use of the previous lemma allows to compute at a point z_0 the velocity U due to the hydrodynamical forces of the points $(z_i)_{1 \leq i \leq N}$, on which acts a scalar field $q_i, i = 1 \dots N$, and verifying $|z_{c_1} - z_i| < |z_{c_1} - z_0|$ for all $i = 1 \dots N$. The calculation gives directly

$$U(z_0) = Q \ln(z_0 - z_{c_1}) + \sum_{k=1}^{\infty} \frac{a_k}{(z_0 - z_{c_1})^k} \quad (\text{E.8})$$

where

$$Q = \sum_{i=1}^N -q_i \quad \text{and} \quad a_k = \sum_{i=1}^N \frac{q_i (z_i - z_{c_1})^k}{k} \quad (\text{E.9})$$

Note that the terms of the series above (equation (E.8)) separate into a product of a coefficient depending on the source point alone (a_k depends on $q_i(z_i - z_{c_1})$) and a function depending on the evaluation point alone, namely $(z_0 - z_{c_1})^{-k}$. By using the formula (E.8), we store only the effect of the matrix on the force field by approximating the matrix-vector product via the truncation at an order $p \ll N$ of the series given in equations (E.4) and (E.8), and compress by regrouping the surface elements. This implies a regrouping of the lines and the columns outside a certain band, whose width is determined by the dept of the tree. We finally arrive to an allocation space $O(N \text{Log} N)$ instead of $O(N^2)$.

In order to attain an even more efficient computation, we can proceed to a further expansion of equation (E.4), as shown in the following

Lemma 2. For every complex numbers z_{c_1} , z_0 and z_{c_2} such that $|z_0 - z_{c_2}| < |z_{c_1} - z_{c_2}|$, we have the following equality:

$$\frac{1}{(z_0 - z_{c_1})^k} = \sum_{l=0}^{\infty} b_l (z_0 - z_{c_2})^l \quad (\text{E.10})$$

where

$$b_l = \frac{(-1)^k \binom{l+k-1}{k-1}}{(z_{c_1} - z_{c_2})^{k+l}} \quad (\text{E.11})$$

Proof. In a similar way as done for the previous lemma, we intercalate z_{c_2} in the left hand side of (E.10), and we obtain the equality:

$$\frac{1}{(z_0 - z_{c_1})^k} = \frac{1}{(z_{c_1} - z_{c_2})^k} \frac{1}{\left(\frac{z_0 - z_{c_2}}{z_{c_1} - z_{c_2}} - 1\right)^k} \quad (\text{E.12})$$

By using the following expansion

$$\frac{1}{(1-u)^k} = \sum_{l=0}^{\infty} \binom{l+k-1}{k-1} u^l \quad \text{for } k \geq 1 \quad (\text{E.13})$$

we obtain directly the result. \square

E.2 Local expansion

Suppose that we have to measure the effect of the hydrodynamical forces on a point z_0 and that the information about the effect of the source points are

calculated and stored on a certain point z_{c_1} . Then, under the hypothesis $|z_0 - z_{c_2}| < |z_{c_1} - z_{c_2}|$, the multipole expansion (E.8) converges inside a circle C_2 of a certain radius r containing the target point z_0 and centered at z_{c_2} . So we have:

$$U(z_0) = \sum_{l=0}^{\infty} b_l (z_0 - z_{c_2})^l \quad (\text{E.14})$$

where

$$b_0 = a_0 \ln(-(z_{c_1} - z_{c_2})) + \sum_{k=1}^{\infty} \frac{a_k}{(z_{c_1} - z_{c_2})^k} (-1)^k \quad (\text{E.15})$$

and

$$b_l = -\frac{a_0}{l \cdot (z_{c_1} - z_{c_2})^l} + \frac{1}{(z_{c_1} - z_{c_2})^l} \sum_{k=1}^{\infty} \frac{a_k}{(z_{c_1} - z_{c_2})^k} \binom{l+k-1}{k-1} (-1)^k \quad (\text{E.16})$$

The series is truncated to the same order p used for the multipole expansion. In comparison with the previous section we have factorized the series as a product of two coefficients, one depending on a given point z_0 where the effect is to be calculated, and the other depending on z_c where the moment is to be evaluated. In some sense the operation consists now in regrouping elementary charges (in the electrostatics language) to build a multipole moment in a certain area. A set of charges at distant point is also regarded now as a multipole moment. The resulting interaction is thus between multipoles.

Using the previous formulas, we need to store only the local moments that summarize the whole information resulting from all the far field interactions calculated based on equality (E.10). Indeed, these quantities are converted, condensed and regrouped in only one local moment. That is to say we do not have to store the multipole moments. The storage of the local moment, that uses only a memory space about $O(N)$ (see figure E.1), is largely sufficient to obtain a good approximation of the matrix-vector product.

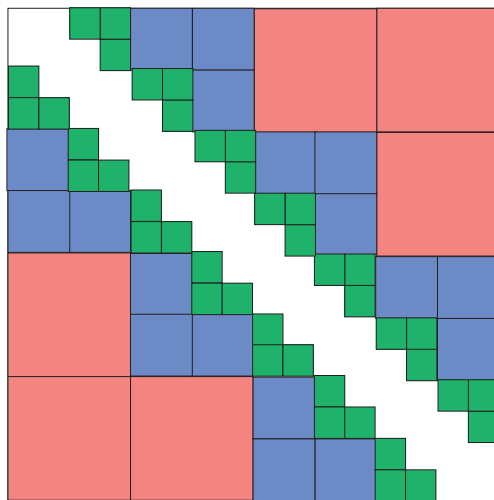


Figure E.1: Representation of the matrix storage by blocks using a tree of depth 4.

BIBLIOGRAPHY

- [ALV02] M. Abkarian, C. Lartigue, and A Viallat. Tank treading and unbinding of deformable vesicles in shear flow: Determination of the lift force. *Phys. Rev. Lett.*, 88:068103, 2002.
- [AMB02] M. V. Apostolakis, V. G. Mavrantzas, and A. N. Beris. Stress gradient-induced migration effects in the taylor-couette flow of a dilute polymer solution. *J. Non-Newtonian Fluid Mech.*, 102:409–445, 2002.
- [ASM⁺92] M. Angelova, S. Soleau, P. Meleard, J.F. Faucon, and P. Bothorel. Preparation of giant vesicles by external a.c. electric fields. kinetics and applications,. *Prog. Colloid Polym. Sci.*, 89:127–131, 1992.
- [AV08] M. Abkarian and A. Viallat. Vesicles and red blood cells in shear flow. *Soft Matter*, 4:653–657, 2008.
- [BAH87] R. B. Bird, R. C. Armstrong, and O. Hassager. *Dynamics of polymeric liquids. Vol. 1, 2nd Ed. : Fluid mechanics.* John Wiley and Sons Inc., New York, NY, 1987.
- [Bat70] G. Batchelor. The stress system in a suspension of force-free particles. *J. Fluid Mech.*, 41(3):545–570, 1970.
- [BBBC81] M. Belzons, R. Blanc, J.-L. Bouillot, and C. Camion. Viscosité d’une suspension diluée et bidimensionnelle de sphères. *C. R. Acad. Sc. Paris*, 292:5, 1981.
- [BBM04] J. Beaucourt, T. Biben, and C. Misbah. Optimal lift force on vesicles near a compressible substrate. *Europhys. Lett.*, 67:676–682, 2004.
- [BCMS02] S Boskovic, JWM Chon, P Mulvaney, and JE Sader. Rheological measurements using microcantilevers. *J. Rheol.*, 46(4):891–899, 2002.

- [BG72] G. K. Batchelor and J. T. Green. The hydrodynamic interaction of two small freely-moving spheres in a linear flow field. *J. Fluid Mech.*, 56(02):375–400, 1972.
- [Bib05] T. Biben. Phase-field models for free-boundary problems. *Eur. J. Phys.*, 26:47–55, 2005.
- [Bit86] M. Bitbol. red blood cell orientation in orbit $c=0$. *Biophys. J.*, 49:1055–1068, 1986.
- [BKM05] T. Biben, K. Kassner, and C. Misbah. Phase-field approach to three-dimensional vesicle dynamics. *Phys. Rev. E*, 72:041921, 2005.
- [BM02] T. Biben and C. Misbah. An advected-field method for deformable entities under flow. *Eur. Phys. J. B*, 29:311–316, 2002.
- [BM03] T. Biben and C. Misbah. Tumbling of vesicles under shear flow within an advected-field approach. *Phys. Rev. E*, 67:031908, 2003.
- [Bra84] J. Brady. The Einstein viscosity correction in n dimensions. *Int. J. Multiphase Flow*, 10:113–114, 1984.
- [BRS⁺04] J. Beaucourt, F. Rioual, T. Séon, T. Biben, and C. Misbah. Steady to unsteady dynamics of a vesicle in a flow. *Phys. Rev. E*, 69:011906, 2004.
- [Bru84] P. O. Brunn. Nonuniform concentration profiles of dilute macromolecular solutions in rotational viscometric flows. *J. Chem. Phys.*, 80(7):3420–3426, 1984.
- [Can70] P. B. Canham. The minimum energy of bending as a possible explanation of the biconcave shape of the human red blood cell. *J. Theoret. Biol.*, 26:61–81, 1970.
- [CKM03] I. Cantat, K. Kassner, and C. Misbah. Vesicles in haptotaxis with hydrodynamical dissipation. *Eur. Phys. J. E*, 10:175–189, 2003.
- [CKPM08] G. Coupier, B. Kaoui, T. Podgorski, and C. Misbah. Non-inertial lateral migration of vesicles in bounded Poiseuille flow. *Phys. Fluids*, 20:111702, 2008.

-
- [CL79] P. C. H. Chan and L. G. Leal. The motion of a deformable drop in a second-order fluid. *J. Fluid. Mech.*, 92:131–170, 1979.
- [CL81] P. C. H. Chan and L. G. Leal. An experimental study of drop migration in shear flow between concentric cylinders. *Int. J. Multiphase Flow*, 7:83–99, 1981.
- [CM99a] I. Cantat and C. Misbah. Dynamics and similarity laws for adhering vesicles in haptotaxis. *Phys. Rev. Lett.*, 83(1):235–238, Jul 1999.
- [CM99b] I. Cantat and C. Misbah. Lift force and dynamical unbinding of adhering vesicles under shear flow. *Phys. Rev. Lett.*, 83(4):880–883, Jul 1999.
- [CMC⁺08] N. Callens, C. Minetti, G. Coupier, M.-A. Mader, F. Dubois, C. Misbah, and T. Podgorski. Hydrodynamic lift of vesicles under shear flow in microgravity. *Europhys. Lett.*, 83:24002, 2008.
- [CN61] B. Coleman and W. Noll. Foundations of linear viscoelasticity. *Rev. Mod. Phys.*, 33:239–249, 1961.
- [CRB⁺02] P. Coussot, J. S. Raynaud, F. Bertrand, P. Moucheron, J. P. Guilbaud, H. T. Huynh, S. Jarny, and D. Lesueur. Coexistence of liquid and solid phases in flowing soft-glassy materials. *Phys. Rev. Lett.*, 88(21):218301, 2002.
- [CZM68] R. G. Cox, I. Y. Z. Zia, and S. G. Mason. Particle motions in sheared suspensions. xxv. streamlines around cylinders and spheres. *J. Colloid Interface Sci.*, 27(1):12, 1968.
- [DB08] S. K. Doddi and P. Bagchi. Lateral migration of a capsule in a plane poiseuille flow in a channel. *Int. J. Multiphase Flow*, 34:966–986, 2008.
- [DBP⁺07] G. Danker, T. Biben, T. Podgorski, C. Verdier, and C. Misbah. Dynamics and rheology of a dilute suspension of vesicles: Higher-order theory. *Phys. Rev. E*, 76:041905, 2007.
- [DCLR05] H Diamant, B Cui, B Lin, and S A Rice. Hydrodynamic interaction in quasi-two-dimensional suspensions. *J. Phys.: Condens. Matter*, 17(31):S2787–S2793, 2005.

- [dHBvdE⁺97] K. de Haas, C. Blom, D. van den Ende, M. Duits, and J. Mellema. Deformation of giant lipid bilayer vesicles in shear flow. *Phys. Rev. E*, 56:7132–7137, 1997.
- [DKS90] H.P. Duwe, J. Kaes, and E. Sackmann. Bending elastic moduli of lipid bilayers : modulation by solutes. *J. Phys. France*, 51(10):945–961, 1990.
- [DKS09] J. Deschamps, V. Kantsler, and V. Steinberg. Phase diagram of single vesicle dynamical states in shear flow. *Phys. Rev. Lett.*, 102(11):118105, 2009.
- [DKSS09] J. Deschamps, V. Kantsler, E. Segre, and V. Steinberg. Dynamics of a vesicle in general flow. *PNAS*, 106(28):11444–11447, 2009.
- [DM07] G. Danker and C. Misbah. Rheology of a dilute suspension of vesicles. *Phys. Rev. Lett.*, 98:088104, 2007.
- [DVM08] G. Danker, C. Verdier, and C. Misbah. Rheology and dynamics of vesicle suspension in comparison with droplet emulsion. *J. Non-Newton. Fluid Mech.*, 152(1-3):156 – 167, 2008.
- [DVM09] G. Danker, P. M. Vlahovska, and C. Misbah. Vesicles in Poiseuille flow. *Phys. Rev. Lett.*, 102(14):148102, 2009.
- [DZ79] K. A. Dill and B. H. Zimm. A rheological separator for very large DNA molecules. *Nucl. Acids Res.*, 7(3):735–749, 1979.
- [Ein06] A. Einstein. Eine neue Bestimmung der Moleküldimensionen. *Ann. Phys.*, 19:289–306, 1906.
- [Ein11] A. Einstein. Berichtigung zu meiner Arbeit: Eine neue Bestimmung der Moleküldimensionen. *Ann. Phys.*, 34:591–592, 1911.
- [ELP08] P. Estellé, C. Lanos, and A. Perrot. Processing the couette viscometry data using a bingham approximation in shear rate calculation. *J. Non-Newton. Fluid Mech.*, 154(1):31 – 38, 2008.
- [FA70] N. A. Frankel and A. Acrivos. The constitutive equation for a dilute emulsion. *J. Fluid Mech.*, 44(1):65–78, 1970.

-
- [FCHMRP99] R. Folch, J. Casademunt, A. Hernández-Machado, and L. Ramírez-Piscina. Phase-field model for Hele-Shaw flows with arbitrary viscosity contrast. i. theoretical approach. *Phys. Rev. E*, 60:1724–1733, 1999.
- [FL31] R. Fåhræus and T. Linqvist. The viscosity of the blood in narrow capillary tube. *Am. J. Physiol.*, 96:562–568, 1931.
- [FLSG08] R. Finken, A. Lamura, U. Seifert, and G. Gompper. Two-dimensional fluctuating vesicles in linear shear flow. *Eur. Phys. J. E*, 25:309–321, 2008.
- [FSLSS78] T. M. Fischer, M. Stöhr-Lissen, and H. Schmid-Schönbein. The red cell as a fluid droplet: tank tread-like motion of the human erythrocyte membrane in shear flow. *Science*, 202:894–896, 1978.
- [GBM10] G. Ghigliotti, T. Biben, and C. Misbah. Rheology of a dilute two-dimensional suspension of vesicles. *J. Fluid Mech.*, 653:489–518, 2010.
- [GD06] N. A. Gumerov and R. Duraiswami. Fast multipole method for the biharmonic equation in three dimensions. *J. Comp. Phys.*, 215(1):363 – 383, 2006.
- [GR87] L. Greengard and V. Rokhlin. A fast algorithm for particle simulations. *J. Comp. Phys.*, 73:325–348, 1987.
- [GR88] L. Greengard and V. Rokhlin. On the efficient implementation of the fast multipole algorithm. Technical report, Yale University, Department of Computer Science, 1988.
- [GSK⁺09] G. Ghigliotti, H. Selmi, B. Kaoui, G. Biros, and C. Misbah. Dynamics and rheology of highly deflated vesicles. *Esaim: proceedings*, 28:212–227, 2009.
- [Hel73] W. Helfrich. Elastic properties of lipid bilayers: theory and possible experiments. *Z. Naturforschung*, 28:693–703, 1973.
- [HH77] P. Hohenberg and B. Halperin. Theory of dynamic critical phenomena. *Rev. Mod. Phys.*, 49:435–479, 1977.

- [HJ06] K.G. Hollingsworth and M.L. Johns. Droplet migration in emulsion systems measured using mr methods. *J. Colloid Interface Sci.*, 296(2):700–709, APR 15 2006.
- [HV10] J. A. Hanna and P. M. Vlahovska. Surfactant-induced migration of a spherical drop in stokes flow. *Phys. Fluids*, 22:013102, 2010.
- [JM07] D. Jamet and C. Misbah. Towards a thermodynamically consistent picture of the phase-field model of vesicles: Local membrane incompressibility. *Phys. Rev. E*, 76:051907, 2007.
- [JM08a] D. Jamet and C. Misbah. Thermodynamically consistent picture of the phase-field model of vesicles: Elimination of the surface tension. *Phys. Rev. E*, 78:041903, 2008.
- [JM08b] D. Jamet and C. Misbah. Toward a thermodynamically consistent picture of the phase-field model of vesicles: Curvature energy. *Phys. Rev. E*, 78:031902, 2008.
- [KBM09] B. Kaoui, G. Birois, and C. Misbah. Why do red blood cells have asymmetric shapes even in a symmetric flow? *Phys. Rev. Lett.*, 103:188101, 2009.
- [KCMP09] B. Kaoui, G. Couplier, C. Misbah, and T. Podgorski. Lateral migration of vesicles in microchannels: effects of walls and shear gradient. *Houille Blanche*, 5:112–119, 2009.
- [KFM09] B. Kaoui, A. Farutin, and C. Misbah. Vesicles under simple shear flow: Elucidating the role of relevant control parameters. *Phys. Rev. E*, 80:061905, 2009.
- [KL10] Y. Kim and M.-C. Lai. Simulating the dynamics of inextensible vesicles by the penalty immersed boundary method. *J. Comput. Phys.*, 229:4840–4853, 2010.
- [Kob93] R. Kobayashi. Modeling and numerical simulations of dendritic crystal growth. *Physica D*, 63:410–423, 1993.
- [KPS94] M. R. Kennedy, C. Pozrikidis, and R. Skalak. Motion and deformation of liquid drops, and rheology of dilute emulsions in simple shear flow. *Comput. Fluids*, 23(2):251–278, 1994.

-
- [KRC⁺08] B. Kaoui, G. H. Ristow, I. Cantat, C. Misbah, and W. Zimmermann. Lateral migration of a 2D vesicle in unbounded Poiseuille flow. *Phys. Rev. E*, 77:021903, 2008.
- [KS82] S. Keller and R. Skalak. Motion of a tank-treading ellipsoidal particle in a shear flow. *J. Fluid Mech.*, 120:27–47, 1982.
- [KS05] V. Kantsler and V. Steinberg. Orientation and dynamics of a vesicle in tank-treading motion in shear flow. *Phys. Rev. Lett.*, 95:258101, 2005.
- [KS06] V. Kantsler and V. Steinberg. Transition to tumbling and two regimes of tumbling motion of a vesicle in shear flow. *Phys. Rev. Lett.*, 96:036001, 2006.
- [KSS08] V. Kantsler, E. Segre, and V. Steinberg. Dynamics of interacting vesicles and rheology of vesicle suspension in shear flow. *Europhys. Lett.*, 82(5):58005, 2008.
- [KWSL96] M. Kraus, W. Wintz, U. Seifert, and R. Lipowsky. Fluid vesicles in shear flow. *Phys. Rev. Lett.*, 77:3685–3688, 1996.
- [Lar99] R. G. Larson. *The structure and rheology of complex fluids*. Oxford University Press, Oxford, UK, 1999.
- [LdGdSVG⁺07] A. C. Lisboa, M. das Graças da Silva Valenzuela, G. Graziolia, F. R. Valenzuela Díazb, and M. Cleide Sogayar. Polymeric microcapsules production from sodium alginic acid for cell therapy. *Mater. Res.*, 10:353–358, 2007.
- [LLW01] C.-H. Lee, W.-C. Lin, and J. Wang. All-optical measurements of the bending rigidity of lipid-vesicle membranes across structural phase transitions. *Phys. Rev. E*, 64(2):020901, Jul 2001.
- [Low09] J. S. Lowengrub. Phase-field modeling of the dynamics of multicomponent vesicles: Spinodal decomposition, coarsening, budding, and fission. *Phys Rev. E*, 79:031926, 2009.
- [LTV08] V.V. Lebedev, K.S. Turitsyn, and S.S. Vergeles. Nearly spherical vesicles in an external flow. *New J. Phys.*, 10(4):043044 (35pp), 2008.

- [Mis06] C. Misbah. Vacillating breathing and tumbling of vesicles under shear flow. *Phys. Rev. Lett.*, 96:028104, 2006.
- [MNG09] J. L. McWhirter, H. Noguchi, and G. Gompper. Flow-induced clustering and alignment of vesicles and red blood cells in microcapillaries. *PNAS*, 106:6039–6043, 2009.
- [MSNG09] S. Messlinger, B. Schmidt, H. Noguchi, and G. Gompper. Dynamical regimes and hydrodynamic lift of viscous vesicles under shear. *Phys. Rev. E*, 80(1):011901, 2009.
- [MT00] S. Mortazavi and G. Tryggvason. A numerical study of the motion of drops in poiseuille flow. part 1. lateral migration of one drop. *J. Fluid. Mech.*, 411:325–350, 2000.
- [MVA⁺06] M.-A. Mader, V. Vitkova, M. Abkarian, A. Viallat, and T. Podgorski. Dynamics of viscous vesicles in shear flow. *Eur. Phys. J. E*, 19:389–397, 2006.
- [NEPW07] C. R. Nugent, K. V. Edmond, H. N. Patel, and E. R. Weeks. Colloidal glass transition observed in confinement. *Phys. Rev. Lett.*, 99(2):025702, Jul 2007.
- [NG04] H. Noguchi and G. Gompper. Fluid vesicles with viscous membranes in shear flow. *Phys. Rev. Lett.*, 93:258102, 2004.
- [NG05] H. Noguchi and G. Gompper. Shape transitions of fluid vesicles and red blood cells in capillary flows. *PNAS*, 102:14159–14164, 2005.
- [Nis02] N. Nishimura. Fast multipole accelerated boundary integral equation methods. *Appl. Mech. Rev.*, 55(4):299–324, 2002.
- [Oll97] P. Olla. The role of tank-treading motions in the transverse migration of a spheroidal vesicle in a shear flow. *J. Phys. A: Math. Gen.*, 30(1):317–329, 1997.
- [Pal00] R. Pal. Shear viscosity behavior of emulsions of two immiscible liquids. *J. Colloid Interface Sci.*, 225:359–366, 2000.
- [Pes02] C. S. Peskin. The immersed boundary method. *Acta Numerica*, 11:1–39, 2002.

-
- [PF90] O. Penrose and P. Fife. Thermodynamically consistent models of phase-field type for the kinetics of phase transitions. *Physica D*, 43:44–62, 1990.
- [Poz92] C. Pozrikidis. *Boundary Integral and Singularity Methods for Linearized Viscous Flow*. Cambridge University Press, Cambridge, UK, 1992.
- [Poz93] C. Pozrikidis. On the transient motion of ordered suspensions of liquid drops. *J. Fluid Mech.*, 246:301–320, 1993.
- [Poz01] C. Pozrikidis. Interfacial dynamics for stokes flow. *J. Comp. Phys.*, 169:250–301, 2001.
- [Poz05] C. Pozrikidis. Numerical simulation of cell motion in tube flow. *Ann. Biomed. Eng.*, 33:165–178, 2005.
- [PSG96] A.R. Pries, T.W. Secomb, and P. Gaehtgens. Biophysical aspects of blood flow in the microvasculature. *Cardiovascular Research*, 32:654–667, 1996.
- [RA78] J. M. Rallison and A. Acrivos. A numerical study of the deformation and burst of a viscous drop in an extensional flow. *J. Fluid Mech.*, 89(1):191–200, 1978.
- [RBM04] F. Rioual, T. Biben, and C. Misbah. Analytical analysis of a vesicle tumbling under a shear flow. *Phys. Rev. E*, 69:061914, 2004.
- [RVB10] A. Rahimian, S. K. Veerapaneni, and G. Biros. Dynamic simulation of locally inextensible vesicles suspended in an arbitrary two-dimensional domain, a boundary integral method. *J. Comput. Phys.*, 229(18):6466 – 6484, 2010.
- [SB69] R. Skalak and P I Branemark. Deformation of red blood cells in capillaries. *Science*, 164:717–719, 1969.
- [SBL91] U. Seifert, K. Berndl, and R. Lipowsky. Shape transformations of vesicles: Phase diagram for spontaneous-curvature and bilayer-coupling models. *Phys. Rev. A*, 44(2):1182–1202, Jul 1991.
- [SCB68] W. R. Schowalter, C. E. Chaffey, and H. Brenner. Rheological behaviour of a dilute emulsion. *J. Colloid Interface Sci.*, 26:152–160, 1968.

- [Sei99] U. Seifert. Fluid membranes in hydrodynamic flow fields: Formalism and an application to fluctuating quasispherical vesicles in shear flow. *Eur. Phys. J. B*, 8:405–415, 1999.
- [Sei04] U. Seifert. Fluid vesicles. In *Lecture Notes: ‘Physics meets Biology. From Soft Matter to Cell Biology’*, pages D3.1–D3.28. 35th Spring School, Institute of Solid State Research, Forschungszentrum Julich, 2004.
- [SL91] J. R. Smart and D. T. Leighton. Measurement of the drift of a droplet due to the presence of a plane. *Phys. Fluids A*, 3:21–28, 1991.
- [SLZ74] R. H. Shafer, N. Laiken, and B. H. Zimm. Radial migration of dna molecules in cylindrical flow: I. theory of the free-draining model. *Biophys. Chem.*, 2(2):180 – 184, 1974.
- [SSRP07] T. Secomb, B. Styp-Rekowska, and A. Pries. Two-dimensional simulation of red blood cell deformation and lateral migration in microvessels. *Ann. Biomed. Eng.*, 35:755–765, 2007.
- [STL⁺10] J. S. Sohn, Y.-H. Tseng, S. Li, A. Voigt, and J. S. Lowengrub. Dynamics of multicomponent vesicles in a viscous fluid. *J. Comput. Phys.*, 229:119–144, 2010.
- [Tay32] G. Taylor. The viscosity of a fluid containing small drops of another fluid. *Proc. R. Soc. Lond. Ser. A*, 138:41–48, 1932.
- [TS04] A.-K. Tornberg and M. J. Shelley. Simulating the dynamics and interactions of flexible fibers in stokes flows. *J. Comput. Phys.*, 196:8–40, 2004.
- [UBL07] O. B. Usta, Jason E. Butler, and Anthony J. C. Ladd. Transverse migration of a confined polymer driven by an external force. *Phys. Rev. Lett.*, 98(9):098301, 2007.
- [UNH93] W. S. J. Uijttewaal, E.J. Nijhof, and R. M. Heethaar. Droplet migration, deformation, and orientation in the presence of a plane wall: A numerical study compared with analytical theories. *Phys. Fluids A*, 5(4):819–825, APR 1993.

-
- [VCM⁺09] V. Vitkova, G. Couplier, M.-A. Mader, B. Kaoui, C. Misbah, and T. Podgorski. Tumbling of viscous vesicles in a linear shear field near a wall. *J. Optoelectron. Adv. Mater.*, 11:1218–1221, 2009.
- [vdW79] J. van der Waals. The thermodynamic theory of capillarity under the hypothesis of a continuous variation of density. *J. Stat. Phys.*, 20:200–244, 1979.
- [VG07] P. M. Vlahovska and R. Serral Gracia. Dynamics of a viscous vesicle in linear flows. *Phys. Rev. E*, 75(1):016313, 2007.
- [VGZB09] S. K. Veerapaneni, D. Gueyffier, D. Zorin, and G. Biros. A boundary integral method for simulating the dynamics of inextensible vesicles suspended in a viscous fluid in 2D. *J. Comp. Phys.*, 228:2334–2353, 2009.
- [VMP04] V. Vitkova, M. A. Mader, and T. Podgorski. Deformation of vesicles flowing through capillaries. *Europhys. Lett.*, 68:398–404, 2004.
- [VMP⁺08] V. Vitkova, M.-A. Mader, B. Polack, C. Misbah, and T. Podgorski. Micro-macro link in rheology of erythrocyte and vesicle suspensions. *Biophys. J.*, 95:33–35, 2008.
- [WBM93] A. Wheeler, W. Boettinger, and G. McFadden. Phase-field model of solute trapping during solidification. *Phys. Rev. E*, 47:1893–1909, 1993.
- [Wei47] K. Weissenberg. A continuum theory of rheological phenomena. *Nature*, 159:310–311, 1947.
- [WO07] N. Willenbacher and C. Oelschlaeger. Dynamics and structure of complex fluids from high frequency mechanical and optical rheometry. *Curr. Opin. Colloid Interface Sci.*, 12(1):43 – 49, 2007.
- [WSW⁺93] S. Wang, R. Sekerka, A. Wheeler, B. Murray, S. R. Coriell, R. J. Braun, and G. B. McFadden. Thermodynamically-consistent phase-field models for solidification. *Physica D*, 69:189–200, 1993.

BIBLIOGRAPHY

- [Wu79] S. Wu. Order-disorder transitions in the extrusion of fiber-filled poly (ethylene terephthalate) and blends. *Polym. Eng. Sci.*, 19(9):638–650, 1979.
- [YO86] V. Yakhot and S. A. Orszag. Renormalization group analysis of turbulence. i. basic theory. *J. Sci. Comput.*, 1:3–51, 1986. 10.1007/BF01061452.

Abstract

The dynamics and the rheology of a suspension of vesicles (a model for red blood cells) in the limit of small Reynolds number are studied by means of two-dimensional numerical simulations, based on the boundary integral and phase field methods. The focus is on the link between the microscopic dynamics of the particles and the overall behavior of the suspension (i.e. rheology).

A dilute suspension of vesicles in a linear shear flow is analyzed in detail and the influence of the parameters governing the dynamics of a single vesicle is extensively described. The nontrivial behavior of the rheological quantities (effective viscosity and normal stress difference) is explained and the role of the membrane of the vesicle detailed.

The influence of the curvature of the flow lines on the dynamics of the vesicles is investigated for the first time, and consistent inward migration is reported. The suggested interpretation, based on the coupling between the curvature of the flow and the rheological properties of the suspension, remains valid for the flow of the majority of complex fluids, like emulsions and polymer suspensions, and is thus expected to have an impact in other fields. Moreover, the behavior of a suspension of vesicles in a microscopic Taylor-Couette cell is investigated, and a transition to ordered states is reported at very low volume fraction. This phenomenon has been explained with interactions between vortices.

The behavior of sets of vesicles in a parabolic flow, a setup that mimics red blood cells in the microvasculature, is presented. Vesicles submitted to sole hydrodynamical interactions are found to form aggregates of finite size, a fact that may prove of physiological interest.

Finally, the transposition to red blood cells of the results above is discussed.

Résumé

On étudie la dynamique et la rhéologie d'une suspension de vésicules (un modèle pour les globules rouges) dans la limite de faibles nombres de Reynolds en utilisant des simulations numériques basées sur les méthodes des intégrales de frontière et du champ de phase.

L'attention est portée sur le lien entre la dynamique microscopique des particules et le comportement d'ensemble de la suspension (c. à d. la rhéologie). Une suspension diluée de vésicules dans un écoulement de cisaillement linéaire est analysée et l'influence des paramètres qui en gouvernent la dynamique est décrite en détail. On explique le comportement complexe des grandeurs rhéologiques (viscosité effective et différence des contraintes normales) et on détaille le rôle de la membrane de la vésicule.

On examine l'influence de la courbure des lignes d'écoulement sur la dynamique des vésicules, et on reporte une migration non négligeable dans la direction de concavité. L'interprétation donnée reste valable pour la plupart des fluides complexes, comme les émulsions et les suspensions de polymères. De plus, le comportement d'une suspension de vésicules dans un dispositif de Taylor-Couette microscopique a été élucidé, et une transition vers des états ordonnés a été mise en évidence à des fractions volumiques très faibles. Ce phénomène a été expliqué à travers interactions entre vortex.

On étudie aussi le comportement d'ensembles de vésicules dans un écoulement parabolique, une situation rencontrée par les globules rouges dans les capillaires sanguins. Les vésicules, soumises aux seules forces hydrodynamiques, forment des agrégats de taille finie, un fait qui pourrait être d'importance physiologique.

La transposition des résultats ci-dessus aux globules rouges est discutée.